

## **INFORMATION TO USERS**

**This manuscript has been reproduced from the microfilm master. UMI films the text directly from the original or copy submitted. Thus, some thesis and dissertation copies are in typewriter face, while others may be from any type of computer printer.**

**The quality of this reproduction is dependent upon the quality of the copy submitted. Broken or indistinct print, colored or poor quality illustrations and photographs, print bleedthrough, substandard margins, and improper alignment can adversely affect reproduction.**

**In the unlikely event that the author did not send UMI a complete manuscript and there are missing pages, these will be noted. Also, if unauthorized copyright material had to be removed, a note will indicate the deletion.**

**Oversize materials (e.g., maps, drawings, charts) are reproduced by sectioning the original, beginning at the upper left-hand corner and continuing from left to right in equal sections with small overlaps. Each original is also photographed in one exposure and is included in reduced form at the back of the book.**

**Photographs included in the original manuscript have been reproduced xerographically in this copy. Higher quality 6" x 9" black and white photographic prints are available for any photographs or illustrations appearing in this copy for an additional charge. Contact UMI directly to order.**

# **UMI**

**A Bell & Howell Information Company  
300 North Zeeb Road, Ann Arbor MI 48106-1346 USA  
313/761-4700 800/521-0600**



**University of Alberta**

**Modeling Heat and Mass Transport In  
Biological Tissues During Freezing**

by

**Christopher Val Studholme**



**A thesis submitted to the Faculty of Graduate Studies and Research in partial  
fulfillment of the requirements for the degree of Master of Science**

in

**Applied Mathematics**

**Department of Mathematical Sciences**

**Edmonton, Alberta**

**Spring 1997**



National Library  
of Canada

Acquisitions and  
Bibliographic Services

395 Wellington Street  
Ottawa ON K1A 0N4  
Canada

Bibliothèque nationale  
du Canada

Acquisitions et  
services bibliographiques

395, rue Wellington  
Ottawa ON K1A 0N4  
Canada

*Your file* *Votre référence*

*Our file* *Notre référence*

**The author has granted a non-exclusive licence allowing the National Library of Canada to reproduce, loan, distribute or sell copies of his/her thesis by any means and in any form or format, making this thesis available to interested persons.**

**The author retains ownership of the copyright in his/her thesis. Neither the thesis nor substantial extracts from it may be printed or otherwise reproduced with the author's permission.**

**L'auteur a accordé une licence non exclusive permettant à la Bibliothèque nationale du Canada de reproduire, prêter, distribuer ou vendre des copies de sa thèse de quelque manière et sous quelque forme que ce soit pour mettre des exemplaires de cette thèse à la disposition des personnes intéressées.**

**L'auteur conserve la propriété du droit d'auteur qui protège sa thèse. Ni la thèse ni des extraits substantiels de celle-ci ne doivent être imprimés ou autrement reproduits sans son autorisation.**

0-612-21212-2

**University of Alberta**

**Library Release Form**

Name of Author: **Christopher Val Studholme**

Title of Thesis: **Modeling Heat and Mass Transport in Biological Tissues During Freezing**

Degree: **Master of Science**

Year this Degree Granted: **1997**

Permission is hereby granted to the University of Alberta Library to reproduce single copies of this thesis and to lend or sell such copies for private, scholarly, or scientific research purposes only.

The author reserves all other publication and other rights in association with the copyright in the thesis, and except as hereinbefore provided, neither the thesis nor any substantial portion thereof may be printed or otherwise reproduced in any material form whatever without the author's prior written permission.



**Chris Studholme  
8 Windermere Drive  
Spruce Grove, Alberta  
T7X 1P8**

December 9, 1996


**University of Alberta**

**Faculty of Graduate Studies and Research**

The undersigned certify that they have read, and recommend to the Faculty of Graduate Studies and Research for acceptance, a thesis entitled **Heat and Mass Transport In Biological Tissues During Freezing** submitted by **Christopher Val Studholme** in partial fulfillment of the requirements for the degree of **Master of Science in Applied Mathematics**.

  
\_\_\_\_\_  
Dr. H. Van Roessel (Committee Chair)

  
\_\_\_\_\_  
Dr. F.B. Moodie (Supervisor)

  
\_\_\_\_\_  
Dr. L.E. McGann (Co-Supervisor)

  
\_\_\_\_\_  
Dr. E.P. Lozowski

December 3, 1996

***This thesis is dedicated to my parents,  
Lynn and Gordon, for all their love and  
support throughout my life.***

## **Abstract**

**Cryobiology, the study of life at low temperatures, requires modeling to extend understanding and predict responses of living systems. A compartment model was developed to represent complex biological tissues as a hierarchy of compartments. To implement this model, a description of phase behaviour in real solutions was developed using thermodynamic principles. Osmotic pressures in solutions, derived from phase behaviour, were used to predict water and solute movements across semi-permeable membranes. The heat conduction equation was solved with a piece-wise quadratic model of temperature and concentrations profiles. This diffusion model includes effects of moving phase boundaries within tissues, and allows for planar and dendritic ice formation. Constitutional supercooling was calculated for prediction of dendritic breakdown. This model was applied to real tissue systems to predict responses on tissue and cellular scales. The model's generality and use of biophysical mechanisms and parameters allows applications to a wide variety of real tissue systems.**



## **Acknowledgments**

**I wish to express my appreciation and gratitude to the following individuals for all that they have done to aid me in the writing of this thesis.**

**To Dr. Locksley McGann, my co-supervisor and long time friend. His appropriate mix of understanding, encouragement, deadlines, help, and distraction was exactly what I needed to get the job done. I will always be indebted to him for what he has provided me.**

**To Dr. Bryant Moodie for serving as my supervisor and helping to define the format and content of this thesis. His encouragement and review of my work was essential to ensure I would actually finish.**

**To Dr. Henry Van Roessel and Dr. Edward Lozowski for serving as committee members. I greatly appreciate their enthusiasm and interest in this thesis, and the insightful questions and comments they gave during the exam.**

**To Dr. Ken Muldrew for always standing his ground in every one of our many scientific arguments. His challenges have always kept me on my toes and forced me to carefully think about and prepare every statement I make.**

**Finally, to all my friends and relatives. I cannot even begin to list all that I have received from these people. All I can say is that whenever I have needed someone to talk to, drink with, play with, or simply be with, one of them has always been there. Also, whenever I had decided to avoid or ignore them, they always returned when the decision fades. Without all of these people, I would not have even made it far enough in life to start this thesis.**

**Thank you to all.**

## Contents

<b>Chapter 1 – Introduction .....</b>	<b>1</b>
<b>Cryobiology .....</b>	<b>1</b>
<b>Water .....</b>	<b>2</b>
<b>Aqueous Solutions .....</b>	<b>2</b>
<b>Biological Tissues .....</b>	<b>4</b>
<b>Mathematical Modeling in Cryobiology.....</b>	<b>6</b>
<b>Critique.....</b>	<b>9</b>
<b>Approach.....</b>	<b>10</b>
<b>Chapter 2 – Model Design .....</b>	<b>12</b>
<b>Introduction .....</b>	<b>12</b>
<b>Generalized Solution.....</b>	<b>12</b>
<b>Compartment Concept.....</b>	<b>14</b>
<b>Compartment Types.....</b>	<b>16</b>
<b>Implementation Details.....</b>	<b>18</b>
<b>Dynamic Delta Time .....</b>	<b>19</b>
<b>Chapter 3 – Phase Behaviour of Real Solutions.....</b>	<b>23</b>
<b>Introduction .....</b>	<b>23</b>
<b>Theory .....</b>	<b>24</b>
<b>Methods and Results .....</b>	<b>30</b>
<b>Determining <math>b_1</math> .....</b>	<b>30</b>
<b>Determining <math>\delta</math> .....</b>	<b>31</b>
<b>Determining <math>b_2</math> .....</b>	<b>31</b>
<b>Chapter 4 – Membrane Permeability .....</b>	<b>35</b>
<b>Introduction .....</b>	<b>35</b>
<b>Osmotic Pressure.....</b>	<b>36</b>

<b>Impermeant Solutes in Water</b> .....	<b>38</b>
<b>Addition of a Permeant Solute</b> .....	<b>39</b>
<b>Variable Time Step</b> .....	<b>41</b>
<b>Chapter 5 – Diffusion Problem</b> .....	<b>48</b>
<b>Introduction</b> .....	<b>48</b>
<b>Mass Diffusion</b> .....	<b>49</b>
<b>Heat Diffusion with a Phase Change</b> .....	<b>57</b>
<b>Mass and Heat Diffusion with a Phase Change</b> .....	<b>64</b>
<b>Chapter 6 – Constitutional Supercooling</b> .....	<b>78</b>
<b>Introduction</b> .....	<b>78</b>
<b>Constitutional Supercooling</b> .....	<b>79</b>
<b>Stability Condition</b> .....	<b>80</b>
<b>Dendritic Breakdown</b> .....	<b>81</b>
<b>Chapter 7 – Experimental Applications</b> .....	<b>89</b>
<b>Introduction</b> .....	<b>89</b>
<b>Cartilage Simulations</b> .....	<b>90</b>
<b>Ice Formation</b> .....	<b>92</b>
<b>Temperature Profiles</b> .....	<b>93</b>
<b>Intracellular Supercooling</b> .....	<b>94</b>
<b>Initial Conditions</b> .....	<b>96</b>
<b>Chapter 8 – Discussion</b> .....	<b>109</b>
<b>Thesis Objectives</b> .....	<b>109</b>
<b>References</b> .....	<b>114</b>
<b>Appendix 1 – Constants and Parameters</b> .....	<b>117</b>
<b>Appendix 2 – Variable Time Step Calculations</b> .....	<b>119</b>

## **List of Tables**

<b>3-1</b>	<b>Summary of Parameters Required for Phase Behaviour Prediction .....</b>	<b>31</b>
<b>7-1</b>	<b>Summary of Freezing Simulations Performed.....</b>	<b>91</b>

## List of Figures

2-1	Schematic of Skin Tissue With Its Compartmentalized Version .....	21
2-2	Hierarchy of Compartment Types.....	22
3-1	Excess Enthalpy Curves Fitted to Theoretical Equations.....	33
3-2	Phase Diagrams From The Literature Fitted to Theoretical Equations.....	34
4-1	Volume Response Curve For Cell Suspended in Hypertonic Solution ....	45
4-2	Simulation of Cellular Response Due to a Permeating Solute .....	46
4-3	Demonstration of the Variable Time Step Method.....	47
5-1	Subinterval Structure For The Mass Only Diffusion Problem .....	71
5-2	Illustration of Solute Diffusion in an Aqueous Solution.....	72
5-3	Subinterval Structure for the Heat Problem With a Phase Change.....	73
5-4	Temperature Profiles Present During the Freezing of Pure Water.....	74
5-5	Summary of the Extent of Ice Growth in the Pure Water Case .....	75
5-6	Subinterval Structure for the Combined Heat and Mass Problem .....	76
5-7	Planar Ice Growth in an Aqueous Salt Solution .....	77
6-1	Conditional Leading to Constitutional Supercooling .....	86
6-2	Temperature Gradients Necessary for Interface Instability .....	87
6-3	Ice Growth Before and After Dendritic Breakdown.....	88
7-1	Cartilage Diagram .....	98
7-2	Summary of Planar and Dendritic Ice Front Propagation .....	99
7-3	DMSO and NaCl Concentration During Planar Ice Growth .....	100
7-4	Temperature Profiles Present In Cartilage During Slow Cooling.....	101
7-5	Temperature Profiles Present In Cartilage During Fast Cooling.....	102
7-6	Cell Volume Curves Resulting During Freezing of Cartilage.....	103
7-7	Intracellular Supercooling as a Result of Freezing .....	104
7-8	Extending Supercooling Curve for Fast Cooling with DMSO .....	105
7-9	Amount of DMSO Present in Cells During Freezing.....	106
7-10	DMSO Uptake Curves for Cells and Cartilage at Room Temperature ...	107
7-11	Temperature Equilibration Curve for Cartilage in an Alcohol Bath .....	108

## List of Symbols and Abbreviations

### Abbreviations

atm	-	atmosphere
C	-	Celsius
cm	-	centimeter
CPA	-	cryoprotective agent
DMSO	-	dimethyl sulfoxide
g	-	gram
IIF	-	intracellular ice formation
J	-	Joule
K	-	Kelvin
kJ	-	kilojoule
kPa	-	kilopascal
l	-	liter
min	-	minute
ml	-	milliliter
mm	-	millimeter
mol	-	mole
NaCl	-	sodium chloride
sec	-	second

### Mathematical Symbols

$A$	-	surface area
$A(\tilde{C})$	-	slope of the phase diagram at the estimated concentration
$a_w$	-	water activity
$b$	-	intrinsic van der Waals volume
$C$	-	concentration
$c$	-	heat capacity

$\bar{C}$	-	total substance in subinterval
$\tilde{C}$	-	estimated concentration at phase boundary
$C_0$	-	imposed concentration at left boundary
$C_n$	-	imposed concentration at right boundary
$C^l$	-	continuous with continuous gradient
$C^\infty$	-	continuous with continuous derivatives
$D$	-	diffusion coefficient
$dE_F$	-	enthalpy of fusion
$dE_M$	-	enthalpy of mixing
$dS_F$	-	entropy of fusion
$dS_M$	-	entropy of mixing
$E$	-	energy or enthalpy
$E_a$	-	activation energy
$\bar{E}_F$	-	specific enthalpy of fusion
$F$	-	free energy (chapter 3)
$F$	-	freezing temperature (chapters 4, 5, and 6)
$f(t)$	-	some function of time
$g$	-	width of solute subinterval
$G_0$	-	imposed concentration gradient at left boundary
$G_n$	-	imposed concentration gradient at right boundary
$h$	-	step size (chapter 4)
$h$	-	width of heat subinterval (chapter 5)
$H_{-l}$	-	imposed temperature gradient at left boundary
$H_n$	-	imposed temperature gradient at right boundary
$HC$	-	heat capacity
$i$	-	iteration number (chapter 4)
$i$	-	subinterval index (chapter 5)
$J$	-	flux

$j$	-	summation index (chapter 5)
$j$	-	solute index (chapter 5)
$K$	-	thermal conductivity
$L$	-	error limit
$L$	-	width of interval (chapter 5)
$L$	-	latent heat of fusion (chapter 5)
$l$	-	number of heat subintervals on solid side
$L_p$	-	hydraulic conductivity
$M$	-	linear term in freezing temperature equation
$m$	-	number of heat subintervals on liquid side
$MV_w$	-	molecular volume of pure water
$N$	-	constant term in freezing temperature equation
$n$	-	number of moles (chapter 3)
$n$	-	number of iterations per unit time (chapter 4)
$n$	-	number of solute subintervals (chapter 5)
$P$	-	linear coefficient for generic linear equation
$p$	-	hydrostatic pressure
$P_s$	-	permeability coefficient for permeant solute
$Q$	-	constant coefficient for generic linear equation
$R$	-	gas constant
$S$	-	entropy (chapter 3)
$S$	-	amount of permeant solute (chapter 4)
$s$	-	number of moles of solid
$\bar{S}_F$	-	specific entropy of fusion
$T$	-	temperature
$t$	-	time
$V$	-	volume
$v$	-	molar volume (chapter 3)



$v$	-	normalized cell volume (chapter 4)
$v_0$	-	aqueous volume (chapter 6)
$X$	-	phase boundary position
$x$	-	mole fraction (chapters 3 and 4)
$x$	-	space variable (chapter 5)
$w_0$	-	number of moles of water
$w_i$	-	approximation to $f(t)$
$\alpha$	-	quadratic coefficient for piece-wise quadratic function
$\beta$	-	linear coefficient for piece-wise quadratic function
$\gamma$	-	constant coefficient for piece-wise quadratic function
$\Delta t$	-	time interval
$\phi$	-	volume fraction
$\phi(t)$	-	imposed concentration at boundary
$\eta$	-	exponential rate coefficient for $\phi(t)$
$\delta$	-	solubility parameter
$\pi$	-	osmotic pressure (chapter 4)
$\pi$	-	pi
$\mu$	-	chemical potential
$\Delta H_f$	-	latent heat of fusion
$\Delta S_f$	-	latent entropy of fusion
$\sigma$	-	reflection coefficient
$\xi$	-	some point in time
$\theta$	-	temperature
$\theta_{-l}$	-	imposed temperature at left boundary
$\theta_m$	-	imposed temperature at right boundary
$\bar{\theta}$	-	total temperature in subinterval
$\rho$	-	density

# **Chapter 1**

## **Introduction**

### **Cryobiology**

Simply put, cryobiology is the study of life at low temperature. In this definition, the relative term, low temperature, refers to any temperature that is below the temperature at which the specific organism being studied normally exists. For many organisms, this temperature is based on that essential ingredient present in all life on earth: water. Life exists as a result of the very specific properties of water, and in most cases life ceases to exist in the absence of liquid water. Although cryobiologists may consider temperatures above the freezing point of water to be low temperature, the most interesting results in this thesis occur at temperatures below the temperature at which ice begins to form.

Ice is no substitute for water within a biological cell. In fact, very few substances are known which can be substituted for water within a cell, and even in these cases, only a portion of the water may be substituted. With this incredible dependence life has on liquid water, it is a wonder how any cryobiologist can hope to study life at temperatures below that at which water turns to ice; however, as most Canadians are well aware, each year winter covers the land with snow and ice, subjecting the trees, animals, and people to a deep freeze lasting for several months. Yet despite this harsh treatment, each spring life flourishes as if completely unscathed by the icy wrath of our northern climate.

The cryobiologist's goal is to study the effect of low temperature on all forms of living organisms, from single cells to entire plants or animals. This study, however, is not limited to the life of these organisms, but also includes the lack of life that many organisms experience when their liquid water is transformed to ice. In most cases this lack of life provides more information about the effect of low temperature than the life itself. In some cases life in the

frozen state is desirable (such as for preservation of tissues); while in other cases, a lack of life is the goal (as with the cryosurgical removal of tumours and other malignancies). Regardless of the cryobiologist's intent, the degree to which water is present within a biological system ultimately dictates the state of that system; and therefore, an understanding of the mechanisms by which water is moved or transformed within the system is crucial.

## **Water**

Water is one of the most abundant substances on earth and also one of the most versatile. Liquid water exists at physiological temperatures as a result of the water molecule's ability to make hydrogen bonds with its neighbours [Dick 1966]. Also, this liquid is capable dissolving a wide variety of solutes, including electrolytes, sugars, and alcohols.

The structure of water in all of its forms is a subject of intense research. The water molecule's unique ability to form strong hydrogen bonds causes the existence of metastable clusters in the liquid state. These clusters, which are larger and longer lasting at lower temperatures, eventually become the framework for the crystalline lattice structure of ice. Any solutes dissolved within water affect this mechanism by which water is transformed to ice; and thus, result in changes in the freezing point of water.

## **Aqueous Solutions**

When solutes (salt, sugar, alcohol, *etc.*) are dissolved in water, the composite substance is known as an aqueous solution. Solutions have a variety of unique properties; some of which are: freezing point, boiling point, and osmotic pressure. These properties are called colligative properties since they arise as a result of the collection of chemical species that make up a solution. As already mentioned, one of these properties, the freezing point, varies from the freezing point of pure water as solutes are added. Generally, as a solute is dissolved in increasing concentration in water, the freezing point of the solution will decrease

below the usual 0° C freezing point of pure water to temperatures as low as –60° C or lower.

The relationship between the freezing point of a solution and the composition of the solution is called the phase behaviour and is typically graphed as a phase diagram. In the case of aqueous solutions, the phase diagram does not describe solely the temperatures at which liquid water precipitates out of solution as ice, but also indicates the temperatures at which other solutes present may precipitate out of solution to their respective solid forms. In the case of a binary mixture (water and a solute), half of the phase diagram indicates the freezing point of water, while the other half indicates the temperature at which the solute begins to precipitate. Regardless of which species leaves the solution at a particular temperature, as temperature is decreased that species will continue to leave the solution and the other species present will become more concentrated. Eventually, a temperature is reached where both species must leave the solution simultaneously and no further change in composition results as the entire mixture becomes solid. This temperature is called the eutectic temperature.

When more than two species are present in a solution, the situation is considerably more complicated. As one species is precipitating from the solution, due to decreasing temperature, all the other species will be concentrated within that solution; and thus, at any particular temperature, another solute may start to precipitate from the solution as well. The phase diagrams for these systems must be presented in several dimensions and can be very complex with multiple eutectic curves between the various subsets of the solutes present in the solution.

In cryobiology, understanding the phase behaviour of an arbitrary solution is important since the composition of that solution can be determined from the phase diagram for any particular temperature the solution is subjected to. In biological systems, knowledge of the composition of the aqueous solutions present is crucial to predicting the movement of water and solutes within the

system. This knowledge is also necessary to understand the effect that these solutions have on living cells.

The phase diagram for a particular solution is also useful for calculating some of the other colligative properties of that solution. Osmotic pressure is one colligative property that is of particular importance since it must be known to predict the movement of water and permeant solutes across biological membranes. This will be discussed in much greater detail later on.

### **Biological Tissues**

The enormous diversity of life on earth results in an equally enormous diversity of living tissues making up living organisms. These tissues range from plants such as trees, shrubs, fruits, and vegetables to animal tissues such as skin, bone, arteries, and organs. Each of these tissues has its own unique structure, and this structure is generally complex and exists on a variety of scales.

On a macroscopic scale, many tissues have some sort of flesh or matrix in which cells are embedded. These regions of flesh or matrix may have properties that vary spatially, and there may be membranes or other boundaries between individual regions.

At the microscopic scale, individual cells are generally surrounded by a semi-permeable membrane and perhaps even a cell wall, as in the case of plant cells. A semi-permeable membrane is one that allows passage of water and solutes with varying degrees of permeability. A cell membrane typically permits water and some other non-electrolyte solutes to pass, while blocking the passive movement of electrolytes and most large molecular weight solutes. Some of these blocked solutes are transported across the membrane by active membrane pumps. Within each cell a particular intracellular structure is present, depending on the cell type. Cells will typically contain organelles, such as the nucleus if present, which maintain some of the complex chemical reactions that keep the

cell alive, and a scaffolding, called the cytoskeleton, which is composed of microtubules that bind and connect all the various structures within the cell.

This complex, almost fractal, structure of biological tissues makes predicting their behaviour in any particular situation difficult. Food preservation is an important part of food sciences and preservation by freezing is a common technique that is used. Both plant material and animal meat can be preserved by freezing; however, the freezing process must maintain the odor, flavour, and texture of the food being preserved. A cryobiologist also needs to preserve plant and animal tissues by freezing; however, these tissues are not later consumed, but are instead expected to be returned to a normal living condition and transplanted into some system where they need to function as if fresh.

A cryosurgeon has a completely different objective from the cryobiologist or food scientist in that the cryosurgeon's goal is tissue death. In the treatment of cancerous tumours and other malignancies, freezing may be employed. In this case, the purpose of freezing is not to completely preserve the tissue, but to instead, destroy the malignant cells while leaving the tissue structure intact. To the cryosurgeon, even a small amount of cell preservation is unacceptable as these cells can later repopulate the treated tissue. Therefore, an accurate method of predicting the region of cell death is necessary to minimize any recurrence of the malignancy.

Modeling the freezing process in this variety of tissues is of importance to the food scientists, cryobiologists, and cryosurgeons alike. The food scientist, while not too concerned with cell survival, needs to maintain the structure of frozen preserved tissues in order to maintain an acceptable texture in the final product. This requires an understanding of the morphology of ice within the tissue and how that ice affects the structure of the tissue.

A cryobiologist interested in banking tissues for zoological or clinical use typically requires that a large proportion of the cells within the tissue be maintained. The role of these cells within the tissue is usually to maintain and repair the tissue; and therefore, if the cells survive the freezing process, any

tissue damage may be repaired after thawing. Transplantation of a tissue containing a large proportion of live cells is more likely to result in a successful graft.

The cryosurgeon needs to be able to predict the exact region of cell death resulting from a particular treatment. During a cryosurgical procedure, the surgeon can measure the size of the ice ball that results from the freezing probe using techniques such as ultrasound or magnetic resonance imaging; however, the region where ice is present does not necessarily coincide with the region of cell death. Some cells in the region of ice, but near the ice interface, may be preserved by the freezing process. Cells near the probe tip, on the other hand, will be successfully destroyed by the rapid freezing that occurs in that region. As a result of this discrepancy between the region of ice and the region of cell death, a cryosurgeon needs to be able to predict the relationship between these two regions in order to effectively plan successful treatments.

### **Mathematical Modeling in Cryobiology**

Regardless of the ultimate goal of the freezing process, modeling of the underlying mechanisms of water, solute and heat movement as well as the propagation of phase changes and the resulting damage to cells and tissues is an important tool in both research and applied fields. A variety of different approaches to modeling these events has been taken by several researchers. Some typical approaches are presented here.

Kedem and Katchalsky, driven by a real need for effective permeability equations, worked to correct the inadequacies of all previous descriptions of solvent and solute transport through biological membranes [Kedem & Katchalsky 1958]. Using the methods of irreversible thermodynamics, a set of permeability equations were developed which take into account the transport of both water and a permeable solute across a biological membrane. This transport is driven by a difference in osmotic pressure across the membrane and the permeant solute concentration gradient within the membrane. The pair of coupled ordinary

differential equations presented require three coefficients, of which two are the respective permeabilities of water and the permeant solute, while the remaining parameter is a reflection coefficient that had been introduced by Staverman [1952]. This reflection coefficient describes how selective the membrane is by quantifying the probability that a particular solute molecule will be reflected from the membrane and not pass through.

Johnson and Wilson developed a set of permeability transport equations consistent with the Kedem and Katchalsky equations; however, with a few modifications [Johnson & Wilson 1967]. The Johnson and Wilson equations neglect any hydrostatic pressure differences across the membrane and assume that the permeating solute has negligible molecular volume. Further, these equations take into account the possibility of a non-permeating solute present on both sides of the membrane. Johnson and Wilson, after writing the equations in a non-dimensional form, then solved the equations using a first-order perturbation technique. Their results are compared with experimental data from the literature.

Walcerz makes use of the Kedem and Katchalsky equations to predict the movement of water and cryoprotectant agents (CPA's) in a two compartment, single cell model [Walcerz 1995]. The transport parameters used to define these water and solute movements are allowed to vary with temperature according to the Arrhenius relation [Atkins 1990]. Also, the phase behaviour of each compartment is predicted for ternary solutions of water, sodium chloride, glycerol, and water, sodium chloride, dimethyl sulfoxide using equations developed by Pegg [1986]. While this model predicts only water and CPA movements in single cells and makes no attempt to model heat movement or ice front propagation, it is implemented as an easy to use software package that attempts to bring mathematical modeling to a greater proportion of cryobiology researchers.

Rubinsky and Pegg developed a mathematical model to predict the movement of water and the location of ice in biological organs at low temperature [Rubinsky & Pegg 1988]. These organs are modeled by breaking their structure



into repetitive sections of tissue, each containing an axial blood vessel. Osmotic flow into the blood vessel is predicted using the Kedem and Katchalsky equations; assuming that osmotic pressure is related to temperature by the phase diagram. This assumption is valid in the blood vessels since ice present there will maintain equilibrium with the unfrozen aqueous solution.

This Rubinsky model demonstrates that as organs are cooled to freezing temperatures the tissue sections dehydrate while the blood vessels swell. At higher cooling rates this dehydration occurs to a lesser extent which results in a greater degree of supercooling. Supercooling is a state at which the local temperature is below the local freezing point, and in this unstable state, a probability of ice forming in the region exists. Results obtained using this model correlate well both qualitatively and quantitatively with experimental data. In this model, however, no attempt is made to predict the movement of heat. It is assumed that the entire system is always at a uniform (although non-constant) temperature.

Rubinsky later expanded on this model [Bischof & Rubinsky 1993]. They used the same Krogh cylinder model [Krogh 1919], as used in Rubinsky's earlier work, to predict the location and extent of ice formation in their model tissue; however, in this work, some attempt is made to take into account the movement of heat. Temperature distributions along the axis of the blood vessel are calculated, and three different types of ice formation are predicted: solid ice, mushy ice, and liquid (no ice). Intracellular ice formation is also predicted using a probability integral. In this case, the probability of ice nucleation within a cell is related to the degree of supercooling within that cell.

A different approach to modeling net volume changes is employed by Diller [Diller & Dunaway 1991]. This network thermodynamic analysis arose out of a study of pancreas islets and was developed to predict the volume response of these tissues to perfusion with a cryoprotective agent (CPA). Flows of water and CPA across cell membranes are coupled as with the Kedem and Katchalsky model, while the tissue as a whole exhibits a viscoelastic behaviour when

shrinking and swelling. This model also takes into account variations in the transport properties with the volume and temperature of the tissue. The temperature dependence here ensures that the model can be used to predict behaviour during freezing experiments. In other work, Diller uses a solution to the heat equation to model heat transport in biological organisms with possible sources of heat included [Diller 1992]. These solutions are developed for cases with and without a phase change.

From the cryosurgical point of view, Andrushkiw solved the heat conduction problem numerically using an implicit finite-difference scheme [Andrushkiw 1990]. His technique yields temperature profile and ice front location in tissues during cryosurgical procedures. Since these procedures are performed on living tissue that is still attached to the body, metabolic heat generation is also taken into account. No attempt is made here to model salt movement within the tissue or water movement into and out of the cells; however, the model is still a useful tool for testing different cryosurgical techniques.

### **Critique**

The above approaches to modeling all have one or more of the following faults.

Most models developed in cryobiology apply to a limited set of cell or tissue systems. Some models apply only to single cells suspended in some physiological solution while others may apply to simple tissue systems. Models developed for a particular tissue or organ system usually cannot be easily extended to apply to systems with significantly different geometry. Furthermore, models developed to predict diffusion through a tissue and then permeation through a cell membrane may not be easily modified to predict permeation through a cell membrane, followed by diffusion through the cytoplasm, and then permeation into organelles.

Due to the complexities involved with multi-solute solutions and predicting the phase behaviour of these solutions, an ideal dilute solution assumption is typically made. While this assumption is valid for dilute solutions, the errors involved when more concentrated solutions are subject to the same assumption can be significant. Furthermore, many models also make additional assumptions, such as the insignificance of a solute's molecular volume. Again, while this assumption is valid for dilute solutions, errors increase as solutions become concentrated by freezing.

Some of the models depend on the use of empirical equations and non-physical parameters to predict behaviour. These equations are particularly difficult to apply in situations different from those for which the equations were developed; thus making the model specific to a single system. Also, the non-physical parameters used in these equations cannot be easily estimated and must be derived by fitting to experimental data. Extrapolating the use of these parameters to new systems cannot be easily justified, and in most cases parameters have to be determined for each specific case in which the model is to be applied.

Given the ever increasing need to develop effective protocols for tissue preservation (or tissue destruction as the case may be) and the difficulty associated with empirical guesses based solely on experiment evidence, general and effective modeling techniques must be developed and applied to simulate tissue response in low temperature environments. The model developed here combines the effects of heat and mass transport with the phase behaviour of real solutions to predict low temperature responses in a wide variety of geometrically distinct tissues.

## **Approach**

The general approach taken in this work is to make minimal assumptions as to the makeup of the tissue systems that will be modeled while making use of basic thermodynamic concepts and widely accepted theories from the literature.

**Parameters used in this model are all of physical significance and most are obtained from the literature. Only a few of the parameters are fit for by using experimental data.**

**This model uses a concept of a solution as a collection of solutes, not solute and solvent as is usually the case. Treating all chemical species in a consistent manner improves the generality of the model and allows for its application in situations where it was not directly intended to be applied.**

**Geometrically complex tissues can be simulated by making use of a compartment model. Tissues are viewed as a collection of compartments where, within each compartment, the mechanisms of mass and heat transport are uniquely defined, and all compartments interact with neighbouring compartments as a unified system.**

**The model predicts mass transport by two basic mechanisms: diffusion and permeation, while heat transport is governed by the heat conduction equation. The model also simulates the movement of phase boundaries within the system and keeps track of any supercooling that may occur.**

**A result of the generality of this model is that it may be applied to biological systems other than those used in cryobiology and perhaps even in modeling efforts outside biology. New mechanisms of transport along with other physical processes (such as chemical reactions) may be included in the general framework developed here, thus allowing this model to be used in a wide variety of situations.**

## **Chapter 2**

### **Model Design**

#### **Introduction**

The model that is introduced in this chapter is intended to overcome some of the failings of the previous modeling approaches presented in chapter one. This model was developed to be as general in scope as possible, allowing for a wide variety of biological systems to be simulated. To aid in the understanding of the model and the systems it can simulate, basic thermodynamic concepts and commonly known physical parameters are used throughout. All attempts are made to stay away from empirical relations with nonphysical coefficients.

A generalized concept of a solution is presented along with equations to predict the phase behaviour of such solutions regardless of the number of components. Solutes within a solution are allowed to be in any of a number of states simultaneously; thus allowing for a more realistic simulation of nature.

To ensure that each tissue's complex geometrical structure can be effectively represented in this model, the concept of a compartment is employed where the most relevant physical dimensions are used to describe each compartment. This compartment concept aids in the localization of the various mechanisms of solute and heat transport, while ensuring that the model functions as a complete system with each compartment interacting with its neighbours. The compartment concept ensures the generality of the model while allowing for future enhancement of the various components of the model.

#### **Generalized Solution**

In chapter one, an aqueous solution was defined as solutes dissolved in water. This is a classic definition where water plays the role of a solvent while all other molecular species present are called solutes. This definition, however, has certain drawbacks that arise from the treatment of water as a different sort of

entity than the other solutes. One particular drawback can be seen when looking at the phase behaviour. When water is considered as the solvent into which solutes are dissolved, the phase behaviour of the solution typically only includes the temperatures and concentrations at which water freezes from the solution to ice. However, as described in chapter one, the phase behaviour for a general solution can be considerably more complex as many solutes (including water) may precipitate from the solution at some temperature and composition combinations.

A more general definition of a solution is as follows. A solution is simply a collection of solutes, where each solutes' molecules are randomly mixed with the others'. A solute here is defined as an individual chemical species in a solution; thus, even water is considered to be a solute. In the ternary solution of water, dimethyl sulfoxide (DMSO) and sodium chloride (NaCl) there are three solutes present, namely water, DMSO and NaCl. When considering the phase behaviour of such a solution, it is recognized that for a particular temperature and solution composition, any one or more of the solutes may precipitate from the solution. If water is the precipitating solute, it is understood that the water is freezing out as ice.

The model allows each solute within a solution to be present in any one of four states: solid, liquid, aqueous, and glass. Both the solid and the liquid states are considered to be pure states as solutes in these states are not mixed with the other solutes present. The solid state is the result of the freezing or precipitation process while the liquid state can be used to represent a single solute or an immiscible solute. The aqueous and glass states of a solute are states in which the solute is considered to be mixed with all the other solutes present in the same state (aqueous or glass, respectively). All solutes present in an aqueous solution are in the aqueous state, while the glass state is reserved for the result of the vitrification process. Vitrification occurs when an aqueous solution is cooled without freezing to a temperature where viscosity becomes infinite. When this occurs a glassy state is formed as the solution becomes an amorphous solid.

Each solute in a solution may be present in any number of the available states simultaneously, and through phase transitions may be transformed from one state to another. Examples of phase transitions include the freezing and thawing of water and other liquids, the precipitation or dissolution of salts and sugars, and the vitrification or devitrification of aqueous solutions. In addition, it is also possible to include chemical reactions into the model as another mechanism through which solutes are transformed. In this latter case, the transitions would not be among the various states, but from one solute to another. Solute in this model do not need to be restricted to these four states. If the need for additional states (such as a gaseous state) arises, the required states can be introduced.

### **Compartment Concept**

To simulate the geometry of real tissue systems, a hierarchical compartment model is employed. This compartment model is a mechanism by which tissues can be represented as a collection of compartments nested one within another. Within each compartment, a particular set of transport equations describes the behaviour of that compartment, while interactions between a compartment and its neighbouring compartments are defined based on the boundary that separates the particular compartments. This compartment structure allows complex three-dimensional tissues to be modeled in such a way that the one-dimensional nature of the transport mechanisms can be isolated. This greatly simplifies the transport equations required.

The hierarchy of compartments is similar to a family tree. Each compartment may have any number of compartments contained within it, called children, while the compartment can only be contained itself within at most one other compartment, its parent compartment. This hierarchy is illustrated by an example, shown in figure 2-1. Here, human skin is displayed alongside its compartmentalized schematic. It is seen that the compartment representing the stratum corneum is contained within the compartment representing the stratum

granulosum, while that compartment is contained within the compartment representing the stratum spinosum, and so on. Furthermore, some of these compartments also have keratinocyte compartments as children.

Each morphological layer in skin plays a specific role in the dynamic process of skin growth. The stratum germinativum is the germinal layer from which cells are produced and move towards the outer surface of the skin. In the stratum spinosum, cells which are in the process of growth begin early keratin synthesis. When cells reach the stratum granulosum they typically contain granules which contribute to the process of keratinisation. The final layer of the epidermis is the outside layer of skin called the stratum corneum. This layer of fibrous protein and keratin consists of the flattened, fused remnants of cells from all the lower layers of the epidermis. The dermis region of skin is a thick, dense layer of fibro-elastic connective tissue which contains many blood vessels that nourish the stratum germinativum layer of the epidermis [Wheater *et al.* 1987].

Just as each layer in skin has a specific function, each compartment in the compartmentalized representation of skin has specific properties relating to the transport of solutes and heat within that compartment. Mass transport within each compartment is modeled by one basic mechanism; either diffusion or permeation. If diffusion is the case, then a phase boundary may propagate through the compartment and a distinction between planar and dendritic ice formation is maintained. However, if permeation is the mechanism of transport then the compartment is considered to be well mixed and all solute transport occurs through the boundary between the compartment and its parent compartment. Heat transport is handled either by the heat conduction equation or by Fick's law [Crank 1975] (in the case of permeation). These two basic mechanisms of transport are not the only mechanisms that can be implemented with this model. Other mechanisms can be added as will be discussed later in this chapter.

To ensure a minimal dependence on geometry, the physical dimensions of each compartment are summarized as much as possible. The most important



dimensions include: total volume of solute contained, surface area of the compartment boundary, and characteristic length (used in diffusion calculations). The total volume of the compartment is the sum of the volume of the contained solutes and the volume of all the contained child compartments. In some cases it may be necessary to vary these dimensions with time as the size or shape of the compartment varies. A simple rule, such as spherical shape, may be introduced to allow two of the dimensions, say surface area and characteristic length, to be calculated from the third, volume in this case. Compartments are not limited to these physical dimensions and different compartment types may be defined with additional physical dimensions as necessary.

In addition to the specific internal behaviour of each compartment, compartments also interact with both their parent and child compartments. In figure 2-1, each keratinocyte compartment interacts with its parent as predicted by the Johnson and Wilson [1967] transport model. Each epidermal layer compartment interacts with its neighbouring layers as dictated by the diffusion equation, while the top-most compartment in the hierarchy, the dermis compartment, interacts with the external environment as defined by the experimenter. Since planar tissues, such as skin, tend to have interactions with their environment on both sides when removed from the body, a special type of compartment which mirrors the external environment is defined and can be placed at any point within the hierarchy. This special type of compartment is not illustrated in figure 2-1, but is discussed in the next section.

### **Compartment Types**

The compartment is the fundamental structural element present in all the representations of biological tissues used with this model. Compartments come in a variety of types and these compartment types are organized in another sort of hierarchy. The hierarchy of compartment types is illustrated in figure 2-2.

The top (most fundamental) compartment in this hierarchy is the Solution. This Solution is the generalized solution that was described earlier in this

chapter. Immediately below the Solution is a Compartment. The Compartment is defined here as a solution that is bounded by some sort of boundary. This boundary is not explicitly defined in the definition of a Compartment, but is instead left to the specific compartments derived from Compartment to define.

To avoid confusion with the hierarchy of compartments used to describe biological tissues, members of the compartment type hierarchy that appear further up the tree are labeled as ancestors while members that appear further down are termed descendants. A descendant compartment type typically exhibits all of the behaviour of the ancestors it was derived from, however the descendant will expand upon that behaviour by exhibiting new behaviour unique to that compartment. The Compartment type, being a descendant of the Solution type, exhibits all the behaviour of a solution, but also includes added behaviour specific to a solution bound by some boundary.

The basic Compartment type is not useful for describing any real biological system and therefore must have descendants to expand upon its behaviour. These descendants specialize the behaviour of Compartment by defining the nature of the boundary present in the compartment. In figure 2-2, some typical descendant types are illustrated. The JWCompartment defines the compartment boundary as a semi-permeable membrane and implements the transport equations of Johnson and Wilson [1967]. On the other hand, in a DCompartment, concentration and temperature gradients are maintained throughout the compartment while heat and solutes flow freely through the boundary as dictated by Fick's law [Crank 1975].

A special type of compartment, called a MirrorCompartment, reflects the external environment. This compartment is necessary whenever the tissue being modeled is planar and the external environment interacts with the tissue on two or more sides. In these cases, the tissue can still be represented using the hierarchical compartment model.

Also illustrated in figure 2-2 is a JWCompartment. This compartment type is a descendant of the JWCompartment; and therefore, exhibits all the

behaviour of a JWCompartment with the addition of some new behaviour. In this case, the new behaviour is the ability of the compartment to predict the incidence of intracellular ice formation (IIF). A wide variety of theories exist to predict IIF [Levitt & Scarth 1936; Mazur *et al.* 1972; Steponkus *et al.* 1984]; however, one particular theory was chosen here. The osmotic rupture hypothesis was developed by Muldrew and McGann [1994] and predicts the initiation of IIF as the result of the osmotic rupture of the cell membrane. This rupture occurs when a defined critical water flux through the membrane exerts sufficient friction on the membrane to cause a local breakdown, thus allowing extracellular ice to propagate into the cell. The JWCompartment exhibits all the behaviour of a JWCompartment; however, it also includes calculations to determine the probability of IIF. If IIF is sufficiently probable, the compartment can automatically become “leaky” to simulate the breakdown of the cell membrane.

### **Implementation Details**

The model presented here is implemented using the C++ object oriented programming language. The hierarchical structure of object types, called classes, in an object oriented language is very similar to the hierarchical structure of compartment types used in this model. With C++, classes can be a descendant of one or more ancestor classes. The descendant typically inherits the behaviour of the ancestor classes, in addition to defining new, class specific behaviour. Given this similarity to the hierarchy of compartment types, individual compartments are each defined as classes in C++.

The hierarchy of compartments used to represent biological tissues is implemented as follows. Each compartment maintains a variety of pointers to: its parent, its children, and its siblings. Since a compartment has at most one parent, only one pointer is required here. On the other hand, a compartment can have several children; and thus, the pointer to the compartment’s children is a pointer to the first child compartment in a linked list of compartments. To maintain this linked list, each compartment also has pointers to some of its

siblings; namely, the sibling immediately preceding and the sibling immediately following the particular compartment in the parent's child list.

Maintaining links between compartments through the use of pointers allows the model to be constructed such that compartments automatically interact with their child compartments. The only compartment that requires a programmed interaction from the user is the top level compartment in the hierarchy (the compartment adjacent to the exterior environment). This compartment has the exterior environment imposed upon it, and then, through the use of the pointers to its children, the compartment imposes conditions upon the various child compartments. This construction closely models the real world as the experimenter only needs to define the state of the exterior environment and typically does not define the internal interactions between parent compartment and child compartment.

### *Dynamic Delta Time*

Simulations proceed as a series of finite time steps. Since a heterogeneous collection of numerical methods is employed, however, one must ensure that this time step is sufficiently small such that no one part of the simulation generates too much error. Generally, it is found that if this time step is fixed throughout the simulation, the simulation can take an unreasonably long time to perform. Therefore, to expedite calculations, the time step used in this model is considered to be dynamic and is chosen at each iteration of the simulation. To facilitate the choosing of a specific value of  $\Delta t$  for a particular iteration, the iteration is broken down into two steps:

1. *Calculate rates.* In this step all rates of transport are determined. In a JWCompartment, both water flux and permeant solute flux are determined, while in a DCompartment, the entire temperature and solute concentration profiles are calculated. No heat or solute is actually moved at this stage as the value of  $\Delta t$  for the iteration has not yet been determined.

- 2. Choose  $\Delta t$  and finalize movements.** Once all rates have been calculated, an estimate of error is determined, and then  $\Delta t$  is chosen such that the error is bounded above by some pre-selected value. The specific error calculations necessary for this step are presented in later chapters. Once  $\Delta t$  is chosen, all movements can occur at the rates calculated in step 1.

This two-step process ensures that no part of the simulation is occurring at too quick a rate, and therefore, that the specified rate of error accumulation is not exceeded. Furthermore, the simulation will not take a prohibitively long time to execute as “slow” sections of the simulation (times when not much is happening) automatically proceed at a faster rate.

The next several chapters describe specific details of the model. Chapter 3 illustrates the prediction of the phase behaviour of complex solutions. This phase behaviour is necessary to accurately predict the amount of ice and other precipitates that form during the freezing process and to predict the osmotic pressures that must be known to implement the Johnson and Wilson model [1967] of solute transport through a semi-permeable membrane.

Chapter 4 describes the details of how the Johnson and Wilson transport model is implemented, including calculations for the rate of error accumulation and how the value of the time step is derived from these calculations.

Chapter 5 deals with the diffusion problem. A solution to the diffusion equation is developed in stages, starting with a simple, solute only system, and proceeding to a complete system with solute, heat, and moving phase boundaries.

Typical uses of the model are presented in chapters 6 and 7. Constitutional supercooling is explored in chapter 6 with some specific results making use of the diffusion model developed in chapter 5 being presented. In chapter 7 the entire model is used to simulate the responses of a real tissue system with a discussion of the results. Chapter 8 contains concluding remarks and a general discussion of the work.

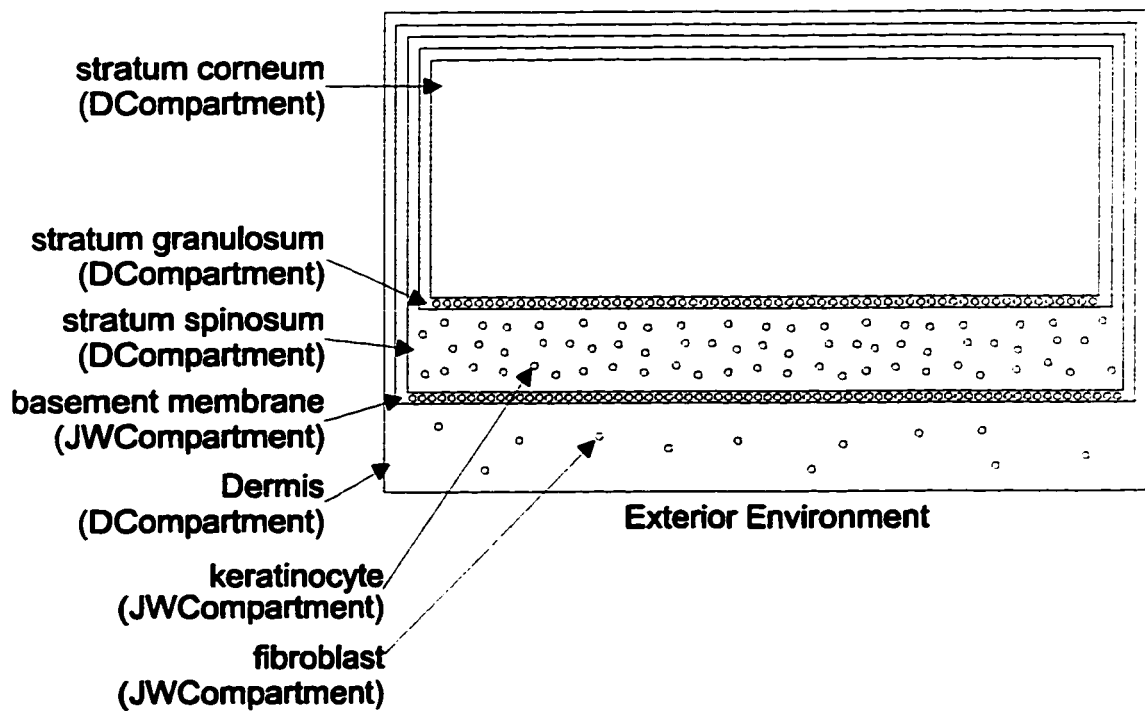
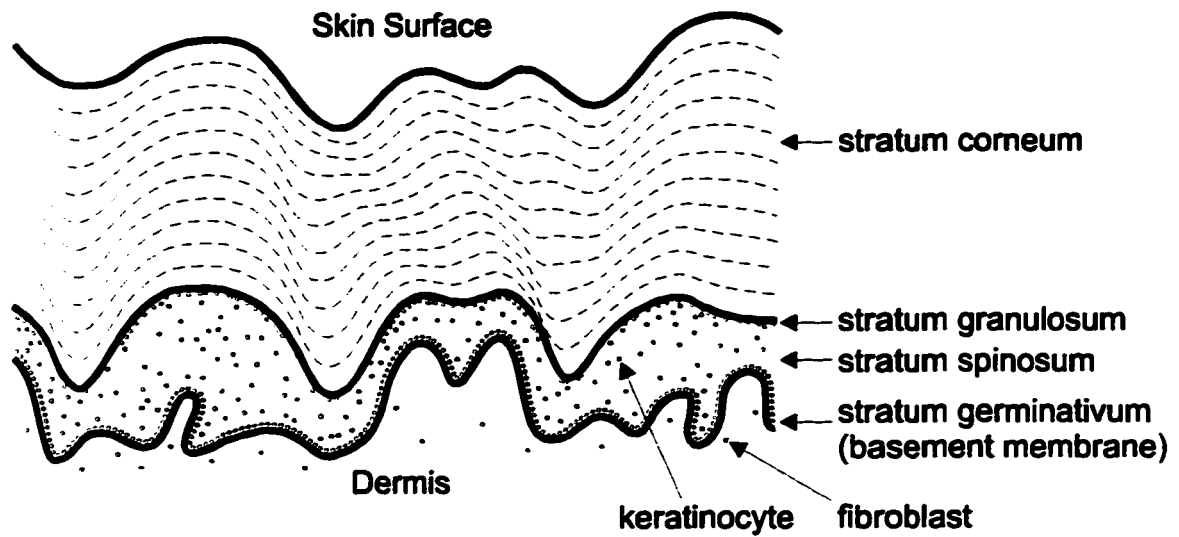


**Figure 2-1.** Schematic of the biological tissue skin along with its compartmentalized version.

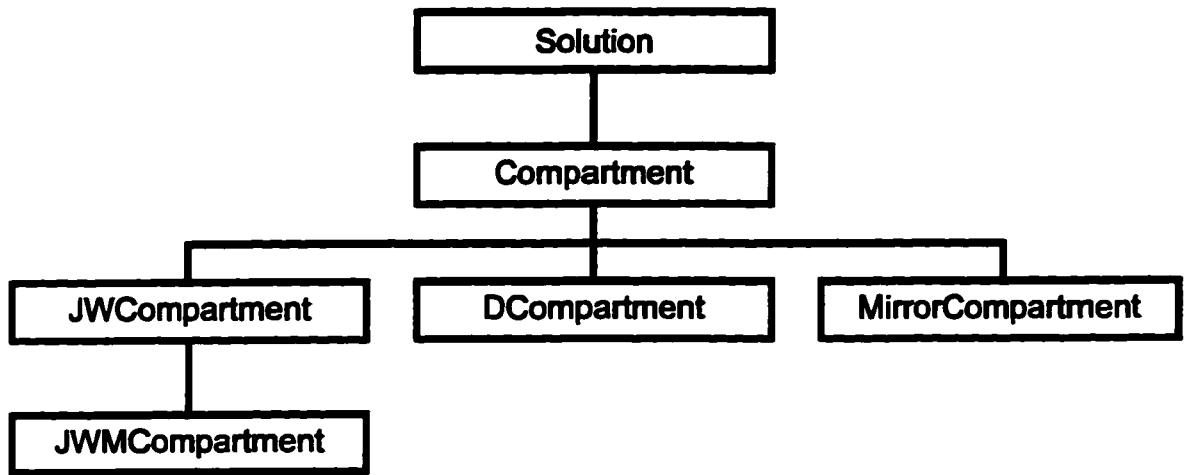


**Figure 2-2.** Hierarchy of compartment types. Compartments near the top of the hierarchy are more general and called ancestors, while compartments lower down are more specialized and called descendants.

## Chapter 3

### Phase Behaviour of Real Solutions\*

#### Introduction

The freezing point of an arbitrary physiological solution is of importance to cryobiologists attempting to model cellular and tissue responses in non-ideal environments. When solutes are added to a liquid, the freezing point of that liquid is depressed due to a disruption of the dynamic equilibrium between the liquid and its solid phase. A phase diagram quantifies the freezing point of a solution over the entire range of composition, and is usually determined by a set of experimental measurements of melting temperatures.

The only general mathematical theory describing these phase diagrams is Raoult's law [Atkins 1990] for ideal dilute solutions. Raoult's law describes the vapour pressure of the solution as a linear function of solute concentration. Since the vapour pressure of a solution is related to the freezing point of that solution, a linear relation between freezing point and solute concentration is derived, but is valid only for very dilute solutions. Raoult's Law is inappropriate for solutions with solute concentrations of interest in cryobiology, since large deviations from linearity are observed at these concentrations [Weast 1983; Rasmussen & MacKenzie 1968].

Others have used empirical mathematical expressions to describe the phase behaviour of specific aqueous solutions [Pegg 1986]. Since these equations have no physical basis for their derivation, they only describe the phase diagram curves for a few selected solutes, and cannot be generalized to arbitrary solutions containing an arbitrary number of solutes. This approach also requires experimental measurement of phase diagram information over the entire

---

\* A version of this chapter has been published. Studholme & McGann 1995. *Advances in Cryogenic Engineering*. 41:47-54.



range of concentration to calculate the empirical parameters required in the equations. As the number of solutes present in a solution increases, experimental measurement of phase diagram information becomes impractical, and a general mathematical theory for predicting this phase behaviour becomes important.

In this chapter, an approach to predicting the phase behaviour of solutions based entirely on thermodynamics is presented. Thermodynamics is, by definition, the study of equilibrium states, and the phase change during freezing is a reversible, hence equilibrium, process. As a result of this equilibrium, one important thermodynamic state variable remains constant -- the Gibb's free energy. Hence, the total derivative of the Gibb's free energy is identically zero. This is the basis for development of a thermodynamic phase behaviour theory.

### Theory

Since the process of freezing is an equilibrium process that occurs at a specific temperature depending on solute concentration, the Gibb's free energy of the system during this state change must remain constant. Free energy is given by

$$F = E - TS , \quad (3-1)$$

where  $F$  is the Gibb's free energy,  $E$  is the enthalpy of the system,  $T$  is the temperature, and  $S$  is the entropy [Atkins 1990]. Since  $F$  is constant, the differential of  $F$  should be identically zero. Formally differentiating equation 3-1 gives

$$dF = dE - TdS - SdT , \quad (3-2)$$

which can be simplified slightly by noting that freezing is an isothermal process, and thus  $dT = 0$ . Furthermore, imposing the equilibrium condition,  $dF = 0$ , equation 3-2 becomes

$$dE - TdS = 0$$

or,

$$T = \frac{dE}{dS}. \quad (3-3)$$

Equation 3-3 is an expression for the freezing point of a solution. To make use of this equation, expressions for  $dE$  and  $dS$  need to be obtained.

Since  $E$  is the enthalpy of the system,  $dE$  is the change in enthalpy that occurs during freezing. Water releases energy, the latent heat of fusion, during the ice formation process and this energy will be one component of  $dE$ . The other component of  $dE$  is a result of the unmixing that is necessary for a phase change to occur. Here, it is assumed that the phase change is the result of one component freezing out of the solution to a pure form. Hence, the unmixing occurs as this component separates from the solution and solidifies. During any mixing process it is generally the case that some energy is absorbed or released, usually called the excess energy of mixing or the heat of mixing. The unmixing process during freezing must therefore be accompanied by an absorption or release of energy, which constitutes the remaining component of the quantity  $dE$ .

An analogous argument for  $dS$  can be presented. Freezing, being an ordering process, results in a decrease in entropy which constitutes one of the two components of  $dS$ . The other component comes from the unmixing that must occur since, as above, the mixing of distinct solutes generally results in a change in entropy. Specifically, mixing results in an increase in entropy since the mixture will be in a less ordered state than the separate components. Therefore, the unmixing process must result in a decrease in entropy and this decrease represents the second component of  $dS$ .

Consider a binary mixture consisting of  $n_1$  moles of the solvent (where the term solvent is used here to label the solute that is being frozen) and  $n_2$  moles of another solute. Since the solvent freezes in a pure form, freezing  $dn_1$  moles of solvent requires that this solvent must first be removed from the solution, and

then solidified. Removing this infinitesimal quantity from solution will cause changes in both the excess enthalpy and the excess entropy of the solution, which will be labeled  $-dE_M$  and  $-dS_M$ , respectively. Here, the subscript  $M$  indicates mixture and the minus sign is included because the substance is being removed from the mixture. Once the substance has been removed from solution, it then undergoes the necessary change of state. Let  $dE_F$  and  $dS_F$  be the changes in enthalpy and entropy, respectively, that result from the process of fusion. The total changes in enthalpy and entropy can now be expressed as follows:

$$dE = dE_F - dE_M, \quad (3-4a)$$

$$dS = dS_F - dS_M. \quad (3-4b)$$

These equations can be substituted into equation 3-3 to give,

$$T = \frac{dE_F - dE_M}{dS_F - dS_M} \quad (3-5)$$

Since the enthalpy and entropy released during freezing is directly proportional to the amount of substance being solidified,

$$dE_F = \bar{E}_F \cdot dn_1, \quad (3-6a)$$

$$dS_F = \bar{S}_F \cdot dn_1, \quad (3-6b)$$

where  $\bar{E}_F$  and  $\bar{S}_F$  are the specific latent heat and specific latent entropy of fusion for the substance being frozen; both are considered constant here. This leaves only  $dE_M$  and  $dS_M$  as unknown quantities that must be examined in greater detail.

In 1947, J. H. Hildebrand expressed the entropy of mixing for a binary solution whose molecules differ in size as

$$\frac{\Delta S^M}{R} = n_1 \ln \frac{V - n_1 b_1 - n_2 b_2}{n_1 (v_1 - b_1)} + n_2 \ln \frac{V - n_1 b_1 - n_2 b_2}{n_2 (v_2 - b_2)} \quad (3-7)$$

where  $\Delta S^M$  indicates the excess entropy, labeled  $S_M$  here,  $V$  is the total volume of the mixture,  $v_1$  and  $v_2$  are the molar volumes of each component, and  $b_1$  and  $b_2$  are geometrical volumes, or intrinsic van der Waals volumes, of each component [Hildebrand 1947].

The partial derivative of  $S_M$  with respect to  $n_1$ , holding  $n_2$  constant, can be calculated from equation 3-7 as

$$\left(\frac{\partial S_M}{\partial n_1}\right)_{n_2} = R \left[ \ln \frac{n_1(v_1 - b_1) + n_2(v_2 - b_2)}{n_1(v_1 - b_1)} + \frac{n_2(v_1 - b_1) - n_2(v_2 - b_2)}{n_1(v_1 - b_1) + n_2(v_2 - b_2)} \right], \quad (3-8)$$

where it is assumed that the volume of the solution is additive, that is

$$V = n_1 v_1 + n_2 v_2, \quad (3-9)$$

and thus

$$V - n_1 b_1 - n_2 b_2 = n_1(v_1 - b_1) + n_2(v_2 - b_2). \quad (3-10)$$

Of the solutes studied in this work, ethanol is the only one with a molar volume that has a significant dependence on concentration (which invalidates equation 3-9). This concentration dependence is evident in the phase behaviour of the solution containing ethanol and water, and therefore, contributes to the error in predicting the phase behaviour of that solution.

For an expression similar to equation 3-8, but involving  $E_M$ , look to a book by Hildebrand, Prausnitz and Scott titled *Regular and Related Solutions* where an expression known as the Scatchard-Hildebrand equation is presented [Hildebrand *et al.* 1970]. This equation results from work done by Scatchard [1931] and describes the enthalpy of mixing of two liquids as

$$\Delta E^M = (n_1 v_1 + n_2 v_2) \phi_1 \phi_2 (\delta_1^2 + \delta_2^2 - 2\delta_{12}), \quad (3-11)$$

where  $\Delta E^M$  represents the excess enthalpy of mixing, labeled  $E_M$  here,  $\phi_i$  represents the volume fraction of each component, and  $\delta_i$  is defined to be a solubility parameter. Here  $\delta_1$  and  $\delta_2$  describe the interactions between like

components in the solution while  $\delta_{12}$  describes the interactions between unlike components. Practically, however, all these parameters cannot be found independently, and therefore, a composite solubility parameter is defined by

$$\delta = \delta_1^2 + \delta_2^2 - 2\delta_{12}, \quad (3-12)$$

and included in equation 3-11 to get

$$E_M = \frac{n_1 v_1 n_2 v_2}{n_1 v_1 + n_2 v_2} \delta, \quad (3-13)$$

where substitutions for the volume fractions,  $\phi_i$ , have also been made. It should be noted that  $\delta > 0$  implies an endothermic mixing process, while  $\delta < 0$  implies exothermic mixing. As before, the partial derivative of this enthalpy of mixing equation with respect to  $n_1$ , holding  $n_2$  constant, is calculated as

$$\left( \frac{\partial E_M}{\partial n_1} \right)_{n_2} = \frac{v_1 n_2^2 v_2^2}{(n_1 v_1 + n_2 v_2)^2} \delta. \quad (3-14)$$

Now, knowing equation 3-8 and equation 3-14, the enthalpy and entropy of unmixing for the  $dn_1$  moles of solvent can be calculated as

$$dE_M = \left( \frac{\partial E_M}{\partial n_1} \right)_{n_2} dn_1, \quad (3-15a)$$

$$dS_M = \left( \frac{\partial S_M}{\partial n_1} \right)_{n_2} dn_1, \quad (3-15b)$$

which, along with equations 3-6, can be substituted into equation 3-5 to get

$$T = \frac{\bar{E}_F \cdot dn_1 - \left( \frac{\partial E_M}{\partial n_1} \right)_{n_2} dn_1}{\bar{S}_F \cdot dn_1 - \left( \frac{\partial S_M}{\partial n_1} \right)_{n_2} dn_1}. \quad (3-16)$$

Cancellation of the  $dn_i$ 's is a requirement since the freezing point of a solution is not expected to depend on the amount of solvent being frozen. Thus, simplifying equation 3-16 gives

$$T = \frac{\bar{E}_F - \left( \frac{\partial E_M}{\partial n_1} \right)_{n_2}}{\bar{S}_F - \left( \frac{\partial S_M}{\partial n_1} \right)_{n_2}} \quad (3-17)$$

By substituting equation 3-8 and equation 3-14 into equation 3-17, the equation for the freezing point of an arbitrary binary mixture is

$$T = \frac{\bar{E}_F - \frac{v_1 n_2^2 v_2^2}{(n_1 v_1 + n_2 v_2)^2} \delta}{\bar{S}_F - R \left[ \ln \frac{n_1(v_1 - b_1) + n_2(v_2 - b_2)}{n_1(v_1 - b_1)} + \frac{n_2(v_1 - b_1) - n_2(v_2 - b_2)}{n_1(v_1 - b_1) + n_2(v_2 - b_2)} \right]}, \quad (3-18)$$

which depends on  $n_1$  and  $n_2$  along with the constants  $\bar{E}_F$ ,  $\bar{S}_F$ ,  $v_1$ ,  $v_2$ ,  $b_1$ ,  $b_2$  and  $\delta$ . To show that this expression does not depend on the total amount of solution,  $n_1 + n_2$ , make a transformation from  $n_1$ ,  $n_2$  to  $x_1$ ,  $x_2$ , the mole fractions. This transformation is

$$x_1 = \frac{n_1}{n_1 + n_2}, \quad x_2 = \frac{n_2}{n_1 + n_2}, \quad (3-19)$$

and results in

$$T = \frac{\bar{E}_F - \frac{v_1 x_2^2 v_2^2}{(x_1 v_1 + x_2 v_2)^2} \delta}{\bar{S}_F - R \left[ \ln \frac{x_1(v_1 - b_1) + x_2(v_2 - b_2)}{x_1(v_1 - b_1)} + \frac{x_2(v_1 - b_1) - x_2(v_2 - b_2)}{x_1(v_1 - b_1) + x_2(v_2 - b_2)} \right]}. \quad (3-20)$$

In this expression  $v_1$  and  $v_2$  are the molar volumes of each component, which are usually well known. However, although  $\delta_i$  may be found in tables for some compounds, the interaction term  $\delta_{12}$  is generally not known, and therefore needs to be fitted using data from experiment or literature and the technique of least

squares. Finally,  $b_1$  and  $b_2$  are the intrinsic van der Waals volumes for each of the components and although this constant is known for several real gases, it is difficult to obtain for most liquids. Therefore it will have to be found by other means, a few of which are proposed by Hildebrand *et al.* [1970]

### **Methods and Results**

Values for the constants  $b_1$ ,  $b_2$  and  $\delta$  are required in order to predict the phase behaviour of an arbitrary two component solution. In the absence of experimental values for these constants obtained from other sources, an effective method of determining these values is by fitting equation 3-20 to known phase information. With three parameters to fit, at least 4 data points are required and can be obtained either experimentally or from previously published tables. A problem with this method pertains to the calculation of  $b_1$ . Since solutions of interest in cryobiology all include water as a primary component, there should be only one value for  $b_1$  that is common to all the mixtures. Therefore, some method for determining  $b_1$ , independent of  $b_2$ , must be found, and then curve fitting techniques can be used to find  $b_2$  and  $\delta$  for each binary solution of interest.

#### *Determining $b_1$*

Hildebrand proposes a few techniques to find this geometrical volume [Hildebrand *et al.* 1970], but due to limitations on the amount of experimental data available in the literature, only one technique was found to be applicable. From a set of steam tables [Haar *et al.* 1984], the value of  $b$  for water was determined by a linear extrapolation of the molar volume of water vapour at constant pressure, but as a function of temperature, to absolute zero temperature. The pressure chosen was 2000kPa because the molar volume data in the range of 50°C to 210°C was nearly linear and thus an extrapolation was possible. By this method, the value of  $b_1$  was determined to be 11.44 ml/mol.

**Table 3-1. Summary of parameters required in equation 3-20.**

<b>Solute</b>	<b>molecular weight g/mol</b>	<b><math>v</math> ml/mol</b>	<b><math>b</math> ml/mol</b>	<b><math>\delta</math> kJ/ml*</b>
water	18.02	18.02	11.44	
ethylene glycol	62.07	54.63	48.05	-0.099
propylene glycol	76.09	71.66	67.18	-0.100
methanol	32.03	38.05	31.48	-0.146
ethanol	46.07	54.84	48.26	-0.021
1-propanol	60.09	70.46	63.89	0.011
2-propanol	60.09	70.23	77.92	0.005
glycerol	92.09	71.70	48.23	-0.004
D-glucose	180.16	113.99	123.84	0.002
sucrose	342.30	214.12	232.74	0.001
acetone	58.05	67.59	60.95	0.015
dimethyl sulfoxide	78.13	70.94	52.49	-0.343

\* negative values indicate exothermic mixing

### *Determining $\delta$*

Since equation 3-13 represents the excess enthalpy of mixing and does not contain the parameter  $b$ , information from the literature on the excess enthalpy of mixing can be used to calculate  $\delta$ . Data on the excess enthalpy of mixing for four of the binary mixtures considered here (ethylene glycol, methanol, propylene glycol, and dimethyl sulfoxide, each as a binary mixture with water) [Christensen *et al.* 1984] was fitted using the technique of least squares with equation 3-13 to determine values for  $\delta$ . Figure 3-1 shows the data and fitted curves.

### *Determining $b_2$*

With these values for  $\delta$ , equation 3-20 was fitted to phase diagram data [Weast 1983; Rasmussen & MacKenzie 1968] for the single parameter  $b_2$ . In the cases where no excess enthalpy data was available, equation 3-20 was fitted for both  $b_2$  and  $\delta$ . In either case, figure 3-2 shows this phase diagram data along with the fitted curves, while table 3-1 summarizes the fitted parameters which are used to predict the phase behavior of these aqueous solutions.



**This phase diagram theory, based on a phase change in one component of a binary solution and the unmixing necessary for the freezing of that component, predicts the freezing point of aqueous solutions of various solutes over a wide range of concentrations. Application of the theory requires three parameters describing the solution – a solubility parameter,  $\delta$ , and the intrinsic van der Waals volume of each solute,  $b_1$  and  $b_2$ . The theory, although developed for binary solutions, can be generalized to mixtures with an arbitrary number of components.**

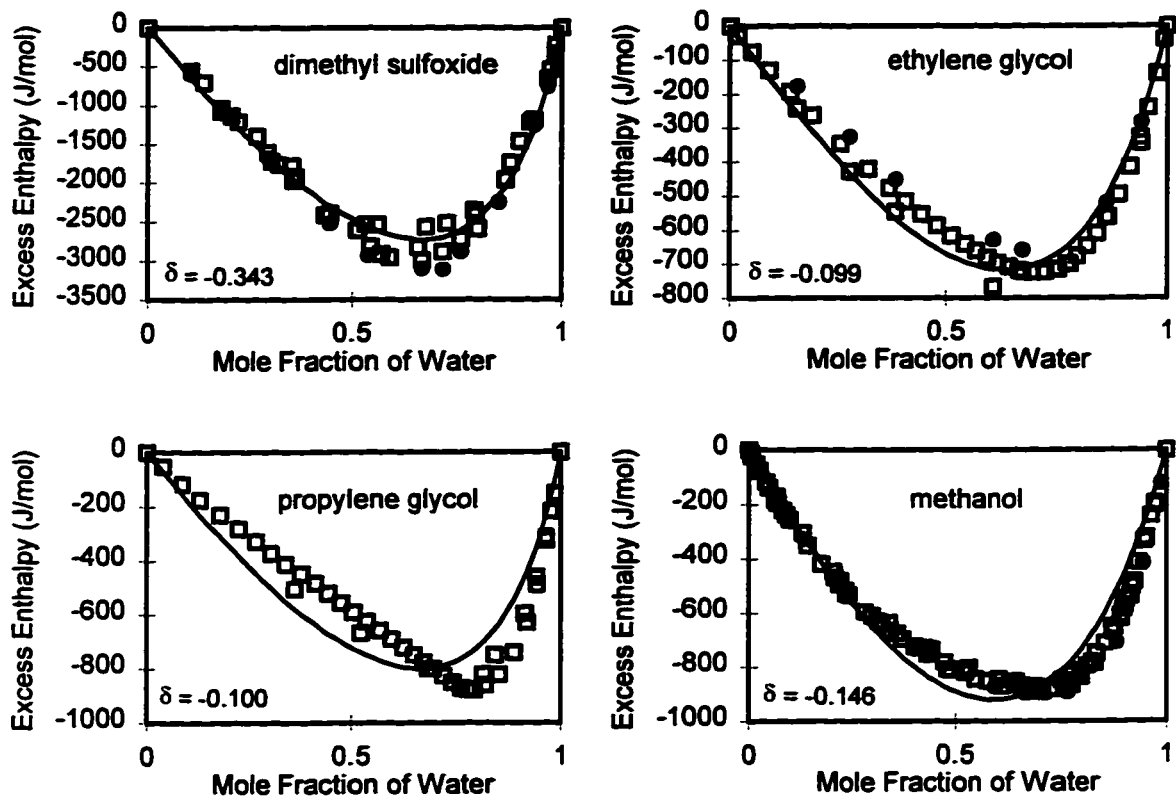


**Figure 3-1.** Excess enthalpy is shown as a function of water concentration. The solid line is the fitted curve using equation 3-13 with the indicated value of  $\delta$ . The open squares represent data at 25°C while the closed circles represent data at 35°C. This latter data was not used during fitting, but is instead just reported for comparison.

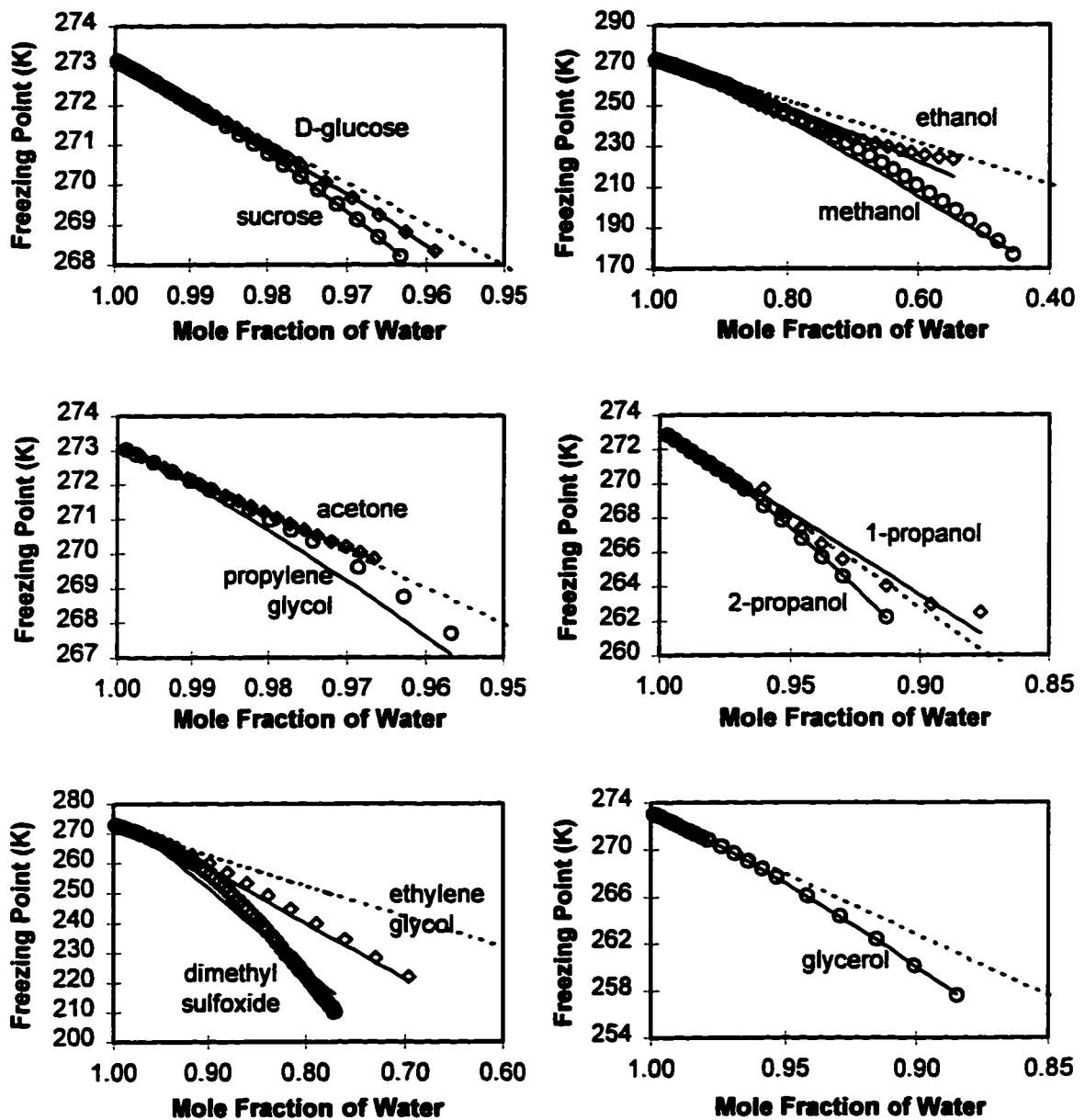


**Figure 3-2.** Phase diagrams from the literature were fitted to equation 3-20. The ethylene glycol, methanol, propylene glycol, and dimethyl sulfoxide curves were fitted for the single parameter  $b_2$ , while all the other curves were fitted for both parameters  $\delta$  and  $b_2$ . The broken line in each graph represents the Raoult's Law prediction of the phase behaviour.

## **Chapter 4**

### **Membrane Permeability**

#### **Introduction**

Most biological cells, and some other biological tissues, are bounded by a semi-permeable membrane which typically allows the passive transport of water, but restricts the passage of salts and other ions. An ideal semi-permeable membrane is one which permits resistance-free movement of one solute, such as water, while completely blocking the movement of all other solutes. The membranes which bind cells, however, are considerably more complex as they will allow transport of many different solutes, each with varying amounts of resistance. In addition, some of this transport is actively done by membrane pumps that vary their rate depending on the state of the cell. Despite these complexities, the membrane of a biological cell can be considered to be passive and semi-permeable. This assumption is generally valid in cryobiology, and it is therefore used in this chapter. It is also assumed that: the membrane is permeable to water with a specified resistance to water flow, the membrane is not permeable to electrolytes and large molecular weight solutes, such as sodium chloride and sugars, respectively, and finally, the membrane is permeable to certain low molecular weight compounds, such as cryoprotectants, with a specified resistance to such flow.

Several researchers have worked, and are working, on this problem of osmotic flow through semi-permeable membranes. Some early papers dealing with this subject are [Jacobs 1952; Staverman 1952; Kedem & Katchalsky 1958; Johnson & Wilson 1967]. The last two papers in this list both present the equations that will be given here to describe osmotic flow. More recent work on membrane permeability can be found in [Kiil 1989; Batycky *et al.* 1996]. Only the specific implementation of the transport equations is given in this chapter; however, a complete derivation of these equations using irreversible

thermodynamics can be found in [Kedem & Katchalsky 1958]. To start off, a calculation of osmotic pressure from the freezing point of a solution is given. Then, the case where only impermeant solutes are present with water is studied. Finally, the complete problem, with both permeant and impermeant solutes in water, is presented along with the equations necessary to implement the dynamic time step numerical method.

### **Osmotic Pressure**

Osmotic pressure is a colligative property of a solution and arises as a result of the fact that water exerts no pressure on an ideal semi-permeable membrane; however, the impermeant solute molecules do. If solute concentration in the exterior region of a cell is greater than that inside the cell, the extra solute outside the cell exerts a net pressure on the cell membrane and literally squeezes the water out of the cell; thus, the cell shrinks. Osmotic pressure is called a colligative property because it arises as a result of the collection of unlike molecules. Freezing point depression, as discussed in chapter 3, is also considered a colligative property, and, in that chapter, it was shown that finding a numerical value for the freezing point of an arbitrary solution based on the known composition of that solution is not a trivial problem. In this chapter, a method of deriving osmotic pressure from the freezing point is given; and thus, if one finds a method of calculating the freezing point of a solution, given the solution's composition, one can find osmotic pressures as well.

The chemical potential of water in solution with other solutes is given by

$$\mu_w(l) = \mu'_w(l) + RT \ln a_w, \quad (4-1)$$

where the  $l$  denotes liquid,  $R$  is the gas constant,  $T$  is the temperature, the prime denotes the value for pure water, and  $a_w$  is the water activity. For an ideal dilute solution, Raoult's law is assumed and the water activity is equal to the mole fraction of water. In this case, the chemical potential would be

$$\mu_w(l) = \mu'_w(l) + RT \ln x_w; \quad (4-2)$$

however, since assuming Raoult's law would limit the scope of these derivations, it will not be assumed here.

Following the methods of Atkins [1990], freezing point depression is derived from the equilibrium condition

$$\mu'_w(s) = \mu'_w(l) + RT \ln a_w, \quad (4-3)$$

where the  $s$  denotes solid. Without going into all the detail, the freezing point of a solution can be expressed as a function of water activity by

$$\frac{F_w - F_s}{F_w F_s} = \frac{R}{\Delta H_f} \ln a_w, \quad (4-4)$$

where  $F_w$  is the freezing point of pure water,  $F_s$  is the freezing point of the solution, and  $\Delta H_f$  is the specific latent heat of fusion for pure water. During this derivation, it was assumed that  $\Delta H_f$  and  $\Delta S_f$  (entropy of fusion) are constants. Also, in equation 4-4,  $\Delta H_f$  must be expressed as a negative number.

An expression for osmotic pressure in terms of water activity can be derived in a similar fashion. Again, following the lead of Atkins [1990], an equilibrium condition involving chemical potentials is written as

$$\mu'_w(p) = \mu'_w(p + \pi) + RT \ln a_w, \quad (4-5)$$

where the  $p$  denotes liquid with hydrostatic pressure  $p$ , and  $\pi$  is the additional pressure (the osmotic pressure) required on the solution side of a semi-permeable membrane to maintain equilibrium. With the details of this derivation also omitted (but found in Atkins [1990]), osmotic pressure can be expressed as

$$\pi = \frac{-RT \ln a_w}{MV_w}, \quad (4-6)$$

where  $MV_w$  is the molecular volume of pure water and is assumed to be constant. The negative sign is necessary to ensure that osmotic pressure is positive since  $a_w \leq 1$ .

Now, by combining equations 4-4 and 4-6, and eliminating water activity, osmotic pressure can be expressed in terms of freezing point by

$$\pi = \frac{-T\Delta H_f}{MV_w} \left( \frac{F_w - F_s}{F_w F_s} \right). \quad (4-7)$$

Since equation 4-7 does not rely on the ideal dilute solution assumption (Raoult's law), it can be used to find the osmotic pressure of any solution provided that the complete phase behaviour of that solution is known.

### Impermeant Solutes in Water

When the only permeant solute is water, the permeability transport equations take a particularly simple form as only one equation is involved. Assuming there is no hydrostatic pressure difference across the membrane, water flux can be written as a linear function of the osmotic pressure difference. The equation for water flux is thus,

$$\frac{d_i V}{dt} = -L_p A \Delta \pi, \quad (4-8)$$

where  $V$  is the volume of the cell,  $L_p$  is the hydraulic conductivity,  $A$  is the surface area of the membrane, and  $\Delta \pi = \pi_e - \pi_i$  is the step change in osmotic pressure across the membrane ( $e$  is for exterior,  $i$  is for interior).

Figure 4-1a illustrates the response of a cell when subjected to an increased osmotic pressure, as dictated by equation 4-8. In this case, the cell was chosen to be a V-79 hamster fibroblast and the parameters describing this cell are given in appendix 1. The initial osmotic pressure within the cell is 5.99 atm (corresponding to a sodium chloride concentration of 0.147 mol/l, which is normal for most animal cells), and the cell is subjected to a 40.02 atm (corresponding to a sodium chloride concentration of 0.976 mol/l) environment at room temperature (22°C). This hypertonic environment causes the cell to shrink until the cellular contents are concentrated enough to make the internal osmotic pressure equal the applied osmotic pressure.

When equilibrium is restored the final volume is given by the Boyle-van't Hoff relation [Lucke & McCutcheon 1932]

$${}_i v = {}_i v_d + \frac{{}_i \pi_o}{e \pi} (1 - {}_i v_d), \quad (4-9)$$

where  ${}_i \pi_o$  is the initial osmotic pressure inside the cell,  $e \pi$  is the exterior osmotic pressure,  ${}_i v$  is the normalized cell volume ( $= V / V_o$ ), and  ${}_i v_d$  is the osmotically inactive fraction of the cell volume. The interior of a typical biological cell is not simply composed of an aqueous solution. Some portion of this interior region is composed of substances that do not participate in the aqueous solution, and therefore, do not affect the osmotic interactions of the cell with its environment. This portion of the cell is termed the osmotically inactive fraction. The Boyle-van't Hoff plot corresponding to the particular system illustrated by figure 4-1a is given in figure 4-1b.

#### **Addition of a Permeant Solute**

When a permeant solute is added to the exterior solution around a cell, this solute will contribute to the osmotic pressure difference; however, since it is also permeable, a concentration gradient will drive the solute into the cell. In this situation, equation 4-8 becomes a pair of coupled ordinary differential equations, given by

$$\left. \begin{aligned} \frac{d{}_i V}{dt} &= -L_p A [\Delta \pi_N + \sigma \Delta \pi_p] \\ \frac{d{}_i S}{dt} &= P_s A \Delta C_s + (1 - \sigma) \bar{C}_s \frac{d{}_i V}{dt} \end{aligned} \right\}, \quad (4-10)$$

where  $\Delta \pi_N$  is the osmotic pressure difference due to the presence of non-permeating solutes,  $\Delta \pi_p$  is the osmotic pressure difference due to the presence of the permeating solute,  $\Delta C_s$  is the difference in permeant solute concentration across the membrane,  $\bar{C}_s$  is the average concentration of permeant solute in the membrane,  ${}_i S$  is the amount of permeant solute in the cell,  $P_s$  is the permeability coefficient for the permeant solute, and  $\sigma$  is a reflection coefficient [Johnson & Wilson 1967]. This reflection coefficient was first introduced by Staverman in 1952 and represents the proportion of permeant solute molecules that will be



reflected from the membrane as opposed to passing through when they approach the membrane. Since some of the permeant solute molecules pass through the membrane, only a portion of the osmotic pressure difference due to the permeant solute contributes to the volume flux. Also, because these molecules pass through the membrane, a portion of the volume flux is due to permeant solute movement, and not water movement. This portion is seen as the second term of the second equation of system 4-10. The water flux is the difference between the volume flux and the permeant solute flux.

To simplify the implementation of system 4-10, the first equation is rewritten as

$$\frac{d_i V}{dt} = -L_p A [(\Delta\pi_N + \Delta\pi_p) - (1 - \sigma)\Delta\pi_p], \quad (4-11)$$

and given that the total osmotic pressure is  $\pi = \pi_N + \pi_p$ , system 4-10 can be rewritten as

$$\left. \begin{aligned} \frac{d_i V}{dt} &= -L_p A [\Delta\pi - (1 - \sigma)\Delta\pi_p] \\ \frac{d_i S}{dt} &= P_s A \Delta C_s + (1 - \sigma) \bar{C}_s \frac{d_i V}{dt} \end{aligned} \right\} \quad (4-12)$$

With this system, the total osmotic pressure difference can be calculated from the freezing point of the solution, as demonstrated in the impermeant only case above. The osmotic pressure difference due to the permeant solute can be calculated from the freezing point depression due to that solute alone in the solution.

A numerical solution to system 4-12 is presented in figures 4-2. In this system, the exterior region of the cell has dimethyl sulfoxide (DMSO) present at a concentration of 1.4 mol/l (10% by volume). The interior of the cell initially contains no DMSO. It can be seen that water is initially forced out of the cell by the greater osmotic pressure found in the exterior region. This greater osmotic pressure is a direct result of the presence of the permeant solute. However, in

addition to water being forced out of the cell, permeant solute also moves into the cell due to the greater permeant solute concentration in the exterior region.

Water continues to leave the cell while solute enters until the osmotic pressure both in and out are equal, which occurs at  $t = 4.6\text{sec}$  in the case of figure 4-2. Beyond this point, since the intracellular concentration of permeant solute will still not equal the extracellular concentration, solute continues to enter the cell. This will result in a greater osmotic pressure (due to a greater permeant solute concentration) within the cell. This greater osmotic pressure causes an influx of water back into the cell, thus expanding it. Both water and permeant solute continue to enter the cell until an equilibrium is reached where both osmotic pressure and permeant solute concentration have zero gradient across the semi-permeable membrane. At this time, the cell has returned to its original volume, but now has some of its water replaced by DMSO. Figure 4-2b displays the fluxes present during the process of volume change illustrated in figure 4-2a.

It should also be mentioned here that the parameters  $L_p$  and  $P_s$  are temperature dependent. This temperature dependence is given by the Arrhenius relation [Atkins 1990]

$$X(T) = X_0 \exp\left[\frac{E_a}{R}\left(\frac{1}{T_0} - \frac{1}{T}\right)\right], \quad (4-13)$$

where  $X_0$  is the value of  $X$  at temperature  $T_0$ , and  $E_a$  is the activation energy which governs the temperature dependence.

### **Variable Time Step**

Many variable step size methods operate by approximating the local truncation error at each iteration, and then, if the local truncation error is in excess, the iteration will be redone with a sufficiently smaller step size. This technique requires that iterations can be repeated as many times as necessary; however, due to the complexity of the systems that may be modeled here, this is unacceptable. The computational and memory overhead required to undo iterations outweigh the gain. To overcome this problem it is necessary to be

able to predict the local truncation error before each iteration begins, then choose the step size for the iteration.

The Euler initial value method is a first order Taylor method [Burden & Faires 1993] with each successive approximation given by

$$w_{i+1} = w_i + hf'(w_i, t_i), \quad (4-14)$$

where  $w_i$  is the approximation of  $f(t)$  and  $h$  is the step size. In this case, the local truncation error is also given by the Taylor theorem as

$$\left| \frac{h^2}{2} f''(\xi) \right|, \quad (4-15)$$

where  $\xi \in [t_i, t_{i+1}]$ . Assuming that the step size is bounded above and that the initial data are smooth, it is reasonable to approximate the local truncation error by

$$\left| \frac{h^2}{2} f''(t_i) \right|. \quad (4-16)$$

In the case of the permeability equations 4-10 the local truncation error is calculated from the second derivatives,

$$\frac{d^2 V}{dt^2} = -L_p A \left[ \frac{d\Delta\pi}{dt} - (1-\sigma) \frac{d\Delta\pi_p}{dt} \right], \quad (4-17a)$$

$$\frac{d^2 S}{dt^2} = P_s A \frac{d\Delta C_s}{dt} + (1-\sigma) \frac{d\bar{C}_s}{dt} \left( \frac{dV}{dt} \right) + (1-\sigma) \bar{C}_s \left( \frac{d^2 V}{dt^2} \right). \quad (4-17b)$$

If equation 4-7 is used to calculate osmotic pressure from the freezing point of the solution, then

$$\frac{d\pi}{dt} = \frac{T\Delta H_f}{MV_w F_s^2} \cdot \frac{dF_s}{dC} \cdot \frac{dC}{dt}. \quad (4-18)$$

Since the local truncation error accumulates with each iteration, the total error accumulation per unit of time is

$$n \left| \frac{h^2}{2} f''(t_i) \right|, \quad (4-19)$$

where  $n = 1/h$ . If  $L$  is the maximum desired rate of error accumulation, then

$$\left| \frac{h}{2} f''(t_i) \right| \leq L, \quad (4-20)$$

which gives the following limitation on the step size

$$h \leq \frac{L}{\left| \frac{1}{2} f''(t_i) \right|}. \quad (4-21)$$

In the case of the permeation equations,  $\Delta t$  ( $= h$ ) is constrained by

$$\Delta t \leq \frac{L \min[V_e, V]}{\text{abs}\left(\frac{1}{2} \frac{d^2 V}{dt^2}\right)}, \quad (4-22a)$$

$$\Delta t \leq \frac{L \min[S_e, S]}{\text{abs}\left(\frac{1}{2} \frac{d^2 S}{dt^2}\right)}, \quad (4-22b)$$

where  $L$  is the desired error limit in units of fraction error per second. The  $\min[ ]$  function in the numerator ensures that all errors are expressed as a non-dimensional fraction of the actual value.

Figures 4-3 illustrate the effect of this variable time step method. In each figure the solid line is the volume curve presented in figures 4-1 and 4-2, respectively, while the dashed lines represent the time step for each iteration. The simulation was run for two different error tolerances:  $10^{-5}/\text{sec}$  and  $10^{-6}/\text{sec}$ . In both cases the time step was limited to a maximum of 0.1sec.

The work presented in this chapter represents an application of basic numerical analysis techniques. Modeling the impermeant only situation and the permeant, impermeant situation has been done time and time again by many researchers in the field. However, applying a variable time step to this process is a seldom-used technique to improve the performance of the analysis. In this case, the variable time step is essential to ensure that this complicated model

can be used to simulate whole tissues in a reasonable length of time while maintaining a high level of accuracy.

Even though the equations presented in this chapter apply only to solutions containing water, a permeant solute, and any number of impermeant solutes, they could be generalized to multiple permeant solutes, increasing the number of required parameters. A better approach would be to improve the theory behind the equations and develop a new set of transport equations. When such work becomes available, the new equations can be implemented in this model with a minimum of effort.

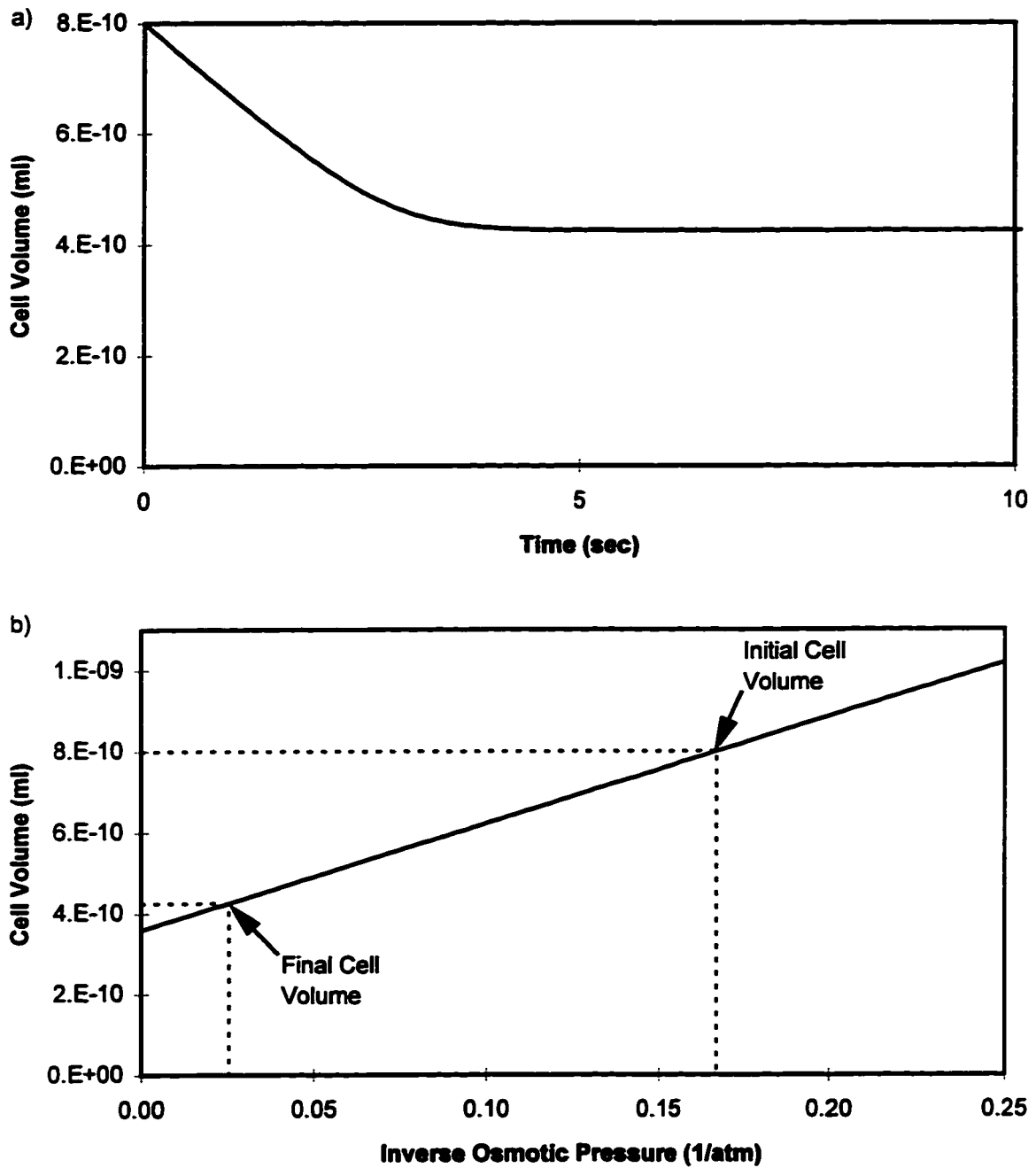


**Figure 4-1.** a) Typical volume response curve for a cell suspended in a concentrated exterior solution. b) The Boyle-van't Hoff plot indicating the equilibrium cell volume as a function of exterior osmotic pressure.

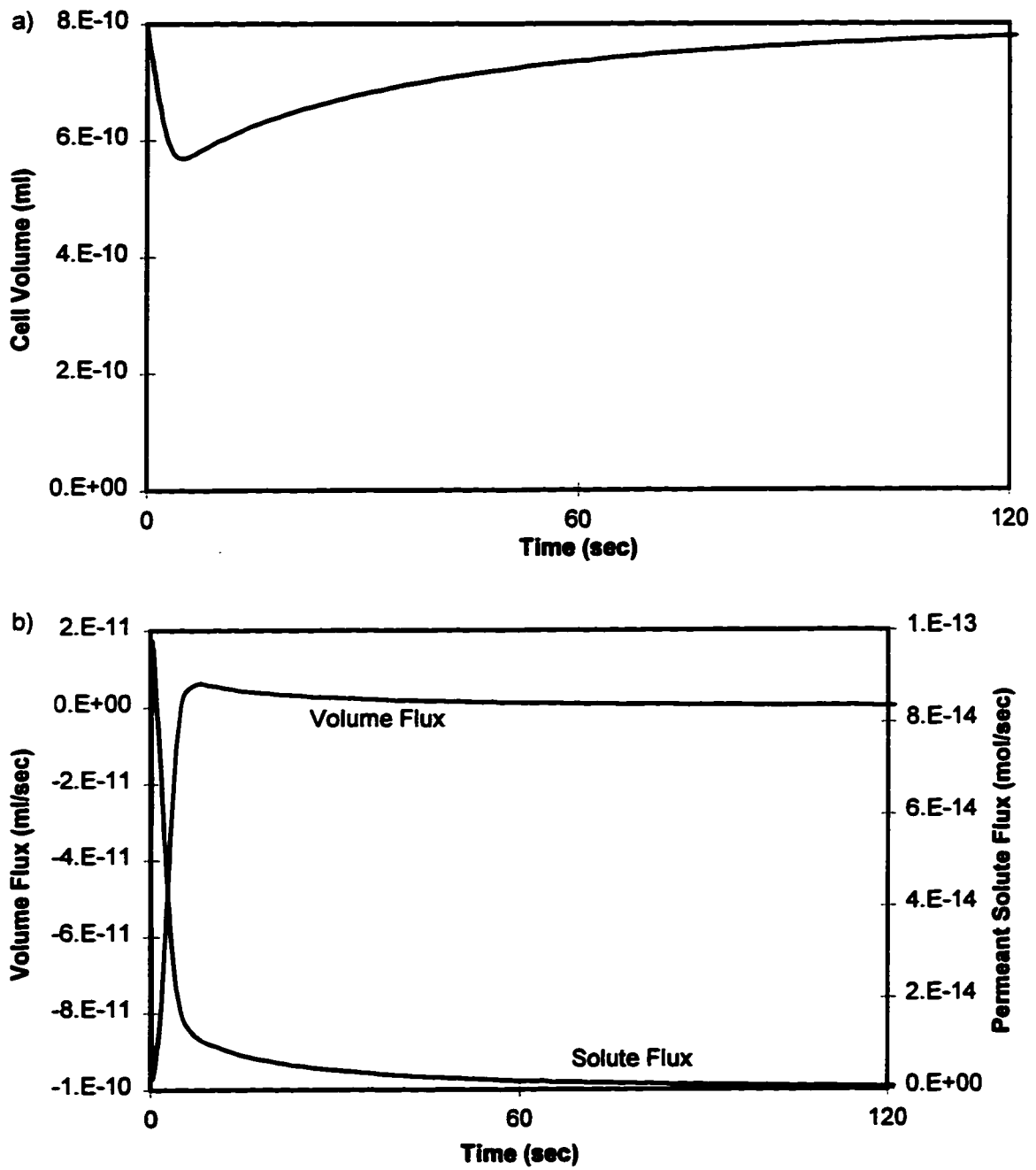


**Figure 4-2.** Simulation of cellular response in the presence of a permeating solute. Volume as a function of time is given in a), while the various fluxes that cause this volume profile are given in b).

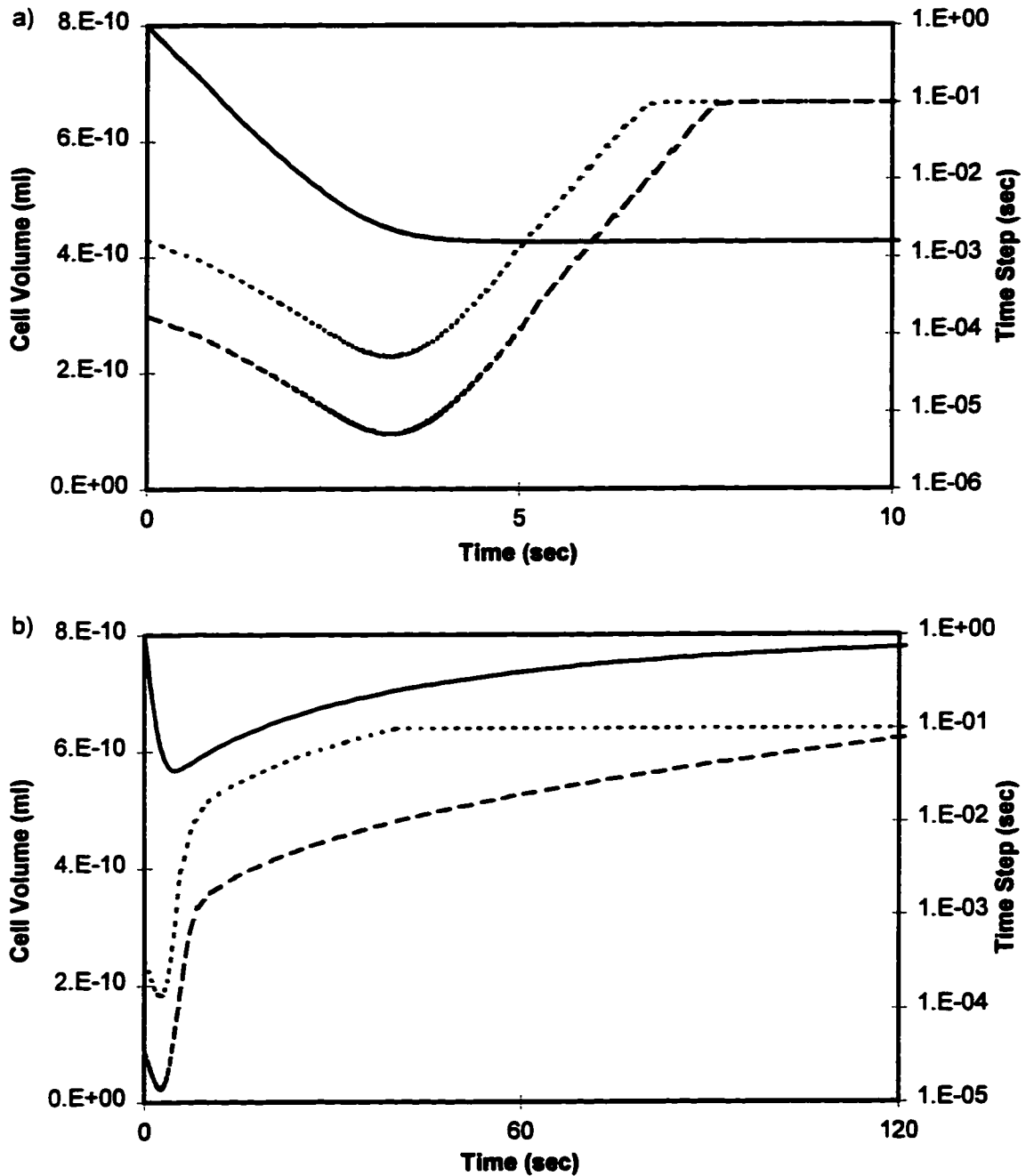


**Figure 4-3.** Demonstration of the variable time step method for a) the impermeant only case, and for b) the permeant case. The short broken line is for the case where the error tolerance was  $10^{-5}/\text{sec}$ , while the long broken line is for the  $10^{-6}/\text{sec}$  case. In each graph, there was no noticeable change in the solid line for the two error tolerances used.



## Chapter 5

### Diffusion Problem

#### Introduction

Unlike the permeation problem discussed in chapter 4, diffusion is a more complicated problem since diffusion occurs not only in time, but in space as well. The JWCompartment discussed in chapter 4 is assumed to be well mixed within, and thus, the differential equations only describe the movement of solutes through the membrane. With diffusion, however, a solute concentration profile must be maintained at the compartment boundary and throughout the compartment. This means that concentration within the compartment is both time dependent and space dependent.

In addition to these concentration profiles, any phase change that occurs within the compartment must be localized and propagate within the compartment at a predicted rate. The propagation rate of the phase change will depend on the local solute concentration profiles, as the solute undergoing the phase change must diffuse towards the phase boundary while all other solutes must diffuse away, and on the temperature profile, as heat is either required or released from the phase boundary as it moves. This coupling between temperature and the various solute concentrations present within the compartment complicates the numerical solution as the entire system must be solved simultaneously.

The basic diffusion equation is

$$\frac{\partial C}{\partial t} = D \frac{\partial^2 C}{\partial x^2}, \quad (5-1)$$

where  $D$  is the coefficient of diffusion and  $C$  is the concentration as a function of space and time. This diffusion equation is a differential form of Fick's law,

$$J = -D \frac{\partial C}{\partial x}, \quad (5-2)$$

which describes the diffusive flux density,  $J$ , across a boundary as a function of the concentration gradient [Crank 1975]. Either form of the diffusion equation can be used to solve diffusion problems.

In order to handle these equations numerically, one of two approaches must be taken. One approach is to solve the diffusion equation exactly in the space dimension and then iterate through discrete time steps. Although solving 5-1 exactly for a general case is a difficult problem, once a solution is found the numerical analysis becomes trivial. The other approach is to partition both the space and time dimensions, and then use either equation 5-1 or equation 5-2 to describe local changes in concentration at each time step. This latter approach is employed here.

The method developed here relies on a piece-wise quadratic fit of the concentration profile. Within each local region of space, the concentration profile is fitted to a quadratic polynomial, and then this quadratic polynomial is used with equation 5-1 to determine the time dependence of the concentration profile. To illustrate this method, the problem of mass diffusion alone is considered first. Heat diffusion is completely analogous to mass diffusion; and therefore, follows from the solution for mass diffusion; however, in the case of heat diffusion, a moving phase change is introduced and a solution for this case developed. Finally, mass and heat diffusion are combined with the phase change, and a general solution to the problem is derived.

### **Mass Diffusion**

Consider a one-dimensional system, bounded in space by  $[0, L]$ , and containing some aqueous solution with a known initial concentration profile. In general this concentration profile is  $C^\infty$  in space. Fick's law (equation 5-2) dictates that the gradient of this concentration profile must exist at all locations in space to ensure that solute fluxes remain finite. Furthermore, if the diffusion coefficient is continuous, the concentration gradients must be continuous to ensure conservation of mass. If the concentration gradient was discontinuous at

a particular point, it can be seen from equation 5-2 that the flux of solute into that region from the left would not equal the flux out to the right; thus implying that a source or sink of solute was located at that point.

This argument suggests that the concentration profile within the region  $[0, L]$  must be at least a  $C^1$  function in the space variable, at all times. To achieve this, suppose that the interval  $[0, L]$  is divided into  $n$  subintervals of varying widths, and that within each subinterval the concentration profile is fitted to a 2<sup>nd</sup> order polynomial. This situation is illustrated in figure 5-1. To ensure that the entire concentration profile is a  $C^1$  function in space, two constraints must be imposed at each of the boundaries between subintervals. One constraint ensures continuity of the profile, while the other ensures continuity of the gradient. Since each constraint dictates the value of one parameter, two of the three available parameters will be constrained in each subinterval. The third parameter will be used to describe the actual concentration profile.

To better understand how the various parameters are determined, the entire system will be described. The piece-wise quadratic function outlined in figure 5-1 requires values for  $3n$  parameters, namely the  $\alpha_i$ 's,  $\beta_i$ 's, and  $\gamma_i$ 's. To accomplish this, a total of  $3n$  constraints must be found such that the resulting  $3n \times 3n$  system can be solved. The first  $n$  of these constraints are derived from conservation of mass. Assuming that each subinterval contains a total amount of solute,  $\bar{C}_i$ , known at a particular moment in time, the following expression can be given:

$$\bar{C}_i = \int_{-x/2}^{x/2} [\alpha_i x^2 + \beta_i x + \gamma_i] dx = \frac{g_i^3}{12} \alpha_i + g_i \gamma_i, \quad i = 0 \dots n-1, \quad (5-3)$$

which then gives a constraint for  $\gamma_i$ ,

$$\gamma_i = \frac{\bar{C}_i}{g_i} - \frac{g_i^2}{12} \alpha_i, \quad i = 0 \dots n-1. \quad (5-4)$$

Further constraints arise from the continuity of the concentration profile and the continuity of the concentration gradient at each of the  $n-1$  boundaries between subintervals. Note that, contrary to what was implied above, since there are only  $n-1$  boundaries between subintervals, only  $2n-2$  constraints are required to impose the  $C^1$  condition; not  $2n$ . This means that there will be 2 constraints remaining to impose boundary conditions on the interval  $[0, L]$ . The continuity constraints are

$$\frac{g_i^2}{4}\alpha_i + \frac{g_i}{2}\beta_i + \gamma_i = \frac{g_{i+1}^2}{4}\alpha_{i+1} - \frac{g_{i+1}}{2}\beta_{i+1} + \gamma_{i+1}, \quad i=0\dots n-2, \quad (5-5)$$

for continuity of the concentration profile, and

$$g_i\alpha_i + \beta_i = -g_{i+1}\alpha_{i+1} + \beta_{i+1}, \quad i=0\dots n-2, \quad (5-6)$$

for continuity of the concentration gradient. Equation 5-5 can be simplified to eliminate the  $\gamma_i$ 's by substituting the conservation equation 5-4 to get

$$\frac{g_i^2}{6}\alpha_i + \frac{g_i}{2}\beta_i + \frac{\bar{C}_i}{g_i} = \frac{g_{i+1}^2}{6}\alpha_{i+1} - \frac{g_{i+1}}{2}\beta_{i+1} + \frac{\bar{C}_{i+1}}{g_{i+1}}, \quad i=0\dots n-2. \quad (5-7)$$

Given the constraints that have now been presented, only 2 more constraints are required to make the necessary  $3n \times 3n$  system. These last 2 constraints will be chosen at the boundaries  $x=0$  and  $x=L$ . Since the conditions at these boundaries may apply to either the concentration itself, or the concentration gradient, four possible choices for these constraints exist. The possibilities are

$$\frac{g_0^2}{6}\alpha_0 - \frac{g_0}{2}\beta_0 + \frac{\bar{C}_0}{g_0} = C_0, \quad (5-8a)$$

$$-g_0\alpha_0 + \beta_0 = G_0, \quad (5-8b)$$

$$\frac{g_{n-1}^2}{6}\alpha_{n-1} + \frac{g_{n-1}}{2}\beta_{n-1} + \frac{\bar{C}_{n-1}}{g_{n-1}} = C_n, \quad (5-8c)$$

$$g_{n-1}\alpha_{n-1} + \beta_{n-1} = G_n. \quad (5-8d)$$

Two of these constraints must be chosen to complete the system. Typically, this choice will include one from 5-8a and 5-8b, as well as one from 5-8c and 5-8d. This ensures that both boundaries of the interval  $[0, L]$  have conditions limiting solute transport. In the case of a semi-infinite system, both conditions 5-8a and 5-8b may be used at the left boundary; however, in this case, these conditions would then dictate the solution to the entire system. For the purposes of this work, 5-8a and 5-8d are the constraints that are chosen; however, calculations for all four constraints will still be given where applicable.

Now, equations 5-4, 5-5, 5-6 and the appropriate choices of 5-8 represent  $3n$  constraints on the  $3n$  unknowns,  $\alpha_i$ ,  $\beta_i$ , and  $\gamma_i$ . Alternatively, equations 5-6, 5-7 and 5-8 can be considered as  $2n$  constraints on the  $2n$  unknowns,  $\alpha_i$  and  $\beta_i$ , and then later used to get the  $\gamma_i$ 's from equations 5-4. In matrix notation, the  $2n \times 2n$  system is given by

$$\begin{pmatrix} \frac{g_0^2}{6} & -\frac{g_0}{2} & 0 & 0 & \dots & 0 & 0 \\ \frac{g_0^2}{6} & \frac{g_0}{2} & -\frac{g_1^2}{6} & \frac{g_1}{2} & \dots & 0 & 0 \\ g_0 & 1 & g_1 & -1 & \dots & 0 & 0 \\ \vdots & \vdots & \vdots & \vdots & \ddots & \vdots & \vdots \\ 0 & 0 & 0 & 0 & \dots & g_{n-1} & 1 \end{pmatrix} \cdot \begin{pmatrix} \alpha_0 \\ \beta_0 \\ \alpha_1 \\ \beta_1 \\ \vdots \\ \alpha_{n-1} \\ \beta_{n-1} \end{pmatrix} = \begin{pmatrix} C_0 - \frac{\bar{C}_0}{g_0} \\ -\frac{\bar{C}_0}{g_0} + \frac{\bar{C}_1}{g_1} \\ 0 \\ \vdots \\ G_n \end{pmatrix}. \quad (5-9)$$

This large system can be solved as a series of small systems, each formed by combining particular subsets of the equations in system 5-9 with results from the other small systems. To see how this is accomplished, consider the last three equations in system 5-9,

$$\left. \begin{aligned} g_{n-2}\alpha_{n-2} + \beta_{n-2} + g_{n-1}\alpha_{n-1} - \beta_{n-1} &= 0 \\ \frac{g_{n-2}^2}{6}\alpha_{n-2} + \frac{g_{n-2}}{2}\beta_{n-2} - \frac{g_{n-1}^2}{6}\alpha_{n-1} + \frac{g_{n-1}}{2}\beta_{n-1} &= -\frac{\bar{C}_{n-2}}{g_{n-2}} + \frac{\bar{C}_{n-1}}{g_{n-1}} \\ g_{n-1}\alpha_{n-1} + \beta_{n-1} &= G_n \end{aligned} \right\}. \quad (5-10)$$

Since there are only three equations for four parameters, only three parameters may be solved for, while the fourth remains independent. Suppose the parameters  $\alpha_{n-1}$ ,  $\beta_{n-1}$ , and  $\beta_{n-2}$  are all solved for as functions of  $\alpha_{n-2}$ , then the one equation involving  $\alpha_{n-2}$  and  $\beta_{n-2}$  can be combined with the fourth and fifth last equations of system 5-9. These three equations would represent a system for the parameters  $\alpha_{n-2}$ ,  $\beta_{n-2}$ ,  $\alpha_{n-3}$ , and  $\beta_{n-3}$ , of which, only three could be solved for while the fourth is again independent. The equation that is derived in one system and used with the next in the series has a general linear form:

$$P_i \alpha_i + \beta_i = Q_i, \quad (5-11)$$

where  $P_i$  and  $Q_i$  are functions of  $P_{i+1}$  and  $Q_{i+1}$ , and not functions of any of the  $\alpha_i$ 's or  $\beta_i$ 's. By examining the last equation in systems 5-9 and 5-10, it can be seen that this constraint is of the form 5-11. In this case

$$P_{n-1} = g_{n-1}, \quad (5-12a)$$

$$Q_{n-1} = G_n. \quad (5-12b)$$

To make use of this method of solving the large system 5-9, it is necessary to obtain a solution for the smaller, three equation systems

$$\left. \begin{aligned} -g_{i+1}\alpha_{i+1} + \beta_{i+1} - \beta_i &= g_i \alpha_i \\ \frac{g_{i+1}^2}{6} \alpha_{i+1} - \frac{g_{i+1}}{2} \beta_{i+1} - \frac{g_i}{2} \beta_i &= \frac{g_i^2}{6} \alpha_i + \frac{\bar{C}_i}{g_i} - \frac{\bar{C}_{i+1}}{g_{i+1}} \\ P_{i+1} \alpha_{i+1} + \beta_{i+1} &= Q_{i+1} \end{aligned} \right\}, \quad i = 0 \dots n-2. \quad (5-13)$$

With the help of some symbolic math software, the solution to 5-13 is

$$\alpha_{i+1} = \frac{-2g_i^2 \alpha_i + 3(g_i + g_{i+1})Q_{i+1} + 6\left(\frac{\bar{C}_i}{g_i} - \frac{\bar{C}_{i+1}}{g_{i+1}}\right)}{3(g_{i+1} + P_{i+1})(g_i + g_{i+1}) - 2g_{i+1}^2}, \quad (5-14a)$$

$$\beta_{i+1} = \frac{2g_i^2 P_{i+1} \alpha_i + g_{i+1} (3g_i + g_{i+1}) Q_{i+1} - 6P_{i+1} \left( \frac{\bar{C}_i}{g_i} - \frac{\bar{C}_{i+1}}{g_{i+1}} \right)}{3(g_{i+1} + P_{i+1})(g_i + g_{i+1}) - 2g_{i+1}^2}, \quad (5-14b)$$

$$\beta_i = \frac{-g_i(g_{i+1} + P_{i+1})(g_i + g_{i+1}) - 2g_i g_{i+1} P_{i+1}}{3(g_{i+1} + P_{i+1})(g_i + g_{i+1}) - 2g_{i+1}^2} \alpha_i$$

$$+ \frac{-6(g_{i+1} + P_{i+1}) \left( \frac{\bar{C}_i}{g_i} - \frac{\bar{C}_{i+1}}{g_{i+1}} \right) - 2g_{i+1}^2 Q_{i+1}}{3(g_{i+1} + P_{i+1})(g_i + g_{i+1}) - 2g_{i+1}^2}. \quad (5-15)$$

Equation 5-15 can be written in the form 5-11 by letting

$$P_i = \frac{g_i(g_{i+1} + P_{i+1})(g_i + g_{i+1}) + 2g_i g_{i+1} P_{i+1}}{3(g_{i+1} + P_{i+1})(g_i + g_{i+1}) - 2g_{i+1}^2}, \quad (5-16a)$$

$$Q_i = \frac{-6(g_{i+1} + P_{i+1}) \left( \frac{\bar{C}_i}{g_i} - \frac{\bar{C}_{i+1}}{g_{i+1}} \right) - 2g_{i+1}^2 Q_{i+1}}{3(g_{i+1} + P_{i+1})(g_i + g_{i+1}) - 2g_{i+1}^2}. \quad (5-16b)$$

These results are almost sufficient to solve system 5-9. Equations 5-16 represent a recursive sequence for determining all the  $P_i$ 's and  $Q_i$ 's with initial values given by equations 5-12. Equations 5-14 give a recursive sequence for determining all the  $\alpha_i$ 's and  $\beta_i$ 's; however,  $\alpha_0$  and  $\beta_0$  are not yet known. To find these two initial values needed by equations 5-14, combine the first equation in system 5-9 with the instance of equation 5-11 when  $i = 0$  to get the system,

$$\left. \begin{aligned} \frac{g_0^2}{6} \alpha_0 - \frac{g_0}{2} \beta_0 &= C_0 - \frac{\bar{C}_0}{g_0} \\ P_0 \alpha_0 + \beta_0 &= Q_0 \end{aligned} \right\}, \quad (5-17)$$

and then solve to get

$$\alpha_0 = \frac{3g_0 Q_0 + 6 \left( C_0 - \frac{\bar{C}_0}{g_0} \right)}{g_0 (g_0 + 3P_0)}, \quad (5-18a)$$

$$\beta_0 = \frac{g_0^2 Q_0 - 6P_0 \left( C_0 - \frac{\bar{C}_0}{g_0} \right)}{g_0(g_0 + 3P_0)}. \quad (5-18b)$$

With these initial values to equations 5-14, all the  $\alpha_i$ 's and  $\beta_i$ 's may be determined; thus solving system 5-9.

It should be noted that if boundary condition 5-8b were used instead of 5-8a, the initial values  $\alpha_0$  and  $\beta_0$  would be

$$\alpha_0 = \frac{Q_0 - G_0}{g_0 + P_0}, \quad (5-19a)$$

$$\beta_0 = \frac{g_0 Q_0 + G_0 P_0}{g_0 + P_0}. \quad (5-19b)$$

Furthermore, if boundary condition 5-8c were used instead of 5-8d, the initial values  $P_{n-1}$  and  $Q_{n-1}$  would be

$$P_{n-1} = \frac{g_{n-1}}{3}, \quad (5-20a)$$

$$Q_{n-1} = \frac{2}{g_{n-1}} \left( C_n - \frac{\bar{C}_{n-1}}{g_{n-1}} \right). \quad (5-20b)$$

Two approaches can be taken to use the solution to system 5-9 in solving the diffusion problem. One approach makes use of the diffusion equation 5-1, while the other uses Fick's law (equation 5-2). To use the diffusion equation, first consider that within each subinterval,

$$\frac{\partial^2 C}{\partial x^2} = 2\alpha_i, \quad (5-21)$$

and thus the diffusion equation becomes

$$\frac{\partial \mathcal{C}}{\partial t} = 2D\alpha_i. \quad (5-22)$$



Then, employing an Euler method [Burden & Faires 1993], the iteration equation is

$$\Delta C = \Delta \gamma_i = 2D\alpha_i \Delta t, \quad (5-23)$$

where  $\Delta t$  is the time step used. This method is only appropriate if the diffusion coefficient is spatially constant; otherwise, Fick's law should be used instead. In this case, the flux across each subinterval boundary is given by

$$J_i = -D_i(-g_i\alpha_i + \beta_i) = -D_i(g_{i-1}\alpha_{i-1} + \beta_{i-1}), \quad (5-24)$$

where  $J_i$  is the flux across the left hand boundary of subinterval  $i$ , and  $D_i$  is the local diffusion coefficient. In the case where  $i = n$  the right hand side of equation 5-24 is used instead. Once the fluxes across the subinterval boundaries have been calculated, the iteration equation becomes

$$\Delta \bar{C}_i = (J_i - J_{i+1})\Delta t. \quad (5-25)$$

To see that equation 5-25 is equivalent to equation 5-23 in the case where  $D$  is spatially constant, note that  $\Delta \bar{C}_i = g_i \Delta \gamma_i$ .

At each iteration of the simulation, it is generally the case that the  $\alpha_i$ 's are not equal and therefore continuity will be lost as the  $\gamma_i$ 's are adjusted. To restore continuity, all the  $\alpha_i$ 's,  $\beta_i$ 's, and  $\gamma_i$ 's need to be recalculated at the end of each iteration (that is, solve system 5-9). This process is necessary to ensure that as the model proceeds, a  $C^1$  representation of the concentration profile in  $[0, L]$  is maintained.

To test this numerical method, a problem where the exact solution is known was chosen for comparison. The problem chosen is one in which the interval is initially at zero concentration, the  $x = L$  boundary is a solid barrier to diffusion, and the  $x = 0$  boundary is fixed at a concentration that grows exponentially to an equilibrium value. The boundary condition at  $x = 0$  is given by

$$\phi(t) = C_0 \{1 - \exp(-\eta t)\}, \quad (5-26)$$

and the exact solution [Crank 1975] to this problem is

$$\frac{C}{C_0} = 1 - \exp(-\eta t) \frac{\cos x(\eta/D)^{\frac{1}{2}}}{\cos L(\eta/D)^{\frac{1}{2}}} - \frac{16\eta L^2}{\pi} \sum_{j=0}^{\infty} \frac{(-1)^j \exp(-D(2j+1)^2 \pi^2 t/4L^2)}{(2j+1)\{4\eta L^2 - D\pi^2(2j+1)^2\}} \cos \frac{(2j+1)\pi x}{2L} \quad (5-27)$$

Figure 5-2 displays the exact and numerical solutions to this problem for two different values of  $n$ , a) 5 and b) 10. The solid lines are the numerical results while the broken lines represent the exact solution. The value of the diffusion coefficient for these calculations was chosen to be  $1.0 \times 10^{-5} \text{ cm}^2/\text{sec}$ . It can be seen in figure 5-2 that small values of  $n$  result in significant error and other numerical artifacts (such a negative relative concentrations). Also, these problems can be avoided by using a larger number of subintervals, such as  $n = 10$ .

### Heat Diffusion with a Phase Change

Diffusion of heat occurs in exactly the same manner as solute diffusion; therefore, the equations derived above all apply in the case of heat. However, the heat problem is complicated somewhat by the introduction a moving phase change into the system. This phase change marks a step change in heat capacity, thermal conductivity, and density, and is usually accompanied by the release or absorption of latent heat. Therefore, although this problem is similar to the above mass problem in many respects, the constraints that must hold at the phase boundary are different. Figure 5-3 illustrates the heat problem.

Equations 5-14 and 5-16 still apply for the cases where  $i = 0 \dots m-2$  and  $i = -l \dots -2$ , but are restated here with new variables,

$$\alpha'_{i+1} = \frac{-2h_i^2 \alpha'_i + 3(h_i + h_{i+1})Q'_{i+1} + 6\left(\frac{\bar{\theta}_i}{h_i} - \frac{\bar{\theta}_{i+1}}{h_{i+1}}\right)}{3(h_{i+1} + P'_{i+1})(h_i + h_{i+1}) - 2h_{i+1}^2}, \quad (5-28a)$$

$$\beta'_{i+1} = \frac{2h_i^2 P'_{i+1} \alpha'_i + h_{i+1}(3h_i + h_{i+1})Q'_{i+1} - 6P'_{i+1}\left(\frac{\bar{\theta}_i}{h_i} - \frac{\bar{\theta}_{i+1}}{h_{i+1}}\right)}{3(h_{i+1} + P'_{i+1})(h_i + h_{i+1}) - 2h_{i+1}^2}, \quad (5-28b)$$

$$P'_i = \frac{h_i(h_{i+1} + P'_{i+1})(h_i + h_{i+1}) + 2h_i h_{i+1} P'_{i+1}}{3(h_{i+1} + P'_{i+1})(h_i + h_{i+1}) - 2h_{i+1}^2}, \quad (5-29a)$$

$$Q'_i = \frac{-6(h_{i+1} + P'_{i+1})\left(\frac{\bar{\theta}_i}{h_i} - \frac{\bar{\theta}_{i+1}}{h_{i+1}}\right) - 2h_{i+1}^2 Q'_{i+1}}{3(h_{i+1} + P'_{i+1})(h_i + h_{i+1}) - 2h_{i+1}^2}. \quad (5-29b)$$

The new variables are:  $\theta$  for temperature,  $h$  for the subinterval width, and a prime on all other variables to indicate the heat case. The possible initial values for these recursion relations corresponding to each boundary condition 5-8 are,

$$\alpha'_{-l} = \frac{3h_{-l}^2 Q'_{-l} + 6h_{-l} \theta_{-l} - 6\bar{\theta}_{-l}}{h_{-l}^2 (h_{-l} + 3P'_{-l})} \quad \text{and} \quad \beta'_{-l} = \frac{h_{-l}^3 Q'_{-l} - 6h_{-l} P'_{-l} \theta_{-l} + 6P'_{-l} \bar{\theta}_{-l}}{h_{-l}^2 (h_{-l} + 3P'_{-l})}, \quad (5-30a)$$

$$\alpha'_{-l} = \frac{Q'_{-l} - H_{-l}}{h_{-l} + P'_{-l}} \quad \text{and} \quad \beta'_{-l} = \frac{h_{-l} Q'_{-l} + H_{-l} P'_{-l}}{h_{-l} + P'_{-l}}, \quad (5-30b)$$

$$P'_{m-1} = \frac{h_{m-1}}{3} \quad \text{and} \quad Q'_{m-1} = \frac{2}{h_{m-1}} \left( \theta_m - \frac{\bar{\theta}_{m-1}}{h_{m-1}} \right), \quad (5-30c)$$

$$P'_{m-1} = h_{m-1} \quad \text{and} \quad Q'_{m-1} = H_m. \quad (5-30d)$$

The significant differences between this heat problem and the preceding mass problem all lie at the phase boundary. At this boundary, heat is either released or absorbed depending on the movement of the boundary; and therefore, this source or sink of heat invalidates the continuity of the gradient

condition that was used earlier. In place of this condition, a new constraint is used to describe the step change in the temperature gradient at the phase boundary. This new constraint is

$$K_s \left. \frac{\partial \theta_s}{\partial x} \right|_{x=X} - K_l \left. \frac{\partial \theta_l}{\partial x} \right|_{x=X} = L\rho \frac{dX}{dt}, \quad (5-31)$$

where the subscript  $s$  denotes the solid side of the boundary, while the  $l$  denotes the liquid side. Also,  $K$  is the thermal conductivity,  $L$  is the specific latent heat of fusion and  $\rho$  is the density. In terms of the usual notation, this expression is rewritten as

$$K_s(\alpha'_1 h_{-1} + \beta'_{-1}) - K_l(-\alpha'_0 h_0 + \beta'_0) = L\rho \frac{dX}{dt}. \quad (5-32)$$

The quantity  $dX/dt$  is the speed of the phase boundary and is a new parameter. With this extra parameter, the system will no longer have a unique solution unless a new constraint is introduced. The new constraint results from the fact that the phase boundary always maintains a temperature equal to the freezing point of the substance. That is

$$\theta(X) = F \quad (5-33)$$

or in the appropriate notation

$$\frac{h_{-1}^2}{6} \alpha'_{-1} + \frac{h_{-1}}{2} \beta'_{-1} + \frac{\bar{\theta}_{-1}}{h_{-1}} = \frac{h_0^2}{6} \alpha'_0 - \frac{h_0}{2} \beta'_0 + \frac{\bar{\theta}_0}{h_0} = F. \quad (5-34)$$

Now, with constraints 5-32, 5-34 and the generic linear relation 5-11, a system analogous to 5-13 can be formed,

$$\left. \begin{aligned}
\frac{h_0^2}{6} \alpha'_0 - \frac{h_0}{2} \beta'_0 &= F - \frac{\bar{\theta}_0}{h_0} \\
\frac{h_{-1}}{2} \beta'_{-1} &= -\frac{h_{-1}^2}{6} \alpha'_{-1} + F - \frac{\bar{\theta}_{-1}}{h_{-1}} \\
K_s \beta'_{-1} + K_l h_0 \alpha'_0 - K_l \beta'_0 - L\rho \frac{dX}{dt} &= -K_s h_{-1} \alpha'_{-1} \\
P'_0 \alpha'_0 + \beta'_0 &= Q'_0
\end{aligned} \right\} \quad (5-35)$$

This system is solved to get

$$\alpha'_0 = \frac{3h_0 Q'_0 + 6 \left( F - \frac{\bar{\theta}_0}{h_0} \right)}{h_0 (h_0 + 3P'_0)}, \quad (5-36a)$$

$$\beta'_0 = \frac{h_0^2 Q'_0 - 6P'_0 \left( F - \frac{\bar{\theta}_0}{h_0} \right)}{h_0 (h_0 + 3P'_0)}, \quad (5-36b)$$

$$\begin{aligned}
\frac{dX}{dt} &= \left( \frac{K_s}{L\rho} \right) \frac{2h_{-1}^2 \alpha'_{-1} + 6 \left( F - \frac{\bar{\theta}_{-1}}{h_{-1}} \right)}{3h_{-1}} \\
&+ \left( \frac{K_l}{L\rho} \right) \frac{2h_0^2 Q'_0 + 6(h_0 + P'_0) \left( F - \frac{\bar{\theta}_0}{h_0} \right)}{h_0 (h_0 + 3P'_0)}, \quad (5-37)
\end{aligned}$$

$$\beta'_{-1} = -\frac{h_{-1}}{3} \alpha'_{-1} + \frac{2}{h_{-1}} \left( F - \frac{\bar{\theta}_{-1}}{h_{-1}} \right). \quad (5-38)$$

From equation 5-38, we read off as before,

$$P'_{-1} = \frac{h_{-1}}{3}, \quad (5-39a)$$

$$Q'_{-1} = \frac{2}{h_{-1}} \left( F - \frac{\bar{\theta}_{-1}}{h_{-1}} \right). \quad (5-39b)$$

These equations now provide initial values for equations 5-29 in order to find the  $P_i$ 's and  $Q_i$ 's for  $i = -l \dots -2$ . Equations 5-36 are used to calculate initial values for equations 5-28, which are then used to calculate the  $\alpha_i$ 's and  $\beta_i$ 's for  $i = 1 \dots m-1$ .

To make use of these equations in solving the heat problem, proceed as before by deriving an iteration equation based on either the heat equation or Fick's law. The heat equation is

$$\frac{\partial \theta}{\partial t} = \left( \frac{K}{c\rho} \right) \frac{\partial^2 \theta}{\partial x^2}, \quad (5-40)$$

and results in iteration equations

$$\Delta \gamma'_i = 2 \left( \frac{K_s}{c_s \rho_s} \right) \alpha'_i \Delta t, \quad i = -l \dots -1, \quad (5-41a)$$

$$\Delta \gamma'_i = 2 \left( \frac{K_l}{c_l \rho_l} \right) \alpha'_i \Delta t, \quad i = 0 \dots m-1. \quad (5-41b)$$

In these equations,  $K$  is the thermal conductivity,  $c$  is the specific heat capacity and  $\rho$  is the density. Since the thermal conductivity is discontinuous across the phase boundary, two iteration equations are required, one for each phase.

When using Fick's law to derive the iteration equation, start with

$$J_i = - \left( \frac{K_i}{c_i \rho_i} \right) (-h_i \alpha'_i + \beta'_i) = - \left( \frac{K_i}{c_i \rho_i} \right) (h_{i-1} \alpha'_{i-1} + \beta'_{i-1}), \quad (5-42)$$

where  $K_i$ ,  $c_i$ , and  $\rho_i$  represent the value of each parameter at the left hand boundary of the subinterval. Then define the iteration equation as

$$\Delta \bar{\theta}_i = (J_i - J_{i+1}) \Delta t; \quad (5-43)$$

however, care must be taken when defining the iteration equation for the two subintervals adjacent to the phase boundary. When  $i = -1$ ,  $J_0$  in equation 5-43 must be defined as

$$J_0 = -\left(\frac{K_s}{c_s \rho_s}\right)(h_{-1} \alpha'_{-1} + \beta'_{-1}), \quad (5-44)$$

and when  $i = 0$ ,  $J_0$  in equation 5-43 must instead be defined as

$$J_0 = -\left(\frac{K_l}{c_l \rho_l}\right)(-h_0 \alpha'_0 + \beta'_0). \quad (5-45)$$

This attention is required to ensure that heat is conserved at the phase boundary.

The only difficulty that remains is with the fact that the phase boundary is moving, and thus  $h_0$  and  $h_{-1}$  will vary with time, one eventually reaching zero. There are a variety of ways in which this problem can be approached.

The ideal way is to, at each iteration, calculate the approximate error accumulation within each subinterval. Then choose the subinterval producing the most error and shrink it by some calculated amount, thus increasing the width of the subintervals adjacent to the error prone subinterval. This method still does not preclude the possibility that either  $h_0$  or  $h_{-1}$  may become zero, nor does it allow for the movement of subintervals from the liquid side to the solid side as all the liquid turns to solid. If one of  $h_0$  or  $h_{-1}$  becomes zero it would be necessary to add that subinterval to the opposite phase and then continue the phase change in the next subinterval,  $l$  or  $-2$  respectively.

A simpler approach is to maintain all subintervals, except those two on either side of the phase change, at a constant width. When either  $h_0$  or  $h_{-1}$  becomes zero, that subinterval is transformed to the opposite phase and takes half of the width from the other subinterval,  $h_{-1}$  or  $h_0$  respectively, which would be twice the original, constant width. This way, subintervals that are not adjacent to the phase boundary maintain a uniform constant width, while the two subintervals adjacent to the phase boundary vary in width from zero to double the constant width of the other subintervals. It is, of course, very important to ensure that when subintervals are varied in size that the heat contained within each

subinterval is appropriately transferred to or from the neighbouring subintervals. This is a minor technicality.

Figure 5-4 demonstrates the freezing of water in an insulated rod initially at 0°C when one end is brought into contact with a constant cold source at a) –10°C and b) –100°C. Each graph displays the temperature profile within the rod at various times from the start of freezing to two hours. The various constants used to generate this data are given in appendix 1. It can be seen from this simulation that the farther the ice front moves from the cold end, the slower it moves. This behaviour can be predicted from equation 5-31 by approximating the temperature gradient in the solid phase by a straight line. From figure 5-4 it can be seen that this approximation may be reasonable for the a) case, but perhaps not as reasonable for the b) case; therefore, begin with the a) case. The temperature gradient in the solid phase is approximated as

$$\frac{\partial \theta_s}{\partial x} \cong \frac{(0^\circ \text{C}) - (-10^\circ \text{C})}{X}, \quad (5-46)$$

while the gradient in the liquid phase remains zero at all time. Substituting these in equation 5-31 gives the following ordinary differential equation

$$K_s \frac{(10^\circ \text{C})}{X} = L\rho \frac{dX}{dt}, \quad (5-47)$$

which is solved to get

$$X = \sqrt{\frac{2(10^\circ \text{C})K_s}{L\rho} t}. \quad (5-48)$$

The ice front position as predicted by this equation is compared to the simulation results in figure 5-5. Graphs are plotted for both the a) –10°C case and the b) –100°C case, and in each graph the solid line represents the simulation result while the broken line represents the solution 5-48. It can be seen that in both cases the solution 5-48 overestimates the progress of the ice front. This is understandable since approximating a concave down curve with a straight line between the endpoints of the curve will always overestimate positive slopes at



the right hand endpoint. This situation is demonstrated most clearly in figure 5-5b where the straight line approximation is most inappropriate.

### **Mass and Heat Diffusion with a Phase Change**

Given the development of a numerical method to simulate mass diffusion, and the refined method to simulate heat diffusion with a phase change, a combined solution can now be developed which incorporates the characteristics of both these previous solutions. In this new combined system, the moving phase change excludes solutes which will diffuse away from the phase change. Also, since the freezing point at the phase change generally depends on the concentration of the solutes present, the solutes will serve to hinder the propagation of the phase change. This new combined system is illustrated in figure 5-6.

As one might expect, all the differences between this system and the previous ones discussed occur at the phase boundary. Thus, equations 5-12, 5-14, 5-16, 5-18, 5-19, 5-20, 5-28, 5-29, and 5-30 still apply in this combined case, but only when  $i = 0 \dots m-2$  or  $i = -l \dots -2$ . Therefore, in this case, it is only necessary to derive the equations that describe the new behaviour exhibited at the phase boundary.

There are two significant differences between this combined heat and solute diffusion problem and the heat only problem discussed in the last section. These differences are that the freezing point at the phase boundary now varies with the concentrations of the solutes present, and that solute concentration gradients at the phase boundary depend on the velocity of the phase boundary. To begin, consider the latter difference. At the phase boundary, the solute concentration gradient is given by

$$\frac{\partial C}{\partial x} = -\frac{C}{D} \frac{dX}{dt}, \quad (5-49)$$

where  $C$  is the solute concentration at the phase boundary and  $dX/dt$  is the velocity of the phase boundary. It can be seen here that the concentration

gradient does not depend linearly on the boundary velocity. This difficulty seriously complicates the analysis; and therefore, needs to be rectified. Since this numerical method ultimately depends on calculations at a series of small time increments, it is possible to estimate the solute concentration,  $C$ , at the phase boundary by making use of the concentration at the last time increment. Call this concentration estimate  $\tilde{C}$ . Then, in the standard notation, equation 5-49 becomes

$$-g_0\alpha_0 + \beta_0 = -\frac{\tilde{C}}{D} \frac{dX}{dt}. \quad (5-50)$$

Since  $P_0$  and  $Q_0$  can be calculated from equations 5-12 and 5-16, they are known; and thus, equation 5-50 can be combined with the linear relation 5-11 to get the system

$$\left. \begin{aligned} -g_0\alpha_0 + \beta_0 &= -\frac{\tilde{C}}{D} \frac{dX}{dt} \\ P_0\alpha_0 + \beta_0 &= Q_0 \end{aligned} \right\}. \quad (5-51)$$

This system has the solution

$$\alpha_0 = \frac{Q_0 + \frac{\tilde{C}}{D} \frac{dX}{dt}}{g_0 + P_0} \quad \text{and} \quad (5-52a)$$

$$\beta_0 = \frac{g_0 Q_0 - P_0 \frac{\tilde{C}}{D} \frac{dX}{dt}}{g_0 + P_0}; \quad (5-52b)$$

and thus, once  $dX/dt$  is known, the solution to the mass portion of the problem is known since equations 5-52 can be used as initial values for the recursion relations 5-14.

Now consider the freezing point at the phase boundary. In general, this temperature is some function of the solute concentration at the boundary. In chapter 3, equations to calculate freezing point as a function of concentration

were developed; however, these equations are non-linear and would be very difficult to implement here. Instead, the concentration estimate introduced above,  $\bar{C}$ , is used again. In this case, the freezing point of the solution at the phase boundary is defined based on a first-order Taylor expansion about  $\bar{C}$ . The desired definition of freezing point is

$$F(C) = A(\bar{C})[C - \bar{C}] + F(\bar{C}), \quad (5-53)$$

where  $A = \partial F / \partial C$  and can be calculated from the equations given in chapter 3. In the usual notation, equation 5-53 is

$$F(C) = A \left[ \frac{g_0^2}{6} \alpha_0 - \frac{g_0}{2} \beta_0 + \frac{\bar{C}_0}{g_0} - \bar{C} \right] + \tilde{F}, \quad (5-54)$$

where  $\tilde{F} = F(\bar{C})$  is used for convenience. This calculation of freezing point can be made a function of  $dX/dt$  by substituting equations 5-52, giving

$$F(C) = \frac{A g_0 (g_0 + 3P_0)}{6(g_0 + P_0)} \frac{\bar{C}}{D} \frac{dX}{dt} - \frac{A g_0^2 Q_0}{3(g_0 + P_0)} + A \frac{\bar{C}_0}{g_0} - A \bar{C} + \tilde{F}. \quad (5-55)$$

At this point it is actually possible to generalize this development to allow for an unlimited number of solutes. By denoting individual solutes by a superscript  $j$ , equation 5-53 can be generalized to include the effect of each solute. This generalization is given by

$$F(C) = \sum_j A^j(\bar{C}^j)[C^j - \bar{C}^j] + F(\bar{C}), \quad (5-56)$$

where it is understood that  $C$  and  $\bar{C}$  are the appropriate column vectors consisting of the  $C^j$ 's and  $\bar{C}^j$ 's, respectively. Equation 5-56 can be simplified as

$$F(C) = M \frac{dX}{dt} + N, \quad (5-57)$$

by letting

$$M = \sum_j \frac{A^j g_0 (g_0 + 3P_0^j) \bar{C}^j}{6(g_0 + P_0^j) D^j}, \quad (5-58a)$$

$$N = \sum_j \left( -\frac{A^j g_0^2 Q_0^j}{3(g_0 + P_0^j)} + A^j \frac{\bar{C}^j}{g_0} - A^j \bar{C}^j \right) + \bar{F}. \quad (5-58b)$$

System 5-35 was developed during the heat only analysis in the previous section; however, that system still applies in this case with only minor modification. The only modification is the constraint defining the freezing point at the phase boundary. The new constraint is

$$\frac{h_{-1}^2}{6} \alpha'_{-1} + \frac{h_{-1}}{2} \beta'_{-1} + \frac{\bar{\theta}_{-1}}{h_{-1}} = \frac{h_0^2}{6} \alpha'_0 - \frac{h_0}{2} \beta'_0 + \frac{\bar{\theta}_0}{h_0} = F(C) = M \frac{dX}{dt} + N, \quad (5-59)$$

which, when used in system 5-35, gives the new system

$$\left. \begin{aligned} \frac{h_0^2}{6} \alpha'_0 - \frac{h_0}{2} \beta'_0 - M \frac{dX}{dt} &= N - \frac{\bar{\theta}_0}{h_0} \\ \frac{h_{-1}}{2} \beta'_{-1} - M \frac{dX}{dt} &= -\frac{h_{-1}^2}{6} \alpha'_{-1} + N - \frac{\bar{\theta}_{-1}}{h_{-1}} \\ K_s \beta'_{-1} + K_l h_0 \alpha'_0 - K_l \beta'_0 - L\rho \frac{dX}{dt} &= -K_s h_{-1} \alpha'_{-1} \\ P'_0 \alpha'_0 + \beta'_0 &= Q'_0 \end{aligned} \right\} \quad (5-60)$$

System 5-60 has solution

$$\alpha'_0 = \frac{3L\rho h_{-1} h_0 Q'_0 + 6L\rho h_{-1} \left( N - \frac{\bar{\theta}_0}{h_0} \right) + 4K_s M h_{-1}^2 \alpha'_{-1}}{L\rho h_{-1} h_0 (h_0 + 3P'_0) - 2K_s M h_0 (h_0 + 3P'_0) - 6K_l M h_{-1} (h_0 + P'_0)} + \frac{-12K_s M \left( \frac{\bar{\theta}_{-1}}{h_{-1}} - \frac{\bar{\theta}_0}{h_0} \right) - 6MQ'_0 (K_l h_{-1} + K_s h_0)}{L\rho h_{-1} h_0 (h_0 + 3P'_0) - 2K_s M h_0 (h_0 + 3P'_0) - 6K_l M h_{-1} (h_0 + P'_0)}, \quad (5-61a)$$

$$\beta'_0 = \frac{L\rho h_{-1} h_0^2 Q'_0 - 6L\rho h_{-1} P'_0 \left( N - \frac{\bar{\theta}_0}{h_0} \right) - 4K_s M h_{-1}^2 P'_0 \alpha'_{-1}}{L\rho h_{-1} h_0 (h_0 + 3P'_0) - 2K_s M h_0 (h_0 + 3P'_0) - 6K_l M h_{-1} (h_0 + P'_0)} + \frac{12K_s M P'_0 \left( \frac{\bar{\theta}_{-1}}{h_{-1}} - \frac{\bar{\theta}_0}{h_0} \right) - 2M h_0 Q'_0 (3K_l h_{-1} + K_s h_0)}{L\rho h_{-1} h_0 (h_0 + 3P'_0) - 2K_s M h_0 (h_0 + 3P'_0) - 6K_l M h_{-1} (h_0 + P'_0)} \quad (5-61b)$$

$$\frac{dX}{dt} = K_s \frac{\frac{2}{3} h_{-1}^2 h_0 (h_0 + 3P'_0) \alpha'_{-1} + 2h_0 (h_0 + 3P'_0) \left( N - \frac{\bar{\theta}_{-1}}{h_{-1}} \right)}{L\rho h_{-1} h_0 (h_0 + 3P'_0) - 2K_s M h_0 (h_0 + 3P'_0) - 6K_l M h_{-1} (h_0 + P'_0)} + K_l \frac{2h_{-1} h_0^2 Q'_0 + 6h_{-1} (h_0 + P'_0) \left( N - \frac{\bar{\theta}_0}{h_0} \right)}{L\rho h_{-1} h_0 (h_0 + 3P'_0) - 2K_s M h_0 (h_0 + 3P'_0) - 6K_l M h_{-1} (h_0 + P'_0)} \quad (5-62)$$

$$\beta'_{-1} = -P'_{-1} \alpha'_{-1} + Q'_{-1} \quad (5-63)$$

where

$$P'_{-1} = \frac{\frac{1}{3} L\rho h_{-1}^2 h_0 (h_0 + 3P'_0) - 2M h_{-1} [K_l h_{-1} (h_0 + P'_0) + K_s h_0 (h_0 + 3P'_0)]}{L\rho h_{-1} h_0 (h_0 + 3P'_0) - 2K_s M h_0 (h_0 + 3P'_0) - 6K_l M h_{-1} (h_0 + P'_0)} \quad (5-64a)$$

$$Q'_{-1} = \frac{2L\rho h_0 (h_0 + 3P'_0) \left( N - \frac{\bar{\theta}_{-1}}{h_{-1}} \right) + 4K_l M h_0^2 Q'_0}{L\rho h_{-1} h_0 (h_0 + 3P'_0) - 2K_s M h_0 (h_0 + 3P'_0) - 6K_l M h_{-1} (h_0 + P'_0)} + \frac{12K_l M (h_0 + P'_0) \left( \frac{\bar{\theta}_{-1}}{h_{-1}} - \frac{\bar{\theta}_0}{h_0} \right)}{L\rho h_{-1} h_0 (h_0 + 3P'_0) - 2K_s M h_0 (h_0 + 3P'_0) - 6K_l M h_{-1} (h_0 + P'_0)} \quad (5-64b)$$

It should be noted here that equations 5-61 through 5-64 are actually a generalization of equations 5-36 to 5-39 from the pure water case discussed in the previous section. To see this, just set  $M = 0$ ,  $N = F$  and compare.

The values for  $P'_{-1}$  and  $Q'_{-1}$  calculated using equations 5-64 can now be used in equations 5-29 to find the remaining  $P'_i$ 's and  $Q'_i$ 's for the heat portion of the problem. Then, all the  $\alpha'_i$ 's and  $\beta'_i$ 's can be found along with  $dX/dt$ , with

$dX/dt$  being used to find the  $\alpha_i$ 's and  $\beta_i$ 's for the solute part of the problem. The same iteration equations (5-23, 5-25, 5-41, and 5-43) that were used in the mass only and heat only cases can be employed here to update the simulation at each time interval.

The only additional consideration that must be addressed is that as the ice front moves, solute must remain in the liquid region. This, however, is easily accomplished by maintaining the value of  $\bar{C}_0$ , while  $g_0$  changes as a result of the moving ice front. Solute will automatically concentrate near the ice front when the solid region is growing, and will automatically be diluted near the ice front when the solid region is shrinking.

Numerical results obtained using this method are presented in figures 5-7a and 5-7b. In these simulations,  $D$  was given a value of  $1.545 \times 10^{-5} \text{ cm}^2/\text{sec}$ , which is appropriate for sodium chloride in water [Weast 1983]. All other parameters used in the simulation are given in appendix 1. Figure 5-7a illustrates the results of freezing an aqueous solution initially at 0.150 mol/l with a fixed  $-10^\circ\text{C}$  boundary condition. The dashed line indicates the salt concentration on the right axis. The region of liquid extends from the open square (indicating the phase boundary) to the right hand edge of the graph.

Figure 5-7b displays a summary of ice front position as a function of time. For the purposes of comparison, the ice front position in the pure water case is also presented (from figure 5-5a). Clearly the rate of ice growth in an aqueous solution is slowed by the presence of a solute; however, the buildup of this solute at the phase boundary is not sufficient to halt the progress of the boundary. The primary effect of the solute buildup is the reduction of the temperature at the phase boundary, and thus, a reduction of the thermal gradients in the solid region. These reduced thermal gradients are the primary cause of the reduced rate of phase boundary propagation.

The numerical methods developed here are effective tools for simulating the behaviour of a combined solute and heat system with a propagating phase

change. These methods do not require any special form for either the initial conditions or the boundary conditions; and thus, can be used to simulate the behaviour of any real system. The equations can also be generalized to an arbitrary number of solutes (as described above) and can also be generalized to the case where the diffusion coefficient varies in space. This latter construction is important for simulating three-dimensional systems where diffusion occurs in only one-dimension, but the surface area through which the diffusion is occurring varies along the axis of diffusion. In the next chapter, constitutional supercooling will be introduced along with a description of dendritic breakdown. The formation of dendrites in the liquid region effectively reduces the surface area (in a position dependent manner) available for solute diffusion; and thus, this model must be able to deal with that situation.

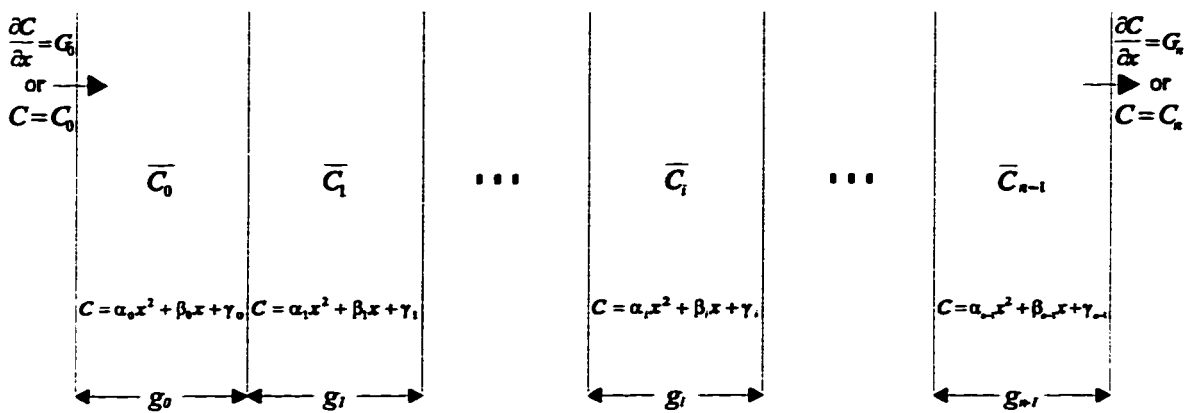


**Figure 5-1.** Subinterval structure for the mass only diffusion problem. The concentration gradient within each subinterval is fitted to a quadratic equation, while observing certain boundary conditions.



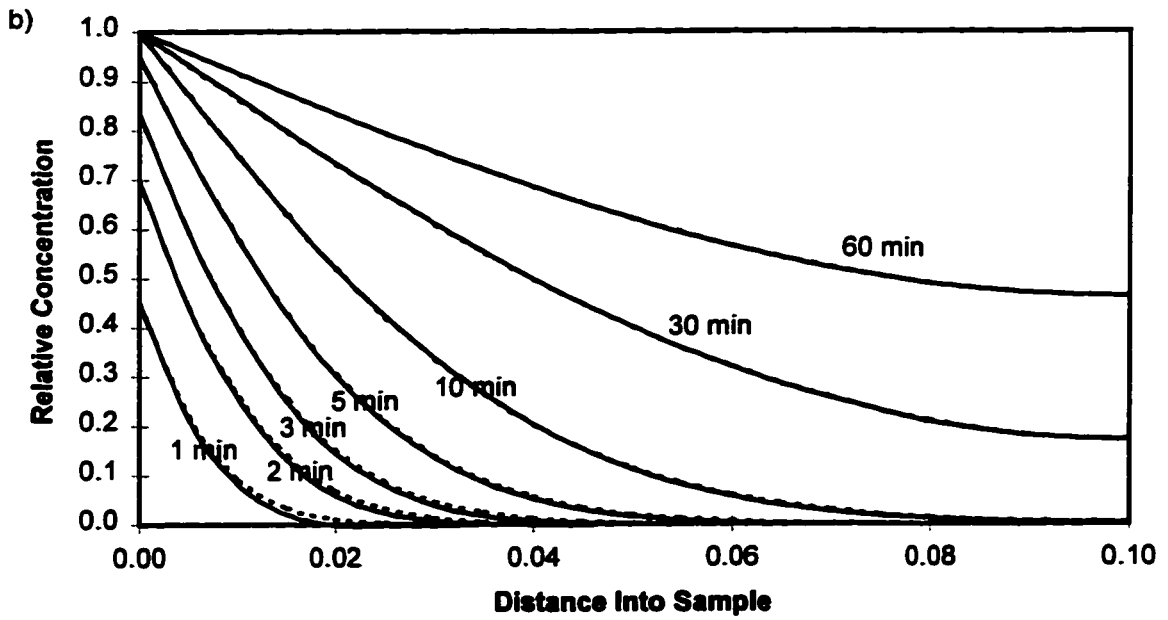
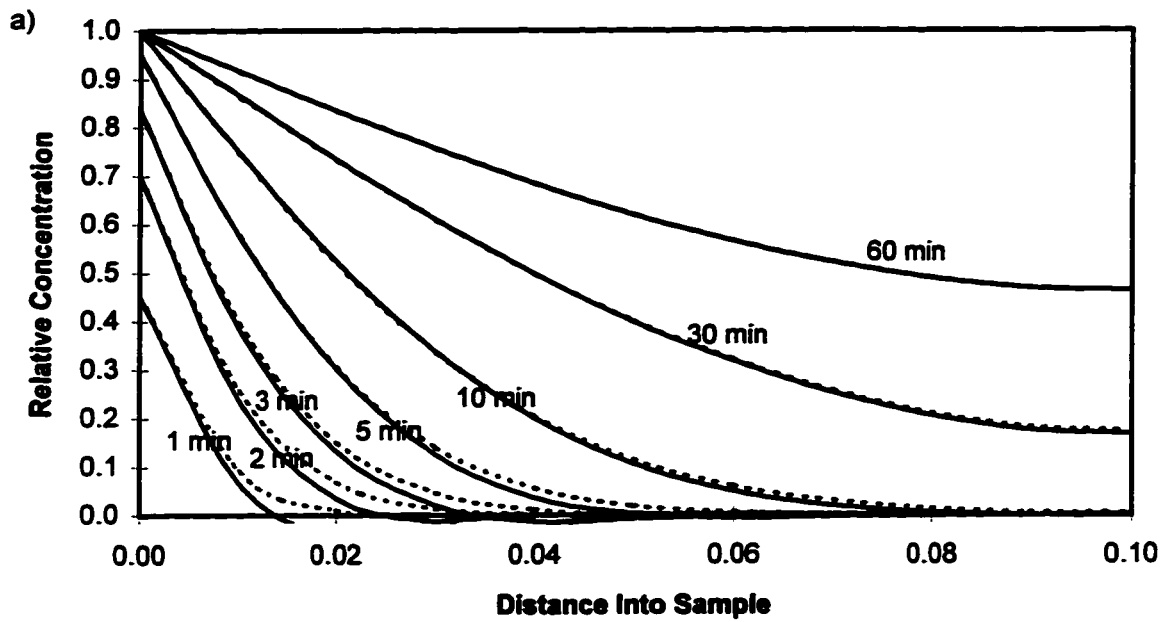


**Figure 5-2.** Illustration of solute diffusion in an aqueous solution. The simulation was done for the case where a)  $n=5$  and b)  $n=10$ . In both cases, the broken line represents the exact solution to the problem.

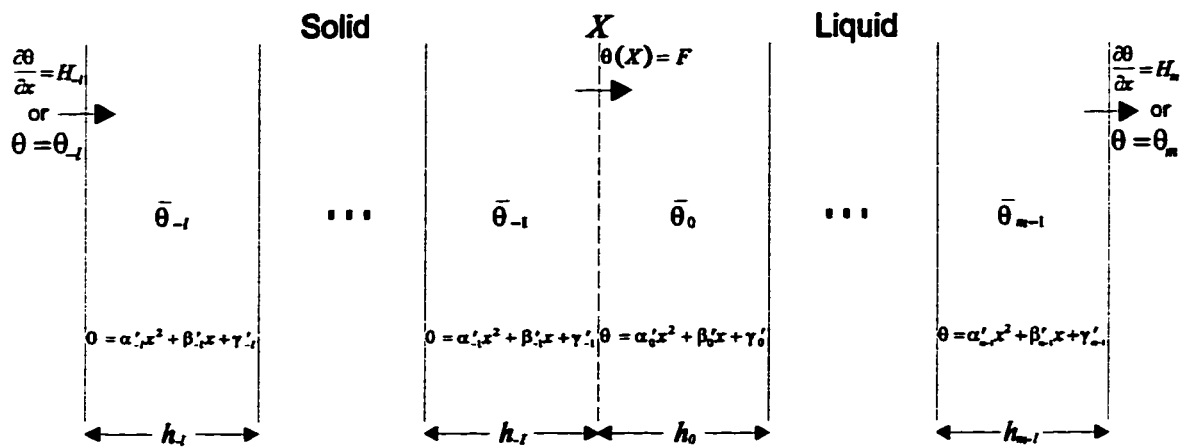


**Figure 5-3.** The heat diffusion problem is similar to the mass diffusion problem; however, it has been revised to include a phase boundary at  $X$ . This phase boundary propagates with time, and is always maintained at a temperature equal to the freezing point of the liquid.

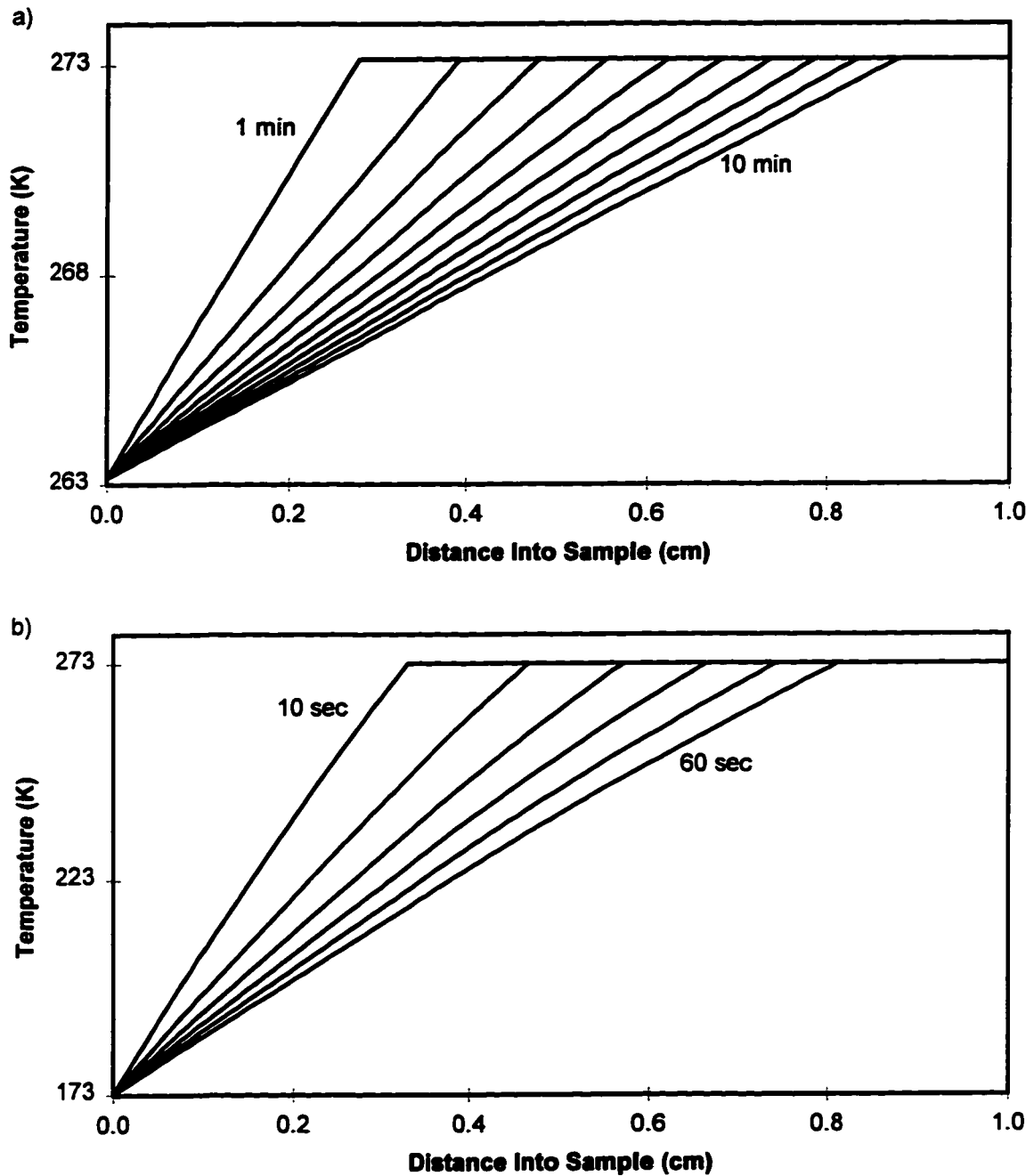


**Figure 5-4.** Temperature profiles present during the freezing of a pure water sample by a fixed temperature at the left boundary. The fixed temperatures used are a)  $-10^{\circ}\text{C}$  and b)  $-100^{\circ}\text{C}$ . In both cases the right boundary can be considered to be either insulated or fixed at  $0^{\circ}\text{C}$ .

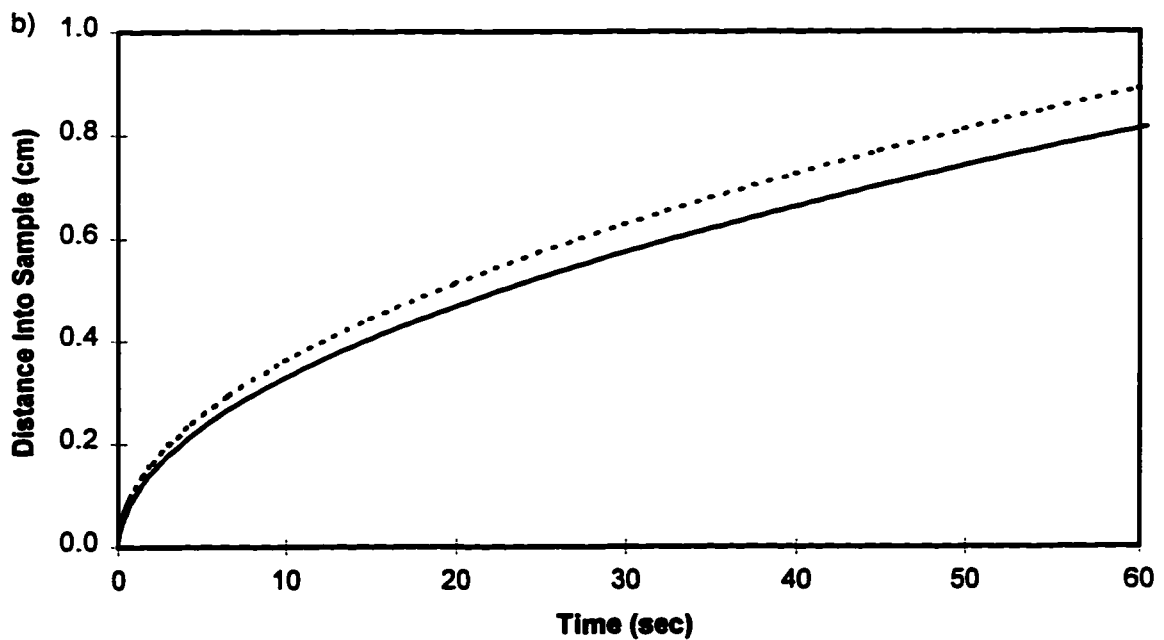
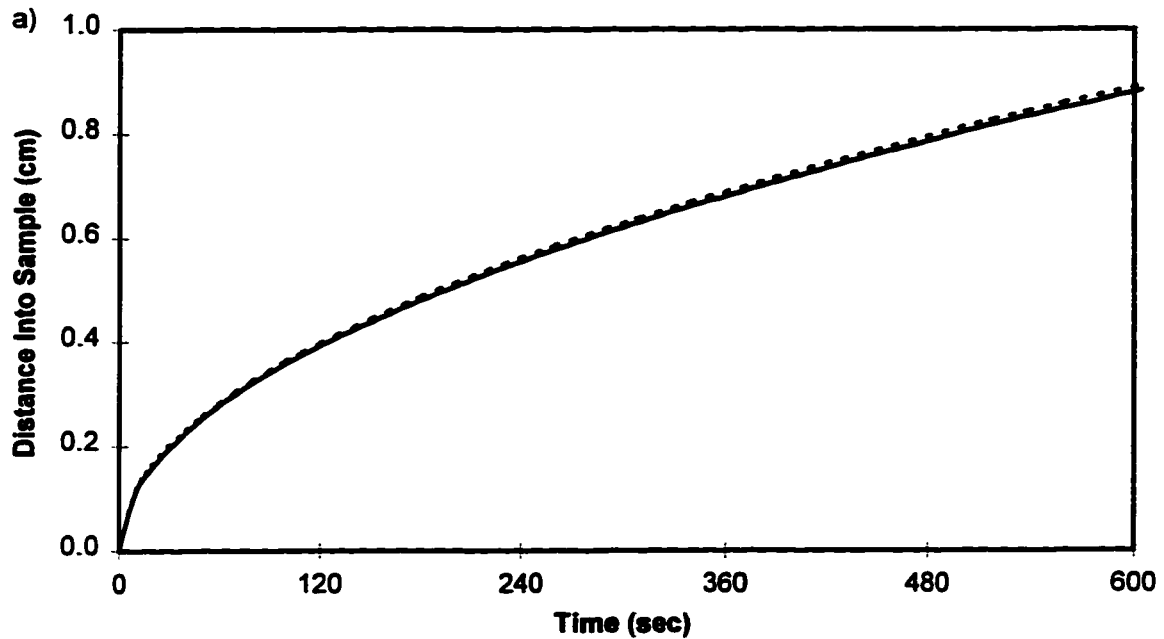


**Figure 5-5.** Summary of the extent of ice growth in the cases presented in figure 5-4. In both figures the solid line is the simulated extent of ice growth (from figure 5-4), while the dashed line is the estimated extent of ice growth (from equation 5-48). The estimated extent of ice growth in the b) graph deviates significantly from the simulated extent of ice growth due to the inappropriateness of the assumption that the temperature profile in the solid phase is linear.

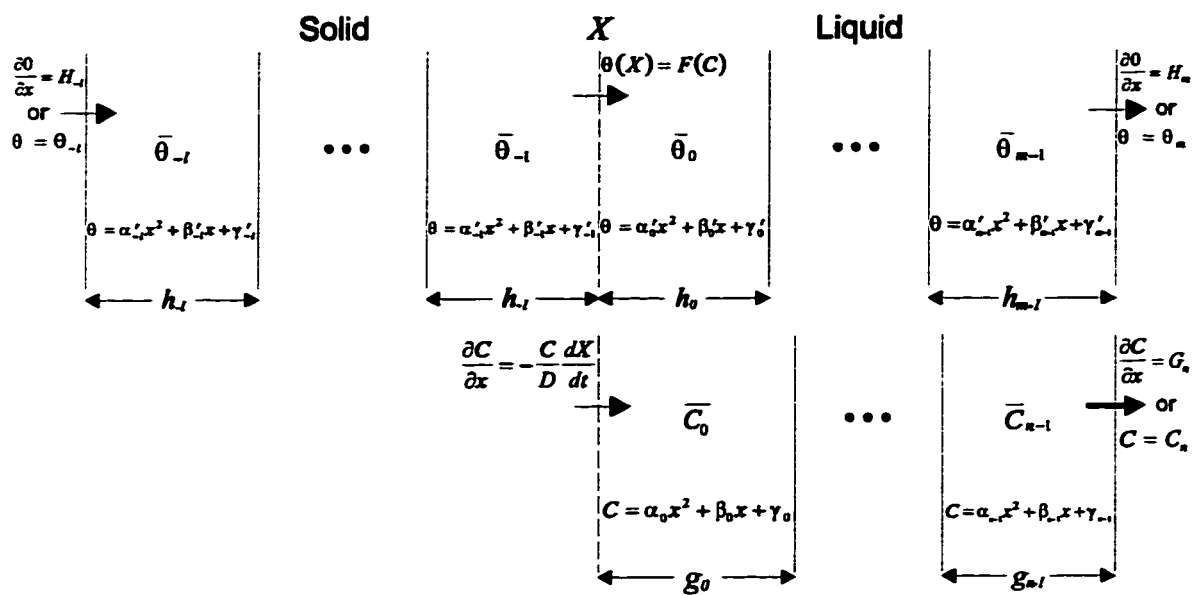


**Figure 5-6.** Mass and heat diffusion are combined into a single problem. The mass gradient boundary condition at the phase change depends on the velocity of the phase change, while the temperature at the phase change depends on the concentration of solutes.

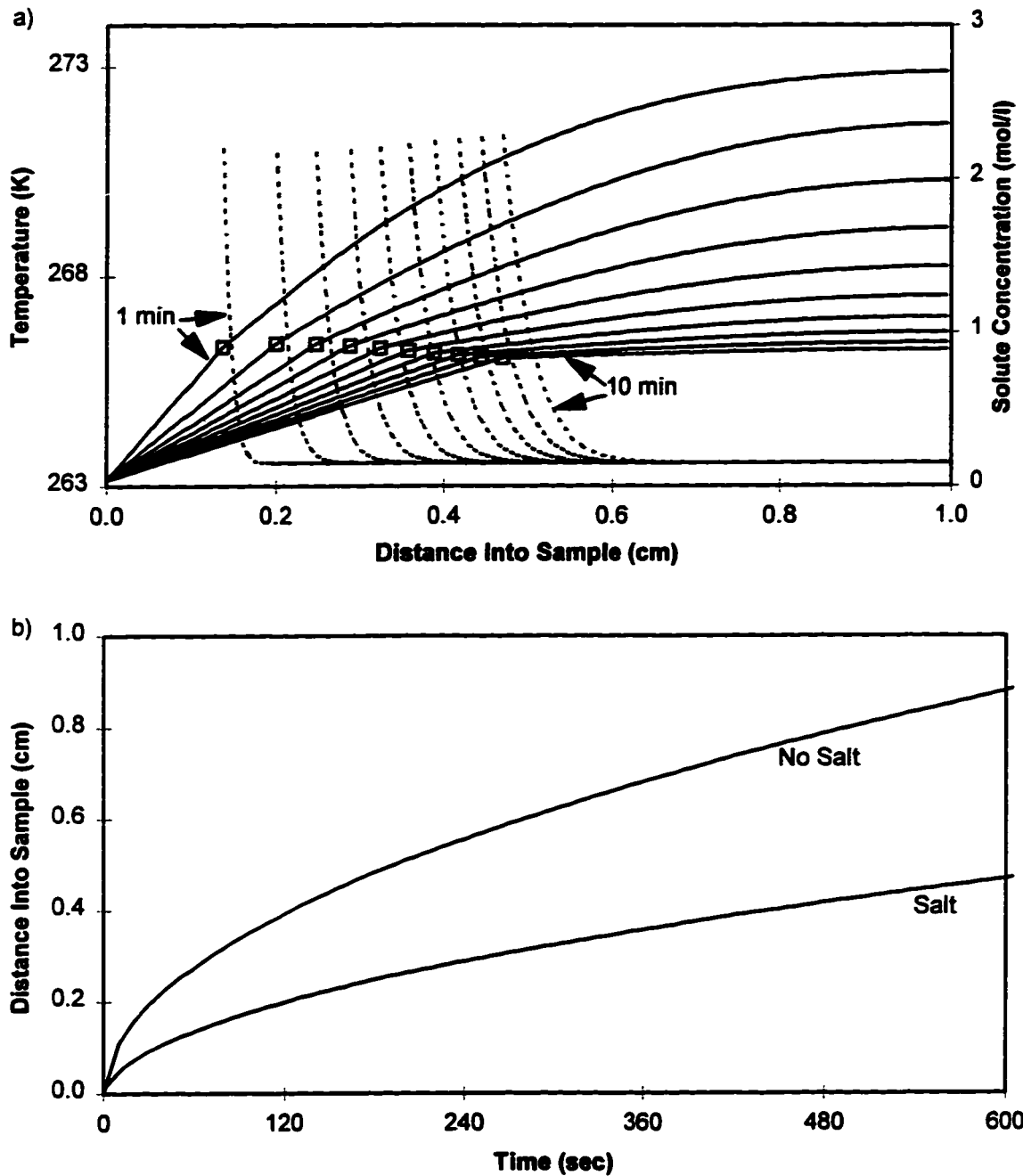


**Figure 5-7.** Simulation of the freezing process in a sample of aqueous solution with an initial concentration of 0.150 mol/l and an initial temperature of 0°C. Graph a) gives the temperature (solid lines) and concentration (broken lines) profiles along with the phase boundary location (open squares), while b) summarizes the extent of ice growth as a function of time. In b), the extent of ice growth in the pure water case (figure 5-5a) is also reported for comparison.

## **Chapter 6**

### **Constitutional Supercooling**

#### **Introduction**

It has been demonstrated that the presence of a solute in liquid water can significantly slow the freezing process. In chapter 5, the progress of the planar ice front was reduced by approximately 47% when a solute at 0.15mol/l is present. This reduction in phase boundary velocity results from the conditions that solute diffuse away from the phase boundary and that the temperature at the phase boundary always equals the local freezing point. The freezing point at the phase boundary is a function of solute concentration, and as solute concentration increases due to the advancing phase boundary, the freezing point decreases. This reduces the temperature gradient in the solid region, and since ice growth is heat limited, the reduction in temperature gradient reduces the amount of heat diffusing from the phase boundary, thus reducing the velocity of the boundary.

On the liquid side of the phase boundary an interesting situation may arise. If the liquid is initially warmer than the freezing point and at a uniform temperature, then, as the phase boundary propagates, a temperature gradient will develop on the liquid side and will be greatest at the phase boundary. Also, since no solute crosses the phase boundary, solute concentration will build immediately adjacent to the phase boundary and decrease to the initial concentration as one moves further from the boundary. Since the freezing point is a function of solute concentration, this concentration profile will lead to a freezing point profile where the freezing point gradient is greatest at the phase boundary. Assuming the solid is on the left, both the temperature and freezing point gradients will be positive and be greatest at the phase boundary, in this case.

If the freezing point gradient is greater than the actual temperature gradient, a condition known as constitutional supercooling arises. Since the

phase boundary is at equilibrium, the temperature and freezing point are equal at the boundary; however, if the freezing point gradient is the greater, the freezing point at locations a small distance from the phase boundary will be greater than the actual temperature. Since liquid exists in this region, the liquid will be in a meta-stable supercooled state. Some early work dealing with constitutional supercooling can be found in [Weinberg & Chalmers 1951; Rutter & Chalmers 1953], while observations (and excellent pictures of dendritic ice growth) more comparable to this work can be found in [Körber & Scheiwe 1983a; Körber *et al.* 1983b].

### **Constitutional Supercooling**

To illustrate how constitutional supercooling may arise and how it may be dealt with, a series of simulations similar to those done at the end of chapter 5 is performed. These simulations, however, only consider a 1.5mm region liquid with the same initial solute concentration of 0.15mol/l as in chapter 5. The simulations will all start with the liquid at a temperature of +10°C and the left boundary at a temperature of -0.5°C (corresponding to the freezing point of a 0.15mol/l solution of sodium chloride in water). The temperature at the left boundary is reduced at fixed rates of -0.02 K/sec, -0.105 K/sec, and -1.0 K/sec. The diffusion coefficient used for these simulations is  $0.72 \times 10^{-5} \text{ cm}^2/\text{sec}$ , which is the diffusion coefficient for a solution of sodium chloride and water as used in [Körber *et al.* 1983b].

Figure 6-1a illustrates the temperature and concentration profiles that arise in the -0.105 K/sec simulation. Since the freezing point of the solution is a function of solute concentration (as described in chapter 3), the concentration profiles in figure 6-1a can be alternatively represented as freezing point profiles. These freezing point profiles are shown in figure 6-1b as the broken lines. Equilibrium at the phase boundary dictates that the freezing point must equal the actual temperature at this boundary, as shown in figure 6-1b; however, since the freezing point is a function of solute concentration, which is in general



independent of the actual temperature, the freezing point will deviate from the actual temperature as the distance from the phase boundary increases.

If the freezing point increases more with distance from the phase boundary than the actual temperature does, then constitutional supercooling will result. Figure 6-1b illustrates the state of the simulation at three distinct times. It can be seen that at 3sec constitutional supercooling has not yet developed, but at 7sec constitutional supercooling is beginning to arise as the actual temperature of the liquid near the phase boundary falls below the freezing point. At 11sec, the temperature is as much as 0.31K below the freezing point at some locations.

This supercooled state is meta-stable and can persist for a finite period of time; however, as the degree of supercooling increases, the probability that random perturbations at the phase boundary will cause some regions to protrude into the supercooled liquid also increases. Since the supercooled liquid presents conditions favourable to an advancing ice front (that is, the possibility of forming ice without having to remove heat), any perturbation in the planar phase boundary that allows ice to protrude past the region of salt buildup and into the supercooled region will cause a dendrite to form. This breakdown of the planar ice front is called dendritic breakdown.

### **Stability Condition**

A necessary condition for interface instability is derived from a comparison of the freezing point gradient and the actual temperature gradient. This condition was first presented in [Rutter & Chalmers 1953], and is given here as

$$\left| \frac{dT}{dx} \right|_{\text{liquid}} > \left| \frac{dT}{dx} \right|_{fp} = \left| \frac{dT}{dC} \right| \left| \frac{dC}{dx} \right|, \quad (6-1)$$

where  $dT/dC$  is the slope of the phase diagram. The condition does not dictate the initiation of dendritic breakdown; but instead, indicates the presence of constitutional supercooling which is a requirement for dendritic breakdown. The actual dendritic breakdown event occurs randomly with a probability that is

dependent on the degree of supercooling. For the purposes of numerical simulation, the exact conditions necessary and sufficient for dendritic breakdown must be specified prior to the execution of the simulation.

Figure 6-2 gives the thermal gradients present during each of the three sample simulations. The solid lines represent the actual temperature gradient as a function of location, while the broken lines indicate the freezing point gradient. The condition for interface instability, equation 6-1, is satisfied when the broken line intersects the solid line and at all points to the right of the intersection. This intersection occurs at  $x = 0.0061\text{cm}$  and  $t = 12.5\text{sec}$  in the  $-0.02\text{K/sec}$  case, at  $x = 0.0060\text{cm}$  and  $t = 5.6\text{sec}$  in the  $-0.105\text{K/sec}$  case, and at  $x = 0.0022\text{cm}$  and  $t = 0.85\text{sec}$  in the  $-1.0\text{K/sec}$  case.

### Dendritic Breakdown

When breakdown of the supercooled state occurs, ice forms in the region of constitutional supercooling. Since the region is at a temperature below the freezing point, ice will form without the removal of latent heat as is usually required, and therefore, can form at an almost unlimited rate. As ice forms in this region, however, the latent heat that is released increases the local temperature. Also, increased solute concentration, due to water removal, decreases the freezing point. Ice may continue to form until the release of latent heat and the concentration of solute results in the restoration of equilibrium; where the local temperature and the freezing point are equal.

To calculate exactly how much ice will form in this situation, suppose that before dendritic breakdown the region contains  $w_0$  moles of water and  $n_0$  moles of solute at a temperature of  $\theta_0$ . Assuming that the freezing point can be calculated from

$$F(C) = F(C_0) + (C - C_0) \frac{\partial F}{\partial C}, \quad (6-2)$$

where  $C_0$  is the initial solute concentration, a relation equating temperature and the freezing point can be derived to calculate how much ice should form.

If  $s$  moles of ice were to form, the sample would be warmed by the latent heat of fusion to a temperature given by

$$\theta = \theta_0 - \frac{L(\theta)}{HC_0} s = \theta_0 - \frac{L(\theta_0)}{HC_0 + (sC_p - lC_p)s}, \quad (6-3)$$

where  $HC_0$  is the initial heat capacity of the sample,  $sC_p$  and  $lC_p$  are the specific heat capacities of solid and liquid water, respectively, and  $L$  is the specific latent heat of fusion as a function of temperature (and is negative, hence the negative sign on the second term). The two different forms of this equation result from the fact that one can either: increase the temperature of the system first and then turn the liquid to solid (first equation), or first turn the liquid to solid and then use the heat to raise the temperature of the system. In nature, the temperature of the system rises as the liquid is turned to solid.

Both versions of equation 6-3 present difficulties in solving the ice growth problem. The difficulty with the first equation lies in its implicit nature and requires one to estimate a value for  $\theta$ , while the second version of the equation increases the complexity of the algebra. There is one valid argument for the use of the first version of equation 6-3 with an estimated, or better, an overestimated value of  $\theta$ . Overestimating the value of  $\theta$  will result in an underestimate of the amount of ice that will form. This underestimate may be desirable since dendritic ice growth will be limited by solute diffusion perpendicular to the axis of the dendrite. Since the effect of solute diffusion on the non-axial growth of a dendrite is not calculated, underestimating the amount of dendrite growth in this direction is a safe alternative.

Equating the freezing point (equation 6-2) and temperature (equation 6-3) gives

$$F_0 + \left( \frac{n_0}{v_0 - lMV_w \cdot s} - C_0 \right) \frac{\partial F}{\partial C} = \theta_0 - \frac{L}{HC_0} s, \quad (6-4)$$

where  $F_0 = F(C_0)$ ,  $n_0/(v_0 - lMV_w \cdot s) = C$ ,  $MV_w$  is the molecular volume of water,  $v_0$  is the initial aqueous volume, and  $L$  is the estimated latent heat of fusion ( $= L(F_0)$  is suggested). Equation 6-4 has a pair of solutions, of which one is applicable:

$$s = \frac{v_0}{2MV_w} - \frac{HC_0}{2L} \left( F_0 - \theta_0 - C_0 \frac{\partial F}{\partial C} \right) - \sqrt{\left[ \frac{v_0}{2MV_w} + \frac{HC_0}{2L} \left( F_0 - \theta_0 - C_0 \frac{\partial F}{\partial C} \right) \right]^2 + \frac{HC_0}{L} \frac{v_0}{MV_w} C_0 \frac{\partial F}{\partial C}}. \quad (6-5)$$

If multiple solutes are present in the solution, equation 6-5 may be generalized to

$$s = \frac{v_0}{2MV_w} - \frac{HC_0}{2L} \left( F_0 - \theta_0 - \sum_j C_j^0 \frac{\partial F}{\partial C^j} \right) - \sqrt{\left[ \frac{v_0}{2MV_w} + \frac{HC_0}{2L} \left( F_0 - \theta_0 - \sum_j C_j^0 \frac{\partial F}{\partial C^j} \right) \right]^2 + \frac{HC_0}{L} \frac{v_0}{MV_w} \sum_j C_j^0 \frac{\partial F}{\partial C^j}}. \quad (6-6)$$

Equation 6-5 is used to calculate ice growth and melt following dendritic breakdown at each iteration of the simulation in each of the liquid subintervals. In the  $-0.105\text{K/sec}$  simulation discussed above, dendritic breakdown was forced to occur at 11sec into the simulation and these results are displayed in figure 6-3. The figure illustrates the situation immediately preceding dendritic breakdown, as it was in figure 6-1b, and then demonstrates the effect of dendritic breakdown immediately after the formation of dendrites and then at a later time.

After dendritic breakdown ice growth is far less limited by the accumulation of solutes at the ice surface since the ice surface is significantly greater in area and the ice now has two options for further growth: extend the length of the dendrites, or increase the width of the dendrites. The option that is preferred in a particular situation depends primarily on the thermal gradients present in the

region of the dendrites. If the thermal gradients are kept large, the dendrites will likely be very thick at the cold end, and taper in width rapidly as one moves towards the warm end. The overall length of the dendrites will be limited as the freezing point is exceeded at the warm end. On the other hand, if the temperature in the region of the dendrites is more uniform and thermal gradients are reduced, dendrite thickness will also be more uniform, and the dendrites will likely grow to longer lengths.

Since ice in the region of the dendrites remains at equilibrium with the liquid at all times, the local temperature will always equal the freezing point, which, of course, is a function of solute concentration. This coupling between solute concentration and temperature can have a profound effect on either the solute concentration or the temperature profile, depending primarily on the specific values of the latent heat of fusion and the heat capacity. Figure 6-3 illustrates the effect on the temperature profile when the specific latent heat of fusion is relatively large compared to the heat capacity, as is the case for water. As the dendrites form in the liquid region, large amounts of latent heat are released and the temperature profile is forced to follow the freezing point profile (as dictated by the concentration profile). In [Körber & Scheiwe 1983] the opposite effect is demonstrated as their experimental setup includes a large glass substrate possessing a heat capacity far greater than that of the liquid. In this case, it is observed that when dendrites form, solutes become increasingly concentrated until the freezing point profile coincides with the temperature profile. The large heat capacity of the glass ensures that the released latent heat had little effect on the local temperature. Since the temperature profile is roughly linear, and the phase behaviour of the solute is also roughly linear, Körber found that the solute concentration profile in the region of the dendrites is approximately linear.

Understanding the effect of constitutional supercooling on a planar ice front is of importance in a range of scientific fields ranging from engineering and chemistry to biology and cryobiology. The techniques presented in this chapter

can be used to model planar ice growth and to predict the temperature gradients that lead to constitutional supercooling. When constitutional supercooling does result, dendritic breakdown may occur as a means to extend the ice front beyond the solute barrier that had built up in the path of the planar ice front. In this way, solute diffusion ceases to limit the growth of ice in a solution when temperature is decreasing. The methods developed here allow the simulation of dendrite growth in both the axial direction and in width.

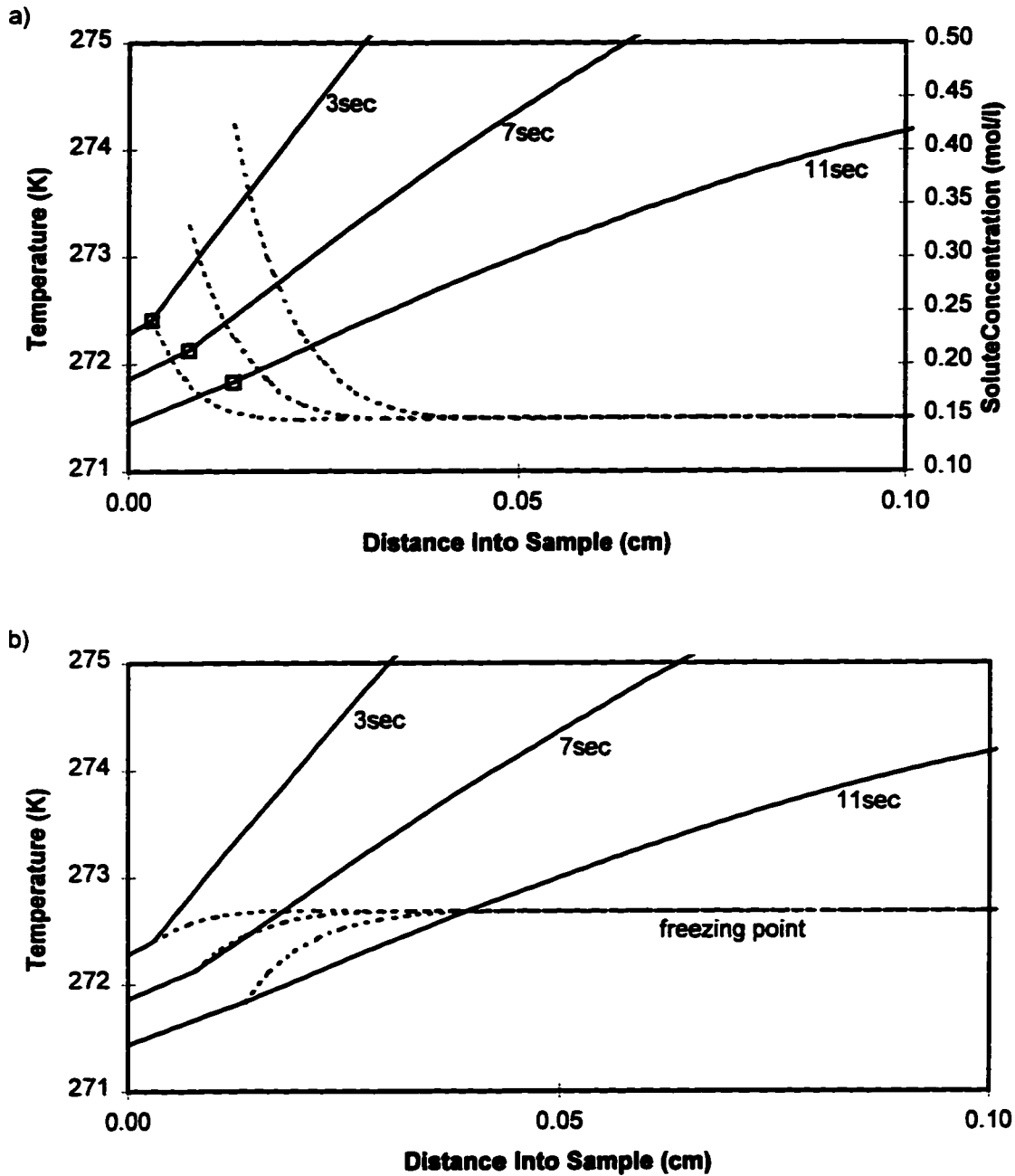


**Figure 6-1.** A sample of aqueous solution is cooled from an initial  $+10^{\circ}\text{C}$  at a constant rate of  $-0.105\text{K/sec}$ . An advancing planar ice front (open squares) leads to a) increased solute concentration, which results in b) a depression of the freezing point near the ice front. It can be seen in b) that at later times, the actual temperature is below the freezing point.

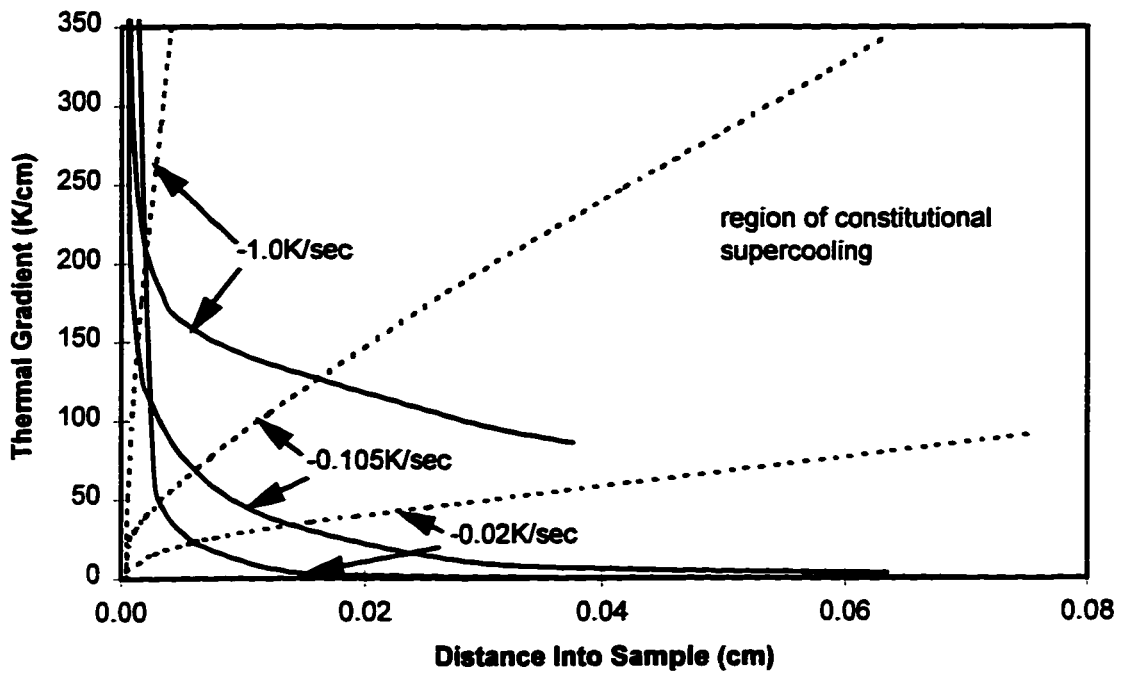


**Figure 6-2.** Actual temperature gradients (solid lines) versus freezing point gradients (broken lines) as a function of phase boundary position for various cooling rates. At positions beyond the intersection of the two temperature gradients, the phase boundary is unstable and may undergo dendritic breakdown.



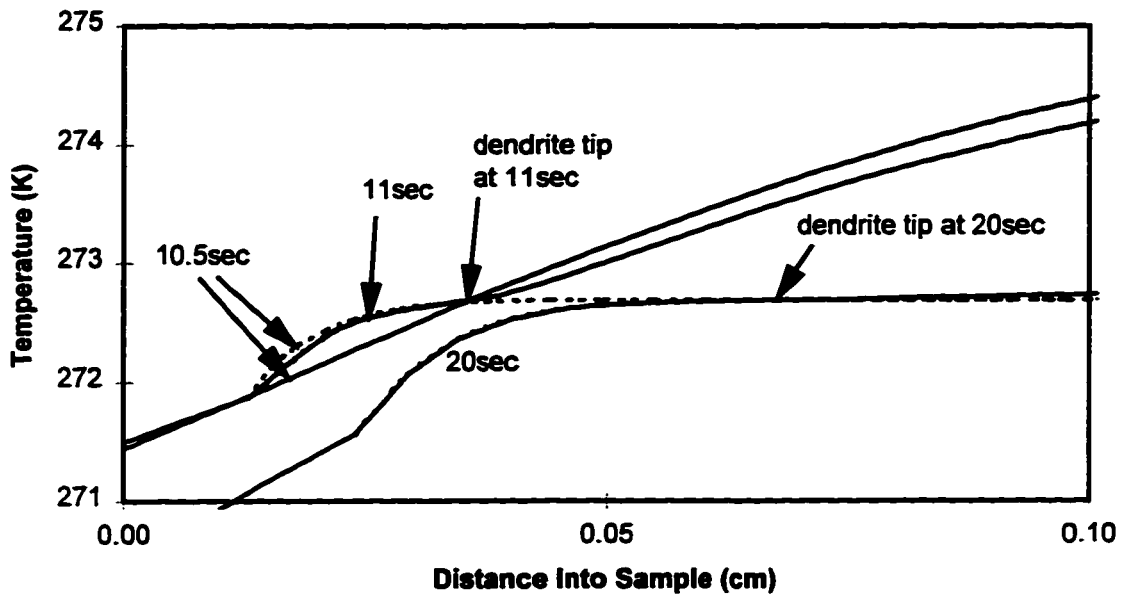


**Figure 6-3.** After dendritic breakdown, dendrites extend from the phase boundary into the supercooled liquid region. Latent heat released from the dendrites causes the temperature profile to exactly match the freezing point profile (11sec). The planar ice front can continue to propagate after dendritic breakdown; however, growth of the dendrites is preferred.

## **Chapter 7**

### **Experimental Applications**

#### **Introduction**

The application of a mathematical model to the simulation of heat and mass transport in biological tissues can be of great value to experimental biologists. These simulations, typically of real experiments done in the lab, can be used to predict the possible outcome of an experiment before it is performed, or to help to understand the results obtained from each experiment.

Furthermore, the simulation can be used to infer measurements that are either difficult or impossible to make during an experiment, or alternatively, to predict the outcome of entire experiments that may be difficult to perform.

The fundamental elements of the model outlined in chapter 2 have been developed, tested, and presented in the preceding chapters. In this chapter, the complete model is employed in the simulation of some typical experiments that may be performed on tissues in the lab. Unfortunately, sufficient experimental data necessary to test the complete model were not available in the literature at the time of this writing, and therefore, since each component of the model was tested as it was developed, simulation results will be presented in this chapter without direct comparison to experimental data. Qualitative assessment of the results is given as data are presented.

The simulations presented in this chapter are all done using human articular cartilage as the tissue model. Cartilage is the tissue found on the exposed surfaces of bones at the joints where one bone meets another. The primary role of cartilage is to absorb compressive forces between the two bones while providing a low friction surface for relative movement between the bones [Muldrew 1993]. Cartilage is composed primarily of a matrix of collagen fibrils with cells, called chondrocytes, interspersed within the matrix. The function of the cells is to maintain the cartilage matrix by repairing damaged collagen fibrils

or by synthesizing new fibrils; and therefore, attempts to preserve cartilage outside the body must focus on the preservation of the function of the chondrocytes [Schachar & McGann 1991]. As a result, an understanding of the local conditions experienced by individual chondrocytes during an experimental procedure is necessary to develop optimal protocols for preservation.

### **Cartilage Simulations**

Cartilage is a tissue well-suited for testing the capabilities of the model developed in the preceding chapters. Cartilage can be considered to be relatively uniform in composition throughout with only the two main components discussed above: the matrix and the chondrocytes. The matrix consists of 80% water [Maroudas 1979] and has three distinct regions: the superficial zone, the intermediate zone, and the deep zone. The composition of the matrix and the function of the chondrocytes does not vary from one zone to the next; only the density and placement of the chondrocytes define each zone. Figure 7-1 illustrates the structure of articular cartilage and how it is represented for simulation.

Since cartilage has a large proportion of water, it can be adequately simulated by an aqueous solution with the diffusion coefficients set as appropriate for the tissue. Also, as little is known about the specific diffusion properties of each region within the cartilage, a single diffusion compartment can be used to model the entire tissue. If it can be assumed that ice and solutes profuse equally and symmetrically at both sides of the tissue, only half of the tissue need be simulated as the other half will be a mirror image of the first.

Four distinct simulations involving the freezing of cartilage are presented in this chapter. In all four simulations, a piece of cartilage 2mm thick and 1cm<sup>2</sup> in surface area is frozen with 1ml of surrounding media (0.15mol/l sodium chloride solution) in a plastic freezing tube that is about 14mm in diameter. As mentioned, only the first 1mm of the cartilage is actually simulated. The thermal conductivity of the plastic freezing tube is estimated to be 0.045J/cm<sup>2</sup> Ksec and

the surface area available for heat transport is estimated to be  $5\text{cm}^2$ . The extratissue media is considered to be well mixed with zero temperature gradient, and thus, a JWCompartment, as described in chapter 4, is used to represent the media. The cartilage is represented by a DCompartment, as described in chapter 5, into which four chondrocytes (JWCompartments) are placed. These chondrocytes are located at positions 0.15mm, 0.40mm, 0.70mm, and 1.0mm within the DCompartment, and, due to their size, they are assumed to have infinite thermal conductivity; thus, they maintain a temperature exactly equal to the local extracellular temperature. The permeability coefficients for the chondrocytes are listed in appendix 1.

Each simulation begins with the entire system at a uniform temperature of  $-5^\circ\text{C}$  and, at  $t = 0$ , ice is nucleated in the extratissue media with planar ice formation beginning at the cartilage surface. Each simulation proceeds with the temperature outside the freezing tube being lowered at a constant rate. Two of the simulations have this rate set at  $-1^\circ/\text{min}$ , while the other two have a cooling rate of  $-5^\circ/\text{min}$ . Of each pair of simulations, one simulation is performed with the additional solute, dimethyl sulfoxide (DMSO), present throughout the system at a concentration of  $1.4\text{mol/l}$  (10% by volume), while the other simulation was done without this extra solute. DMSO is a cryoprotective agent that is commonly used to aid in the cryopreservation of cells and tissues. The protective effect of DMSO for cartilage will be assessed based on the results of these simulations. Table 7-1 details the four simulations performed.

**Table 7-1. Summary of freezing simulations performed.**

Simulation Number	Initial Temperature	Cooling Rate	Final Temperature	Dimethyl Sulfoxide present
1	$-5^\circ\text{C}$	$-1^\circ/\text{min}$	$-30^\circ\text{C}$	none
2	$-5^\circ\text{C}$	$-5^\circ/\text{min}$	$-30^\circ\text{C}$	none
3	$-5^\circ\text{C}$	$-1^\circ/\text{min}$	$-30^\circ\text{C}$	1.4 mol/l
4	$-5^\circ\text{C}$	$-5^\circ/\text{min}$	$-30^\circ\text{C}$	1.4 mol/l

## **Ice Formation**

Each simulation was first run in planar ice mode. This means that dendritic ice formation was disabled and the planar ice front that is initiated at the cartilage surface propagates throughout the cartilage. Since this ice front excludes solutes as it propagates, both salt and DMSO are excluded in the simulations where DMSO is present. The diffusion coefficient used for sodium chloride in cartilage was  $0.68 \times 10^{-5} \text{ cm}^2/\text{sec}$  [Maroudas 1979], while for DMSO in cartilage a diffusion coefficient of  $1.02 \times 10^{-5} \text{ cm}^2/\text{sec}$  [Muldrew 1993] was used.

Since the samples are not at a high temperature to start with, and are not being warmed at the far end, constitutional supercooling develops immediately after  $t = 0$  and grows in magnitude with time. As a result, it is quite possible that dendritic breakdown will occur within the tissue. In the simulations presented here, this dendritic breakdown is arbitrarily chosen to occur at the moment the planar ice front reaches 0.1mm from the cartilage surface. With this particular choice made, dendritic breakdown was chosen for each simulation to occur at times  $t = 95\text{sec}$ ,  $t = 75\text{sec}$ ,  $t = 145\text{sec}$ , and  $t = 98\text{sec}$ , respectively. Figures 7-2a and 7-2b illustrate the progress of the planar ice front in each of the four simulations, both with dendritic breakdown and without dendritic breakdown. The fact that the phase boundary can pass the 1mm mark is due to the reduction in the density of water as it is transformed to ice. If the entire system were capable of freezing, the compartment would increase in width to 1.09mm.

It is seen in figure 7-2b, that the presence of DMSO significantly slows the planar ice front. This is due to the fact that the freezing point at the phase boundary is a function of both the DMSO and salt concentrations. Also, both DMSO and salt must be excluded from the phase boundary. The equations developed in chapter 5 were used to simultaneously predict the diffusion of both DMSO and salt from the phase boundary. Figure 7-3 shows the DMSO and the salt concentration profiles that result in the cartilage at various times for the  $-5^\circ/\text{min}$  simulation.

Since the case of planar ice propagation throughout the cartilage may be seen by some as unrealistic, the remaining data presented in this chapter will deal with the simulations where dendritic breakdown occurs at 0.1mm from the cartilage surface, as mentioned above.

### **Temperature Profiles**

Temperature within each simulation was calculated at a variety of locations throughout the system. In particular, figures 7-4 and 7-5 displays the temperature at six locations within the system: the control temperature, the temperature of the extratissue media, and the temperatures present inside each of the four chondrocytes.

At  $t = 0$  in each simulation, the temperature throughout the system is  $-5^{\circ}\text{C}$ ; however, since the extratissue media also has ice growth nucleated at this time, the temperature in this media instantly rises to the freezing point of the media ( $-0.5^{\circ}\text{C}$  for the no-DMSO case, and  $-1.3^{\circ}\text{C}$  when DMSO is present). Since ice does not form within the cartilage at this time, the temperature there is a little slower to rise than the temperature of the surrounding media.

Temperatures within the cells of the cartilage continue to match the temperature of the extratissue media until dendritic breakdown occurs. At this moment, dendrites quickly form throughout the cartilage and the latent heat that comes with this ice growth increases the temperature in the cartilage. It is seen in figures 7-4 and 7-5 that the cell furthest from the planar phase boundary experiences the greatest increase in temperature. The reason for this is twofold: first, being farther from the cartilage surface, heat takes longer to be extracted by the colder surrounding media; and second, since the planar ice front excludes solutes into the non-frozen region, and these solutes take time to diffuse into the cartilage, the freezing point of the cartilage will be higher as one moves deeper into the cartilage.

Eventually, as enough ice forms and concentrates solutes sufficiently to lower the freezing point, the temperature of the system can begin to fall towards

the control temperature (temperature outside the plastic freezing tube). The amount of time that is required for this to take place depends primarily on how much ice needs to form since all this ice produces a large quantity of latent heat which must be removed. DMSO has the effect of decreasing the freezing point, or alternatively, decreasing to total amount of ice that must be present at a given temperature. In the presence of DMSO, no less ice forms; however, the ice does not form until lower temperatures are reached. This is the reason why the temperature of the system is quicker to return to the control temperature when DMSO is present, as seen in figure 7-4b and 7-5b. Furthermore, since DMSO postpones ice formation to lower temperatures, it can also be seen in figures 7-4b and 7-5b that the system does not match the control temperature as closely when DMSO is present. Despite this, DMSO does help to reduce the overall discrepancy between system temperature and control temperature.

### **Intracellular Supercooling**

When the temperature within the tissue deviates from the control temperature, due to the release of latent heat during ice growth, the tissue temperature must eventually return to the control temperature and this can only be accomplished with cooling rates greater than the externally applied cooling rate. This large cooling rate causes rapid changes in the composition of the extracellular environment, and these changes, in turn, cause supercooling to occur in the chondrocytes as they attempt to maintain osmotic equilibrium with their extracellular environment. When ice forms in the extracellular region, solutes are concentrated, and these solutes will induce an osmotic pressure gradient across the cell membrane. As detailed in chapter 4, this osmotic pressure gradient will cause the cell to dehydrate in order to concentrate its intracellular solutes, and thus, match osmotic pressure with the outside environment. Figures 7-6 illustrate this cell shrinkage. It can be seen that the rate of cell shrinkage reaches a maximum at a time corresponding to the time when the temperature decrease is most rapid, as seen in figures 7-4 and 7-5.

The large water flux from the cells is an attempt to restore equilibrium between the cellular contents and the extracellular environment. The finite value of the hydraulic conductivity of the membrane, however, combined with the fact that this value has an exponential dependence on temperature, ensure that the water flux from the cell remains limited; and therefore, if the external cooling is incessant, equilibrium is not restored in the cell. In this case, intracellular supercooling will result. Figure 7-7 demonstrates the degree of intracellular supercooling present in the four cells within the cartilage. Initially the entire tissue is supercooled, however this ceases shortly after extratissue nucleation. Then, in the planar ice growth stage, supercooling slowly rises, not a result of the cells failing to maintain equilibrium with their environment, but instead, as a result of the constitutional supercooling of the environment due to the propagation of the planar phase boundary.

At the moment of dendritic breakdown, ice quickly grows throughout the cartilage, raising the temperature and thus reducing the degree of supercooling. Also, as the dendrites form, concentration of solutes will initiate cell dehydration. Since the latent heat of fusion maintains a relatively high temperature, the cells are able to quickly equilibrate with their environment; however, as ice formation nears its conclusion, less latent heat is released and the temperature starts to decrease rapidly towards the external control temperature. Under these conditions, the cells fail to maintain equilibrium with their local environment, and thus, intracellular supercooling increases, as seen in figure 7-7.

The external cooling rate has a significant effect on this supercooling, as does the presence of DMSO. Since DMSO acts to postpone ice growth until lower temperatures are reached, more time is available to the cell to dehydrate, and thus, supercooling is reduced. When the external cooling ceases, the cells have time to restore equilibrium with the extracellular solutes, as seen in figure 7-7d when  $t = 300\text{sec}$ . However, if cooling does not cease, the cell must continue to play "catch-up" with the ever-changing extracellular environment, and since the hydraulic conductivity of the cell decreases exponentially with temperature,



the cell soon falls behind. Figure 7-8 demonstrates what can happen if cooling continues at  $-5^{\circ}/\text{min}$  down to a temperature of  $-60^{\circ}\text{C}$ .

In addition to cell dehydration during the supercooled state, DMSO concentration within the cell will be lower than the external DMSO concentration as a result of the excess water in the cell. Since the cell is permeable to DMSO, this reduced DMSO concentration will result in a flux of DMSO into the cell. The increase in DMSO within the cell is illustrated in figure 7-9. Since chondrocyte permeability to DMSO has a greater dependence on temperature than hydraulic conductivity (due to a large activation energy), permeability to DMSO decreases rapidly with decreasing temperature, and thus, only small amounts of DMSO move through the membrane during the freezing simulation.

### **Initial Conditions**

In addition to being a useful tool in predicting experimental outcome, this model can also be used to aid scientists in preparing experiments by predicting the amount of time it takes to equilibrate the system. The simulations presented in this chapter rely on their experimental counterparts being equilibrated in two particular cases. First, at room temperature the cartilage used in DMSO experiments needs to be equilibrated to a  $1.4\text{ mol/l}$  DMSO solution. This involves simply placing the cartilage in media containing DMSO and waiting. Simulation of this equilibration process is an effective way to determine the required amount of time to wait. Figure 7-10 clearly shows that a  $30\text{ min}$  wait is sufficient.

Once the cartilage needed for an experiment is prepared at room temperature, it must be equilibrated at  $-5^{\circ}\text{C}$  before ice formation can be nucleated. Equilibration at this temperature is necessary to ensure that nucleation can be quickly and easily performed when doing these experiments. Figure 7-11 shows that  $2\text{ min}$  is sufficient to ensure thermal equilibrium.

While performing these simulations, it was found that the results could be presented in far more ways than presented in this chapter. Simulations of this kind yield such a large volume of information that it is sometimes difficult to

**decide how to present it. In this chapter, all the data were presented in a consistent way (similar scales, for example); however, this may not have been the most intuitive way to present some of the data. The possibilities are as endless as the data, and this was only a single set of simple experiments. The list of possible experiments that can be aided, or simulated entirely, by this model is limitless.**

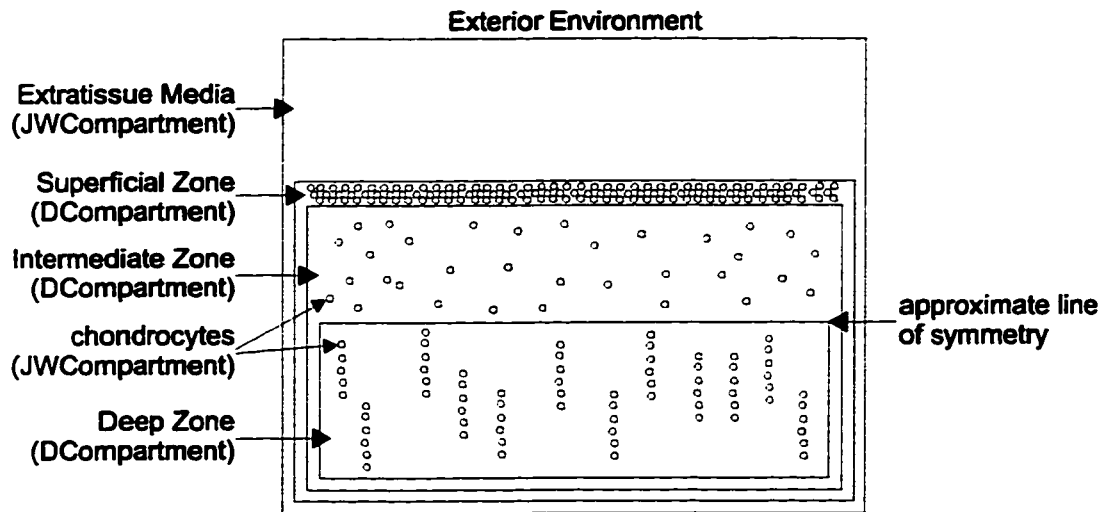


**Figure 7-1. Cartilage diagram.** This diagram illustrates how cartilage may be represented with the hierarchical compartment model. The simulations presented in this chapter were all done using a slightly simpler model consisting of a single DCompartment and four individual chondrocyte compartments.

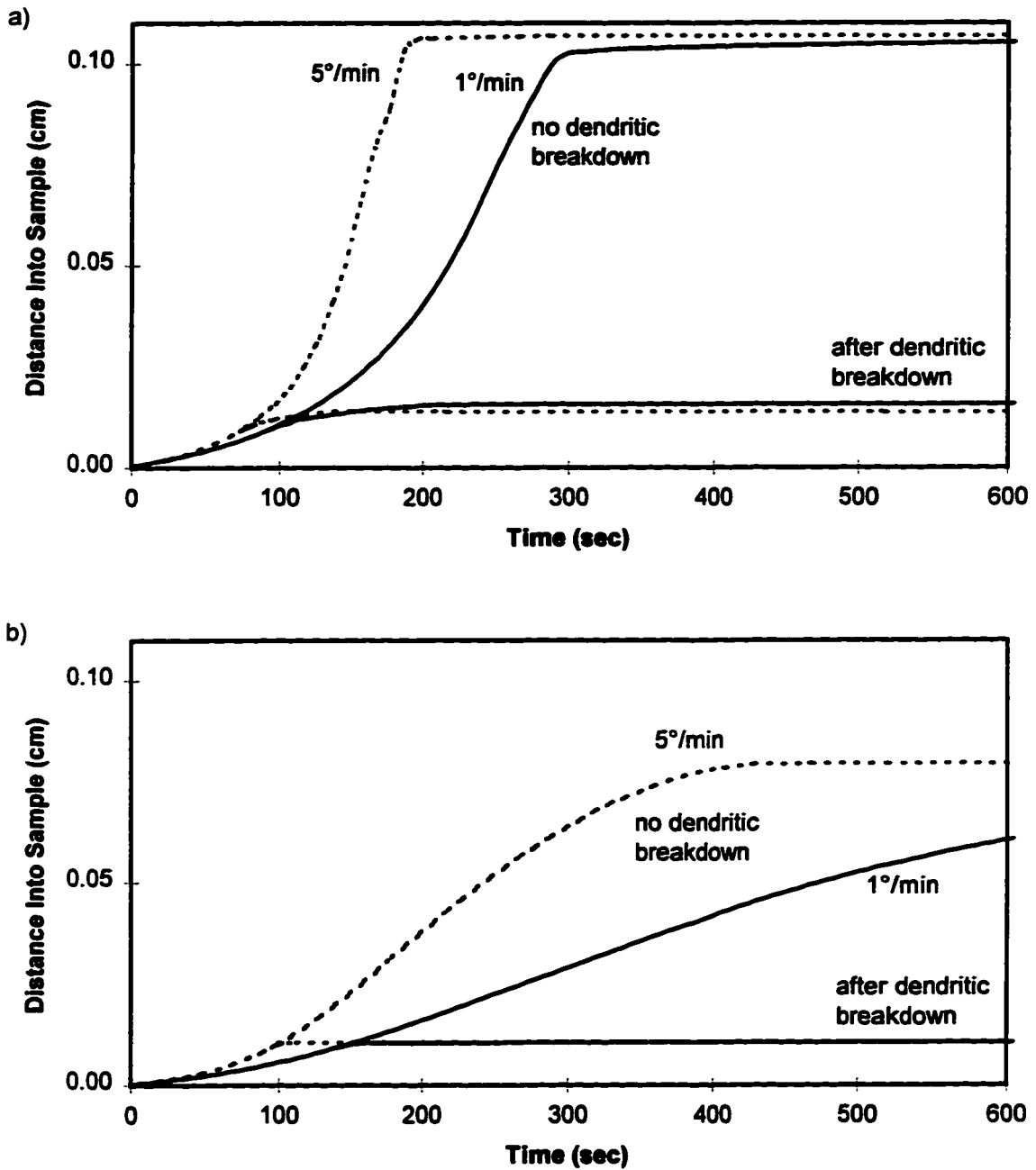


**Figure 7-2.** Summary of planar phase boundary propagation in the absence of, and following dendritic breakdown. Simulations for the a) salt only case, and b) the DMSO case are presented.

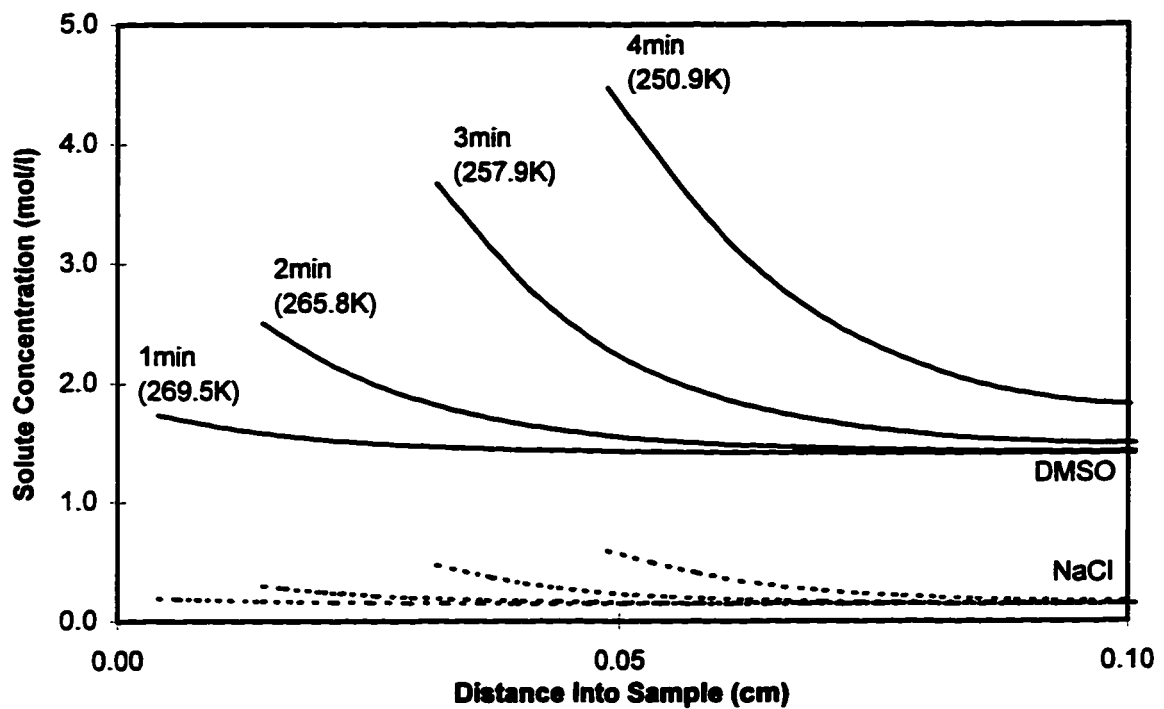


**Figure 7-3.** During planar ice growth, both DMSO and NaCl are excluded from the phase boundary. DMSO (solid lines) and NaCl (broken lines) concentration profiles are presented at various times during the fast cooling simulation. The temperatures quoted are the freezing points at the phase boundary.

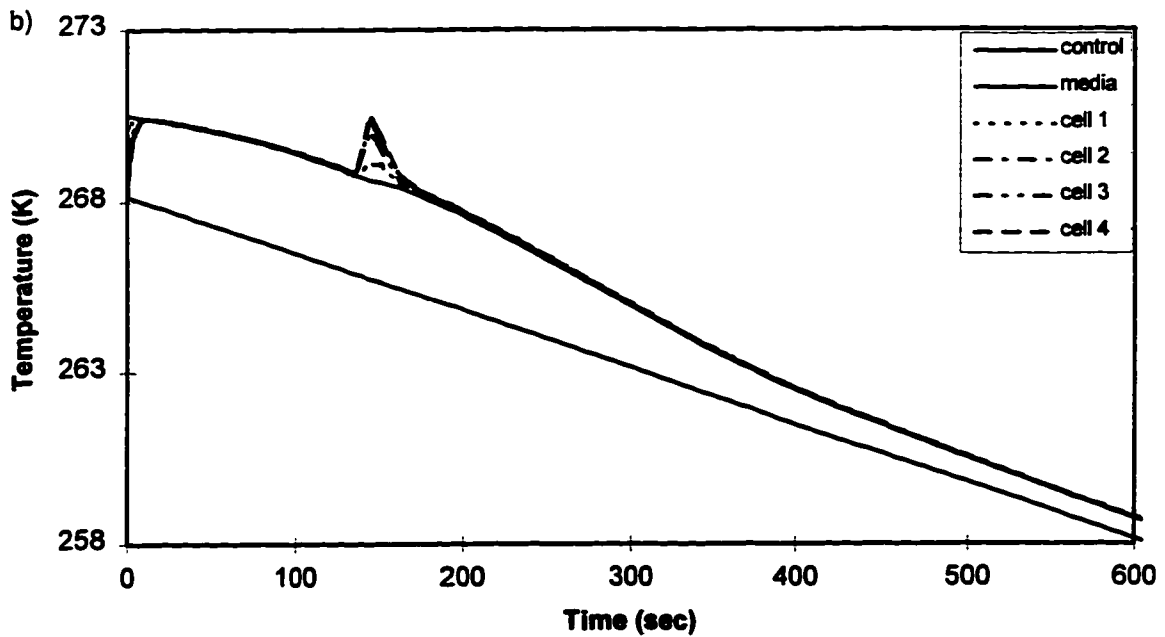
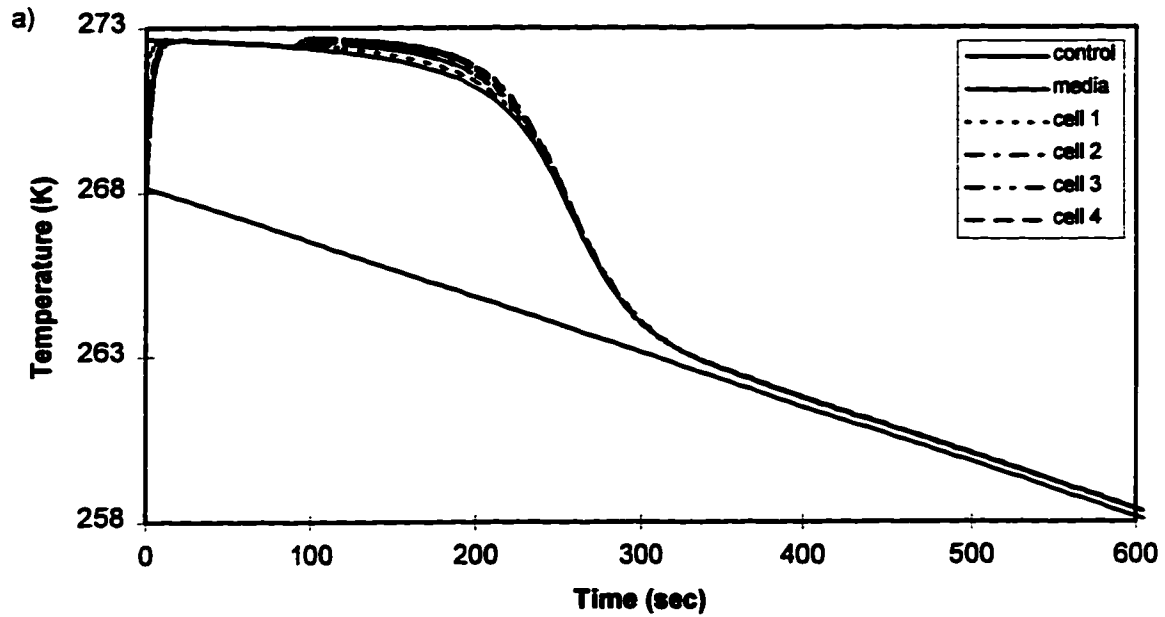


**Figure 7-4.** Temperature profiles present during the  $-1^{\circ}/\text{min}$  simulations. The effect of DMSO can be seen in b) as ice formation is postponed to lower temperatures than in a).

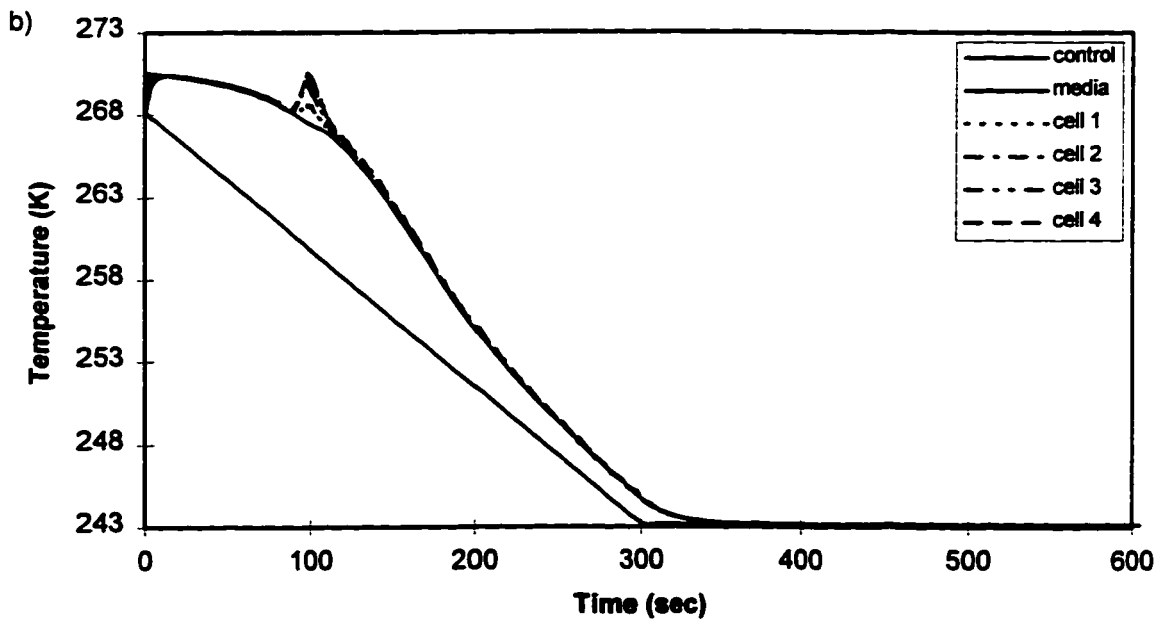
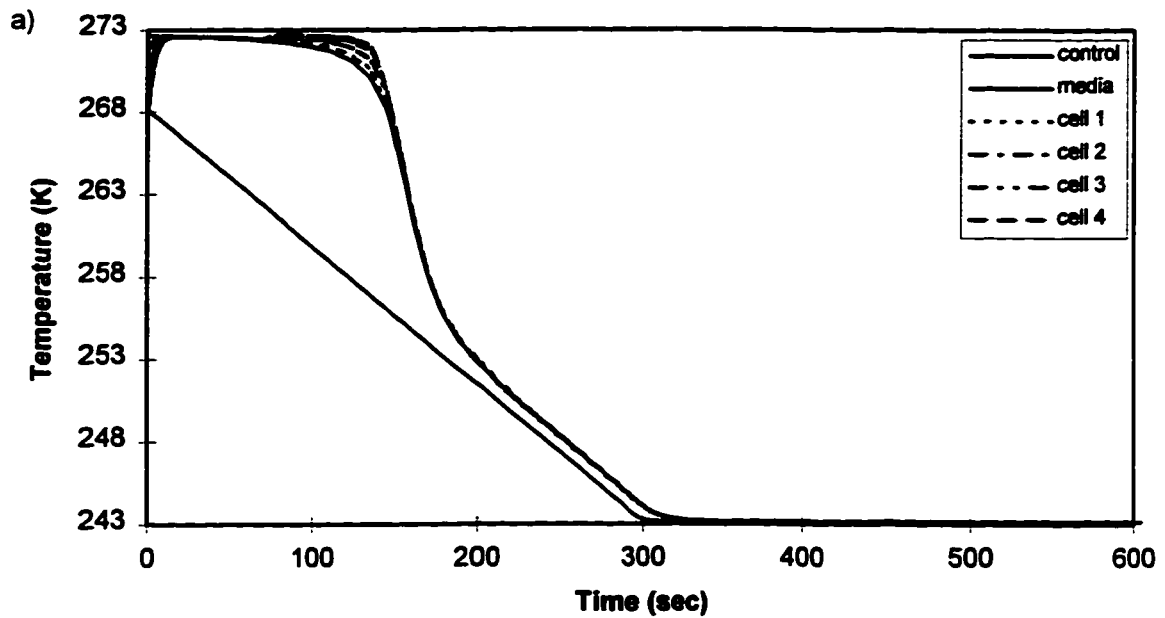


**Figure 7-5.** Temperature profiles present during the  $-5^{\circ}/\text{min}$  simulations. The effect of DMSO can be seen in b) as ice formation is postponed to lower temperatures than in a). Cooling ceases at 300sec when the control temperature reaches  $-30^{\circ}\text{C}$ .

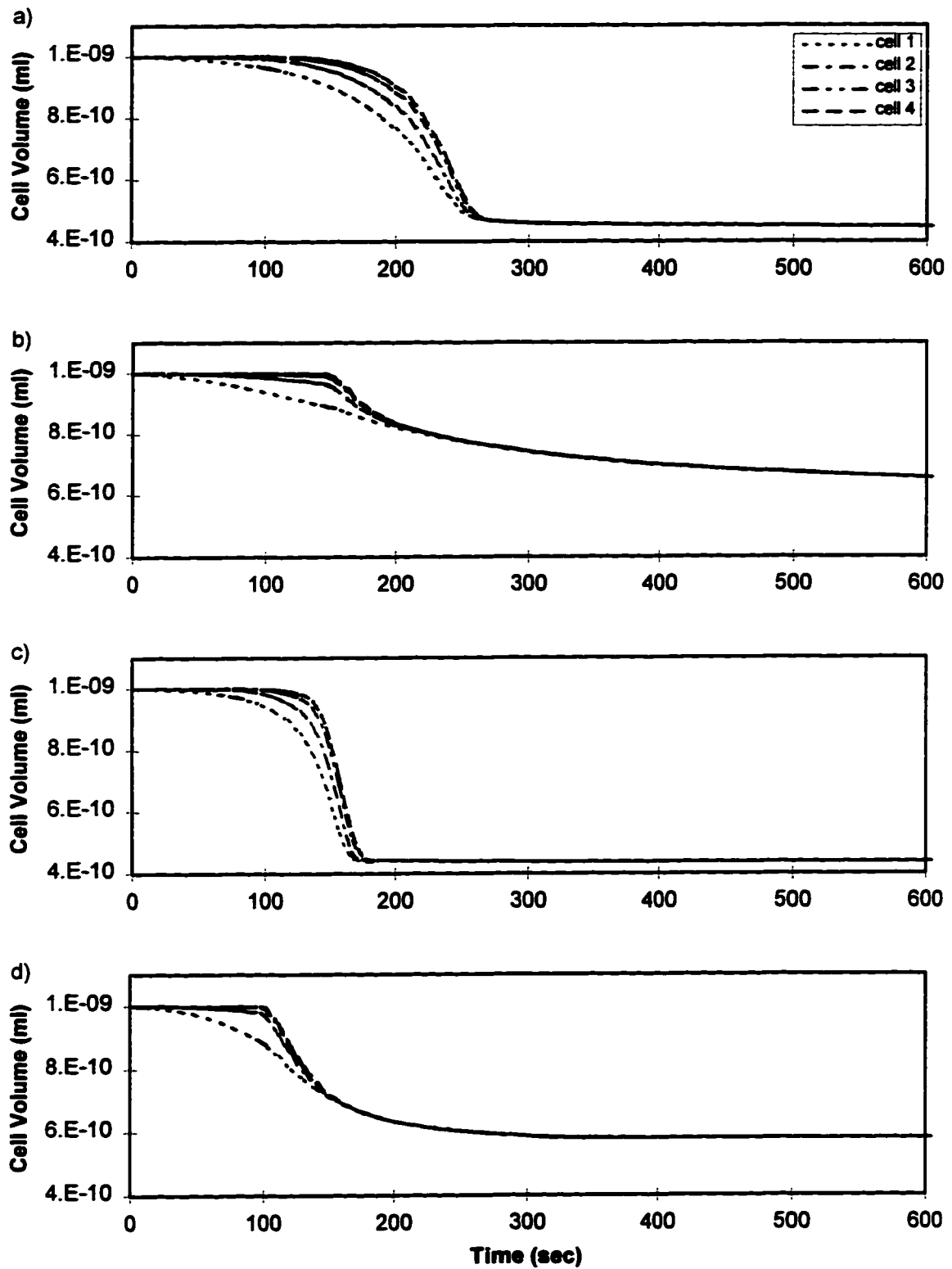


**Figure 7-6.** Cell volume curves for the a) slow cooling, b) slow cooling with DMSO, c) fast cooling, and d) fast cooling with DMSO simulations.



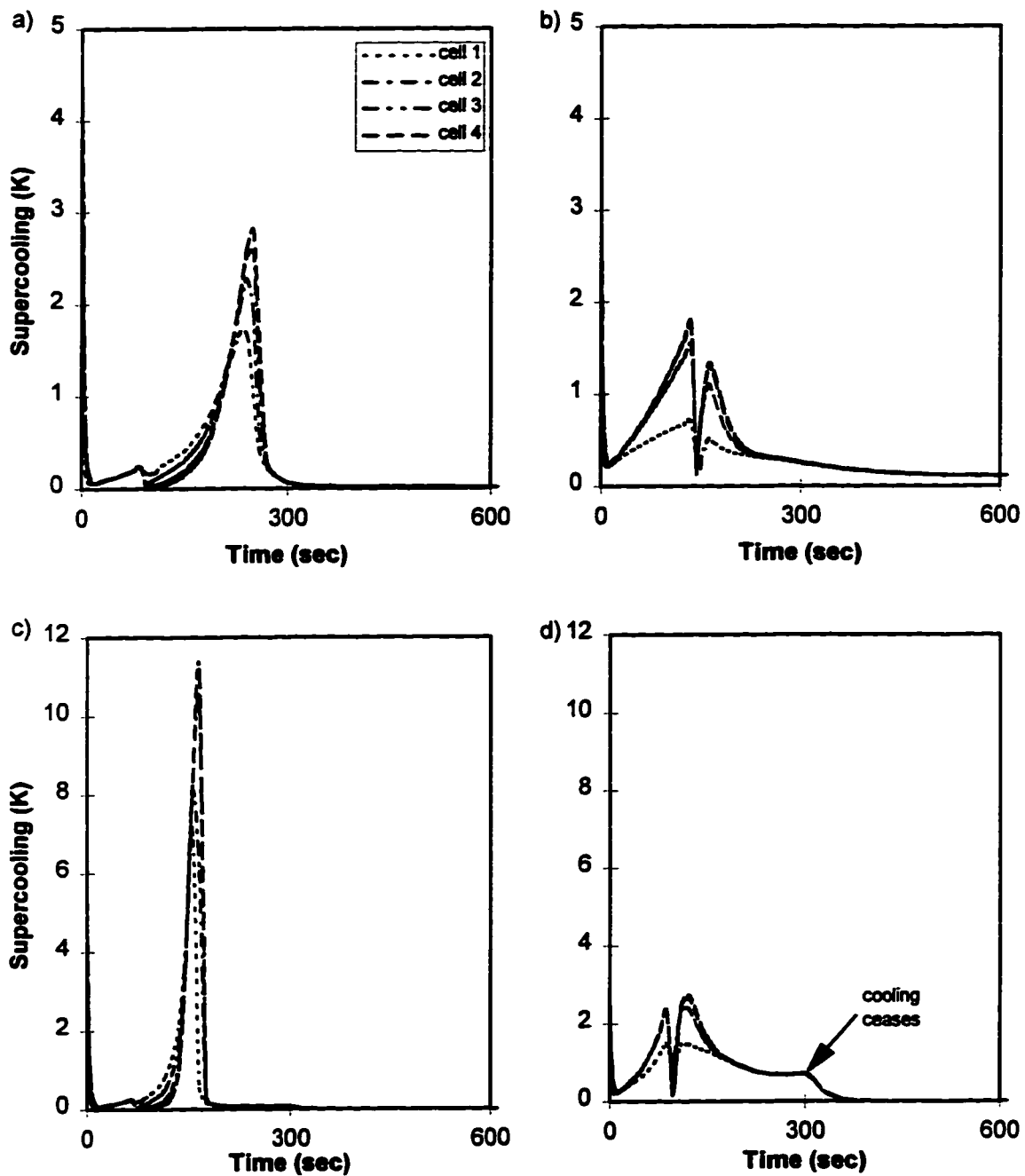


**Figure 7-7.** Degree of supercooling present within each chondrocyte. Curves a) and b) demonstrate the effect of DMSO, curve b), in the slow cooling case, while curves c) and d) demonstrate the same effect in the fast cooling case. In figure d), the cessation of cooling allows the cells to equilibrate with their extracellular environment.

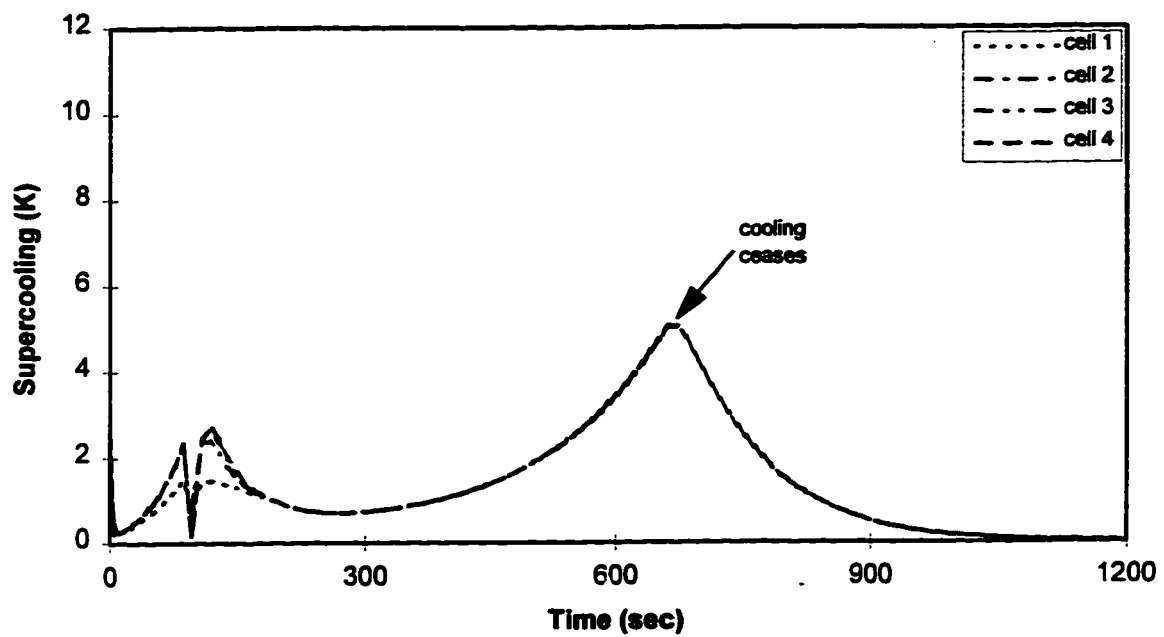


**Figure 7-8.** Same curve as that presented in figure 7-7d; however in this case cooling does not cease at  $-30^{\circ}\text{C}$ , but instead continues until  $-60^{\circ}\text{C}$  is reached. Only at this point do the cells have a chance to equilibrate with the extracellular solutes.

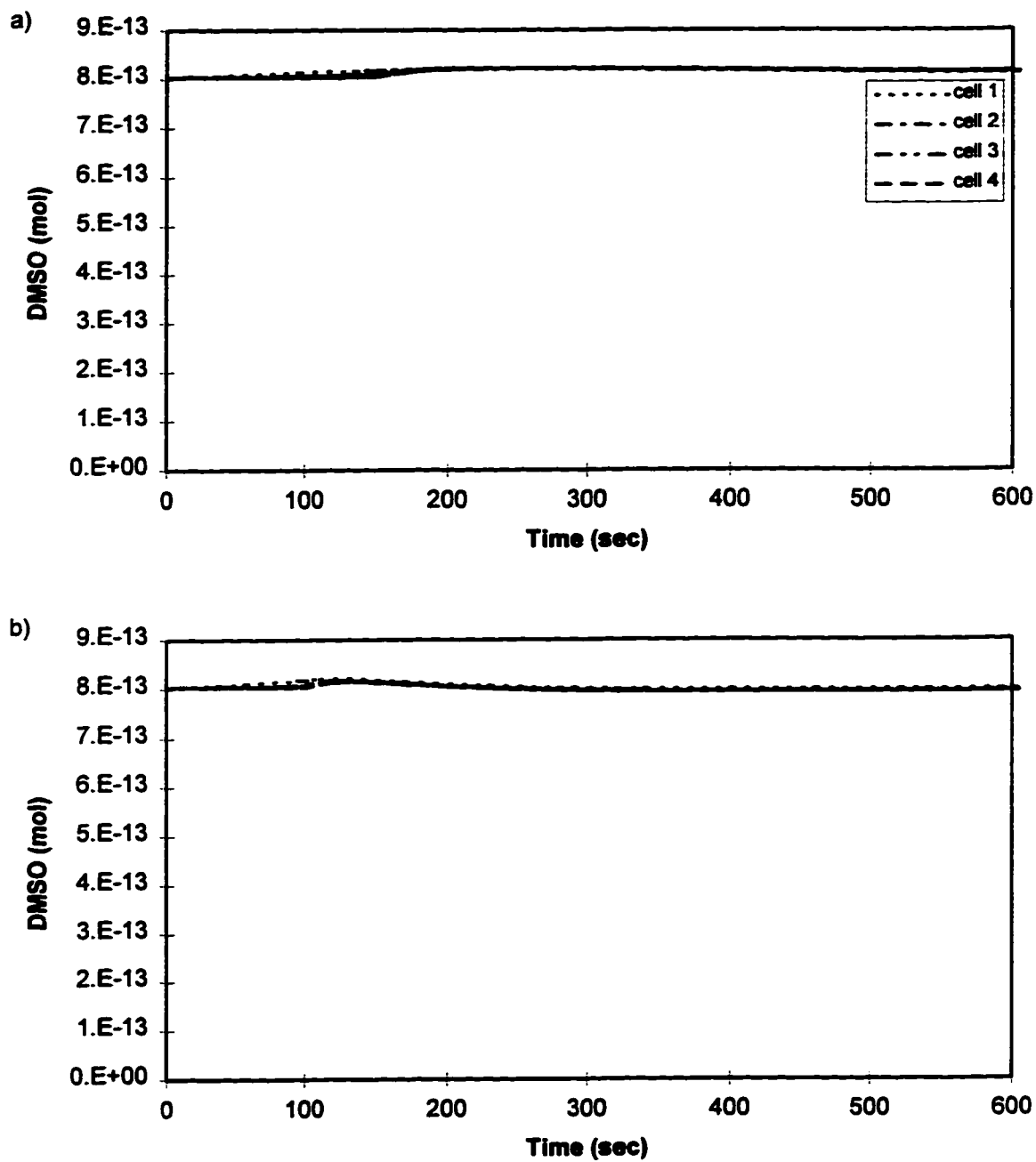


**Figure 7-9.** The amount of DMSO present within the cells during the a) slow cooling simulation and the b) fast cooling simulation. In both cases DMSO enters the cells during the supercooled state, and then very slowly leave the cell.

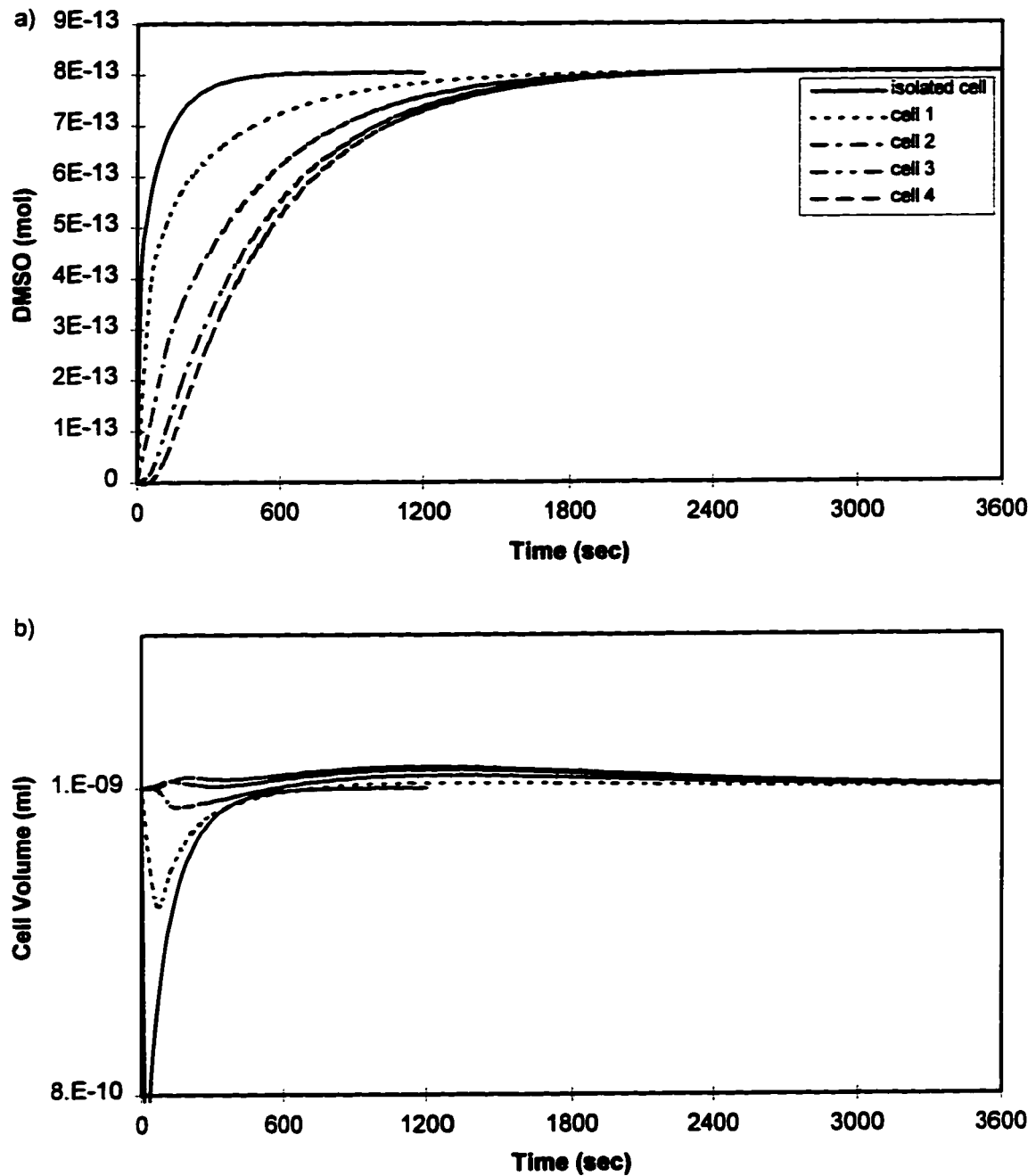


**Figure 7-10.** Equilibration of chondrocytes with 1.4 mol/l DMSO at 22°C. Both the a) DMSO uptake and b) cell volume curves show that 30min is sufficient time for equilibrium to be reached. The cells deep in the cartilage swell slightly as a result of the fact that when DMSO diffuses into the cartilage, it dilutes the salt solution present there.

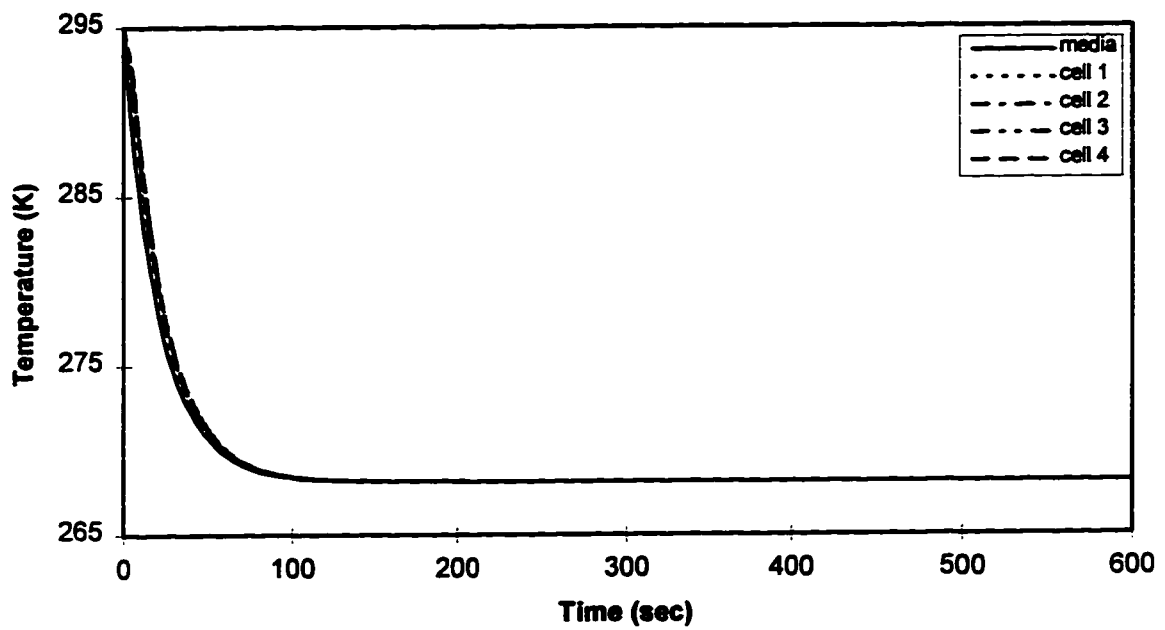


**Figure 7-11.** Thermal equilibration of the cartilage and freezing tube system from room temperature to  $-5^{\circ}\text{C}$ . One need only wait for 2min to ensure that the entire system is at the desired temperature.

## **Chapter 8**

### **Discussion**

#### **Thesis Objectives**

The objective of this thesis was to develop a model of heat and mass transport in biological tissues that is relatively easy to understand, but general enough that it can be applied to a wide range of systems. This model was developed from well-known physical processes and thermodynamic mechanisms, using only parameters with physical significance. The use of empirical relations and meaningless coefficients that must be fit for using experimental data was avoided. The basic framework of the model makes very few specific assumptions regarding the scale and geometry of the system to be modeled. As a result, a wide variety of tissue systems can be effectively modeled by this approach. This framework was also intended to be extendible, and it can have additional geometry or physical mechanisms included as the need arises. This also helps to ensure that the scope of the model is significant.

Since the model was implemented with an object oriented programming language, the compartment type hierarchy corresponds well with the class structure allowed by such a programming language. By implementing each compartment as a specific class, and each descendent as a class derived from its ancestor, the reasons for having a hierarchy of compartment types is realized. A new compartment type that only modifies the behaviour of an existing compartment type by a small amount can be easily and quickly implemented by creating the new compartment type as a descendent of the existing one.

Although this compartment model does allow three-dimensional tissues to be effectively represented by a hierarchy of compartments, the one-dimensional nature of the transport mechanisms cannot be easily avoided. This model, in its current state, is not intended to effectively model situations where the gradients in solute concentration and temperature are not parallel. In terms of modeling

situations of interest to cryobiologists, however, this is not a major drawback as the need for such complex modeling efforts does not currently exist.

There is, in cryobiology, a definite need to be able to predict the phase behaviour of a solution consisting of an arbitrary number of components, each present in an arbitrary amount. It is easily seen that large deviations from the ideal dilute solution model do occur with many solutions that are currently being used by cryobiologists. The theory presented in this thesis effectively describes the phase behaviour of some typical binary solutions of interest to the cryobiologist; however, this theory has not been extensively tested with other binary solutions, nor has it been tested with solutions containing more than two solutes. There is an obvious way to generalize the equations that have been presented such that they apply to solutions containing more than two solutes; however, these generalized equations would require that more parameters be provided to accurately describe the phase behaviour. The parameters required by the theory are physical in nature and some may be found in the literature; however, most remain unknown and would have to be fitted from known phase behaviour. Of course, as the number of components in a solution increases, measurement of the phase behaviour quickly becomes a very tedious endeavor.

The transport mechanism known as osmosis has been well studied by a wide range of researchers. Provided that osmotic pressures can be calculated, the transport equations for water and permeant solute movement provide a reasonably accurate description of osmosis. The current description of this transport mechanism can be generalized to allow for multiple permeant solutes, each with its own permeability and reflection coefficients; however, any significant interaction between permeant solutes would require a more precise model.

The calculation of osmotic pressure is a problem similar in difficulty to the problem of calculating phase behaviour. In fact, one can think of a planar phase boundary as an ideal semi-permeable membrane. As the planar phase boundary propagates, it selects out a single solute from the solution being frozen and

allows only this solute to cross the boundary. Also, the boundary has infinitesimal width as an ideal semi-permeable membrane would. In a situation where pure water exists on both sides of a semi-permeable membrane (ie. equilibrium), and then some solute is added to one side, the solute interferes with the dynamic equilibrium at the membrane and causes a net flux of water towards the side of the membrane containing the solute. A completely analogous situation arises when a planar ice front separates ice from pure water, and solute is added to liquid side. Again, the solute will disrupt the dynamic equilibrium between the ice and the liquid, and a net flux of water will cross the phase boundary into the liquid region (the ice melts). This comparison between a phase boundary and an ideal semi-permeable membrane could be useful in further attempts to predict phase behaviour and osmotic pressures.

The variable time step algorithm introduced in chapter 2 and detailed in chapter 4 is actually just an optimization for the model. It is, however, a very effective optimization as some of the simulations done for this thesis take hours to execute on a moderately powered desktop computer. Without the variable time step method, either error tolerance would have to be sacrificed or weeks of computer time would have to be allocated for each simulation.

In chapter 5 a general solution of the diffusion equation was presented. The diffusion equation can be solved exactly in many specific situations; however, as more general solutions are desired, the difficulty associated with finding an exact solution skyrockets. The numerical solution presented in this thesis is general enough to fulfill all the needs of this model. Both heat and solute movements can be modeled, along with moving planar phase boundaries that couple the separate heat and solute movements at their location. In this thesis, however, no attempt was made to model the diffusion of water. Most models that consider diffusion of a solute in water assume that the water is so abundant that the concentration of the water does not vary significantly from one part of the system to another, and thus, water does not diffuse. This may be an erroneous assumption when the dilute solution assumption cannot be made.



The equations presented in chapter 5 are complete and can be used to model the diffusion of water in addition to the other solutes. The only special consideration is that at the phase boundary, water concentration is depressed as freezing proceeds; not elevated as is the case of the other solutes.

The solution to the diffusion problem also allows for dendritic ice formation. When this occurs, solute concentration and temperature are coupled throughout the region of the dendrites via the phase diagram. From experience running the simulations presented in this thesis, dendritic breakdown tends to cause the value of  $\Delta t$  to suddenly plummet as the temperature profile within the system is forced to conform to the distinctly non-linear freezing point profile.

Another realization that comes with experience running these simulations is that there are far more possible ways to graph the data than can be physically accomplished. During a typical experiment in biology, the experimenter must carefully choose what measurements they wish to make before the experiment begins and are then forced to only make those measurements during the course of the experiment. Although the person who simulates their experiments usually must also choose what measurements are desired before the simulation is run, the number of measurements that may be allowed for each simulation is virtually unlimited. Each simulation yields a mountain of numbers, and these numbers can be presented in an equally massive number of possible ways. Chapter 7 presents a simple set of four simulations that mimic experiments that are typical of what a cryobiologist might be interested in performing. The results of these simulations are presented in a few select ways such that the effectiveness of the model can be displayed. The data could, just as easily, have been presented in a variety of other ways that would have, perhaps, made the cryobiology easier to understand, or the mechanisms of transport easier to understand. The possibilities are limitless.

As cryobiologists continue studying tissues of ever increasing complexity, and use solutions containing multiple solutes in extreme concentrations, the need to understand the movement of heat and solutes in these tissue systems, along

**with the growth or absence of ice, is an ever-increasing difficulty. A model that can effectively describe these mechanisms within tissues is of great importance to any researcher that needs a thorough understanding of the state of the tissue they are studying. The modeling efforts presented in this thesis are a necessary first step to understanding more complex mechanisms of damage and injury in biological tissues. With the fundamentals of heat and mass transport grasped, the biological impact of freezing on tissues can now be addressed.**

## References

- Andrushkiw, R. Mathematical Modeling of Freezing Front Propagation in Biological Tissue. *Mathl Comput. Modelling* **13**:10:1-9 (1990).
- Atkins, P. W. "Physical Chemistry," 4th ed. W. H. Freeman and Company, New York (1990).
- Batycky, R., Hammerstedt, R., Edwards, D. Osmotically Driven Intracellular Transport Phenomena. *Submitted to R. Soc. Lond.* April (1996).
- Bischof, J., Rubinsky, B. Microscale Heat and Mass Transfer of Vascular and Intracellular Freezing in the Liver. *Journal of Heat Transfer* **115**:1029-1035 (1993).
- Burden, R., Faires, J. "Numerical Analysis," 5th ed. PWS Publishing Company, Boston (1993).
- Christensen, C., Gmehling, J., Rasmussen, P., Weidlich, U. "Heats of Mixing Data Collection," Deutsche Gesellschaft für Chemisches Apparatewesen, Frankfurt (1984).
- Crank, J. "The Mathematics of Diffusion," 2nd ed. Clarendon Press, Oxford (1975).
- Dick, D. "Cell Water." Butterworth, Inc., Washington, D.C. (1966).
- Diller, K., Dunaway, D. Network Thermodynamic Analysis of Vasomotion in a Microvascular Network. *Biorheology* **28**:369-382 (1991).
- Diller, K. Modeling of Bioheat Transfer Processes at High and Low Temperatures. *Advances in Heat Transfer* **22**:157-357 (1992).
- Haar, L., Gallagher, J., Kell, G. "NBS/NRC Steam Tables." Hemisphere Publishing Corporation, Washington (1984).
- Hildebrand, J. The Entropy of Solution of Molecules of Different Size. *J. Chem. Phys.* **15**:8:225-228 (1947).
- Hildebrand, J., Prausnitz, J., Scott, R. "Regular and Related Solutions." Van Nostrand Reinhold Company, New York (1970).

- Jacobs, M. *In* "Trends in Physiology and Biochemistry." Academic Press, New York (1952).
- Johnson, J., Wilson, T. Osmotic Volume Changes Induced by a Permeable Solute. *J. Theoret. Biol.* **17**:304-311 (1967).
- Kedem, O., Katchalsky, A. Thermodynamic Analysis of the Permeability of Biological Membranes to Non-Electrolytes. *Biochimica et Biophysica Acta* **27**:229-246 (1958).
- Kiil, F. Molecular Mechanisms of Osmosis. *American Physiological Society*. R801-808 (1989).
- Körber, C., Scheiwe, M. Observations on the Non-Planar Freezing of Aqueous Salt Solutions. *Journal of Crystal Growth* **61**:307-316 (1983a).
- Körber, C., Scheiwe, M., Wollhöver, K. Solute Polarization During Planar Freezing of Aqueous Salt Solutions. *Int. J. Heat Mass Transfer* **26**:1241-1253 (1983b).
- Krogh, A. The Number and Distribution of Capillaries in Muscles With Calculation of Oxygen Pressure Heat Necessary for Supplying the Tissue. *J. Physiol.* **52**:409 (1919).
- Levitt, J., Scarth, G. Frost Hardening Studies With Living Cells. II. Permeability in Relation To Frost Resistance and the Seasonal Cycle. *Can. J. Res. Sect. C Bot. Sci.* **14**:285-305 (1936).
- Lucke, B., McCutcheon, M. The Living Cell as an Osmotic System and its Permeability to Water. *Physiol. Rev.* **12**:68-132 (1932).
- Maroudas, A. Physico-chemical Properties of Articular Cartilage. *In* "Adult Articular Cartilage," 2nd ed. Pitman Medical (1979).
- Mazur, P., Leibo, S., Chu, E. A Two Factor Hypothesis of Freezing Injury. *Exp. Cell Res.* **71**:345-355 (1972).
- Muldrew, K., McGann, L. Mechanisms of Intracellular Ice Formation. *Biophys. J.* **57**:525-532 (1990).
- Muldrew, K. Doctoral Dissertation. University of Alberta, Canada (1993).

- Muldrew, K., McGann, L. The Osmotic Rupture Hypothesis of Intracellular Freezing Injury. *Biophys J.* **66**:532-541 (1994).
- Pegg, D. Equations For Obtaining Melting Points And Eutectic Temperatures For The Ternary System Dimethyl Sulphoxide/Sodium Chloride/Water. *Cryo-Letters* **7**:387-394 (1986).
- Rasmussen, D., MacKenzie, A. Phase Diagram for the System Water-Dimethylsulphoxide. *Nature* **220**:1315-1317 (1968).
- Rubinsky, B., Pegg, D. A Mathematical Model for the Freezing Process in Biological Tissue. *Proc. R. Soc. Lond.* **B234**:343-358 (1988).
- Rutter, J., Chalmers, B. A Prismatic Substructure Formed During Solidification of Metals. *Canadian Journal of Physics* **31**:15-39 (1953).
- Scatchard, G. Equilibria in Non-Electrolyte Solutions in Relation to the Vapor Pressures and Densities of the Components. *Chem. Rev.* **8**:321-333 (1931).
- Schachar, N., McGann, L. Cryopreservation of Articular Cartilage, Bone and Cartilage Allografts: Biology and Clinical Applications, Friedlaender and Goldberg, editors, Americal Academy of Orthopaedic Surgeons (1991).
- Staverman, A. Non-equilibrium Thermodynamics of Membrane Processes. *Trans. Faraday Soc.* **48**:176-185 (1952).
- Steponkus, P., Stout, D., Wolfe, J., Lovelace, R. Freeze-induced Electrical Transients and Cryoinjury. *Cryo Lett.* **5**:343-348 (1984).
- Walcerz, D. Cryosim: A User-Friendly Program for Simulating Cryopreservation Protocols. *Cryobiology* **32**:35-51 (1995).
- Weast, C. "CRC Handbook of Chemistry and Physics," 63rd ed. CRC Press, Inc., Boca Raton (1983).
- Weinberg, F., Chalmers, B. *Can. J. Phys* **29**:382 (1951).
- Wheater, P., Burkitt, H., Daniels, V. "Functional Histology," 2nd ed. Longman Group UK Limited, New York (1987).

## Appendix 1

### Constants and Parameters

#### Permeability Parameters

Parameters are given for both V-79-w hamster fibroblasts and bovine chondrocytes. All these values came from [Muldrew 1993].

#### *V-79 Hamster Fibroblasts*

<b>Parameters</b>	<b>Symbol</b>	<b>Value</b>
Isotonic Volume	V	$800\mu\text{m}^3$
Membrane Surface Area	SA	$417\mu\text{m}^2$
Osmotically Inactive Volume	$V_d$	$359\mu\text{m}^3$
Base Temperature for Parameters	$T_g$	273K
Hydraulic Conductivity	$L_p$	$0.145\mu\text{m}^3/\mu\text{m}^2\cdot\text{atm}\cdot\text{min}$
Activation Energy for $L_p$	$E_a$	9.14 kcal/mol
DMSO Permeability	$P_g$	$0.512\mu\text{m}/\text{min}$
Activation Energy for $P_g$	$E_a$	20.1 kcal/mol
Reflection Coefficient	$\sigma$	0.9

#### *Bovine Chondrocytes*

<b>Parameters</b>	<b>Symbol</b>	<b>Value</b>
Isotonic Volume	V	$1000\mu\text{m}^3$
Membrane Surface Area	SA	$484\mu\text{m}^2$
Osmotically Inactive Volume	$V_d$	$430\mu\text{m}^3$
Base Temperature for Parameters	$T_g$	287K
Hydraulic Conductivity	$L_p$	$0.146\mu\text{m}^3/\mu\text{m}^2\cdot\text{atm}\cdot\text{min}$
Activation Energy for $L_p$	$E_a$	12.2 kcal/mol
DMSO Permeability	$P_g$	$2.70\mu\text{m}/\text{min}$
Activation Energy for $P_g$	$E_a$	18.5 kcal/mol
Reflection Coefficient	$\sigma$	0.95

## Physical Parameters

These physical parameters were used in more of the diffusion simulations.

Most of the parameters were found in [Weast 1983].

Solute	Constant	Symbol	Value
H <sub>2</sub> O	Molecule Weight	<i>MW</i>	18.01528 g/mol
H <sub>2</sub> O	Freezing Point (at 1atm)	<i>F</i>	273.15K
H <sub>2</sub> O	Latent Heat of Fusion	<i>L</i>	-6009 J/mol
H <sub>2</sub> O	Molecular Volume of Liquid	<i><sub>l</sub>MV</i>	18.01528 ml/mol
H <sub>2</sub> O	Molecular Volume of Solid	<i><sub>s</sub>MV</i>	19.58 ml/mol
H <sub>2</sub> O	Heat Capacity of Liquid	<i><sub>l</sub>c<sub>p</sub></i>	75.98 J/K·mol
H <sub>2</sub> O	Heat Capacity of Solid	<i><sub>s</sub>c<sub>p</sub></i>	37.8 J/K·mol
H <sub>2</sub> O	Thermal Conductivity of Liquid	<i><sub>l</sub>K</i>	0.00574 J·cm/cm <sup>2</sup> ·K·sec
H <sub>2</sub> O	Thermal Conductivity of Solid	<i><sub>s</sub>K</i>	0.022 J·cm/cm <sup>2</sup> ·K·sec
NaCl	Phase Diagram Coefficient	<i>a</i>	-3115 K·ml/mol
NaCl	Phase Diagram Coefficient	<i>b</i>	-270 K·ml <sup>2</sup> /mol <sup>2</sup>
NaCl	Diffusion Coefficient	<i>D</i>	1.545 × 10 <sup>-5</sup> cm <sup>2</sup> /sec
NaCl	Molecular Volume in Solution	<i><sub>l</sub>MV</i>	19.07 ml/mol
NaCl	Molecular Weight	<i>MW</i>	58.4428 g/mol
DMSO	Phase Diagram Coefficient	<i>a</i>	0
DMSO	Phase Diagram Coefficient	<i>b</i>	-1021856 K·ml <sup>2</sup> /mol <sup>2</sup>
DMSO	Diffusion Coefficient	<i>D</i>	1.02 × 10 <sup>-5</sup> cm <sup>2</sup> /sec
DMSO	Molecular Volume in Solution	<i><sub>l</sub>MV</i>	70.94 ml/mol
DMSO	Molecular Weight	<i>MW</i>	78.1335 g/mol

## Appendix 2

### Variable Time Step Calculations

The variable time step method presented at the end of chapter 4 can also be applied to the diffusion equations derived in chapter 5. As in chapter 4, all that is required is that some time derivatives be calculated.

Since the iteration equation for the diffusion problem is

$$C(t_{j+1}) = C(t_j) + \frac{\partial C}{\partial t} \Delta t, \quad (\text{A2-1})$$

where

$$\frac{\partial C}{\partial t} = 2D\alpha_i, \quad (\text{A2-2})$$

the local truncation error associated with each iteration can be written as

$$\left| D(\Delta t)^2 \frac{d\alpha_i}{dt} \right|. \quad (\text{A2-3})$$

This means that to achieve a desired error limit, one must choose  $\Delta t$  such that

$$\Delta t \leq \frac{L \text{abs}\left(\frac{\bar{C}_i}{g_i}\right)}{\text{abs}\left(D \frac{d\alpha_i}{dt}\right)}, \quad (\text{A2-4})$$

where  $L$  is the desired fraction error per second.

To calculate the derivatives  $d\alpha_i/dt$ , start by calculating  $dQ_i/dt$  for each subinterval. From equation 5-12b,

$$\frac{dQ_{n-1}}{dt} = \frac{dG_n}{dt}, \quad (\text{A2-5})$$

and from equation 5-16b,



$$\frac{dQ_i}{dt} = \frac{-12D(g_{i+1} + P_{i+1})(\alpha_i - \alpha_{i+1}) - 2g_{i+1}^2 \frac{dQ_{i+1}}{dt}}{3(g_{i+1} + P_{i+1})(g_i + g_{i+1}) - 2g_{i+1}^2}. \quad (\text{A2-6})$$

At the phase boundary (from equation 5-64b)

$$\begin{aligned} \frac{dQ'_{-1}}{dt} = & \frac{2L\rho h_0(h_0 + 3P'_0)\left(\frac{dN}{dt} - 2K_s\alpha'_{-1}\right) + 4K_l M h_0^2 \frac{dQ'_0}{dt}}{L\rho h_{-1}h_0(h_0 + 3P'_0) - 2K_s M h_0(h_0 + 3P'_0) - 6K_l M h_{-1}(h_0 + P'_0)}, \quad (\text{A2-7}) \\ & + \frac{24K_l M(h_0 + P'_0)(K_s\alpha'_{-1} - K_l\alpha'_0)}{L\rho h_{-1}h_0(h_0 + 3P'_0) - 2K_s M h_0(h_0 + 3P'_0) - 6K_l M h_{-1}(h_0 + P'_0)} \end{aligned}$$

where (from equation 5-58b)

$$\frac{dN}{dt} = \sum_j \left( -\frac{A^j g_0^2 \frac{dQ^j_0}{dt}}{3(g_0 + P^j_0)} + 2A^j D^j \alpha^j_0 \right). \quad (\text{A2-8})$$

Note that all these calculations rely on the fact that

$$\frac{d\bar{C}_i}{dt} = 2Dg_i\alpha_i. \quad (\text{A2-9})$$

Then, the  $d\alpha_i/dt$ 's may be calculated. From 5-18a,

$$\frac{d\alpha_0}{dt} = \frac{3g_0 \frac{dQ_0}{dt} + 6\left(\frac{dC_0}{dt} - 2D\alpha_0\right)}{g_0(g_0 + 3P_0)}, \quad (\text{A2-10})$$

and from 5-14a,

$$\frac{d\alpha_{i+1}}{dt} = \frac{-2g_i^2 \frac{d\alpha_i}{dt} + 3(g_i + g_{i+1}) \frac{dQ_{i+1}}{dt} + 12D(\alpha_i - \alpha_{i+1})}{3(g_{i+1} + P_{i+1})(g_i + g_{i+1}) - 2g_{i+1}^2}. \quad (\text{A2-11})$$

At the phase boundary equation 5-61a differentiates to

$$\frac{d\alpha'_0}{dt} = \frac{3L\rho h_{-1}h_0 \frac{dQ'_0}{dt} + 6L\rho h_{-1} \left( \frac{dN}{dt} - 2K_I \alpha'_0 \right) + 4K_s M h_{-1}^2 \frac{d\alpha'_{-1}}{dt}}{L\rho h_{-1}h_0(h_0 + 3P'_0) - 2K_s M h_0(h_0 + 3P'_0) - 6K_I M h_{-1}(h_0 + P'_0)} + \frac{-24K_s M (K_s \alpha'_{-1} - K_I \alpha'_0) - 6M (K_I h_{-1} + K_s h_0) \frac{dQ'_0}{dt}}{L\rho h_{-1}h_0(h_0 + 3P'_0) - 2K_s M h_0(h_0 + 3P'_0) - 6K_I M h_{-1}(h_0 + P'_0)} \quad (A2-12)$$

while equation 5-52a gives

$$\frac{d\alpha_0}{dt} = \frac{\frac{dQ_0}{dt} + \frac{\tilde{C}}{D} \frac{d^2 X}{dt^2}}{g_0 + P_0} \quad (A2-13)$$

where (from equation 5-62)

$$\frac{d^2 X}{dt^2} = K_s \frac{\frac{2}{3} h_{-1}^2 h_0 (h_0 + 3P'_0) \frac{d\alpha'_{-1}}{dt} + 2h_0 (h_0 + 3P'_0) \left( \frac{dN}{dt} - 2K_s \alpha'_{-1} \right)}{L\rho h_{-1}h_0(h_0 + 3P'_0) - 2K_s M h_0(h_0 + 3P'_0) - 6K_I M h_{-1}(h_0 + P'_0)} + K_I \frac{2h_{-1}h_0^2 \frac{dQ'_0}{dt} + 6h_{-1}(h_0 + P'_0) \left( \frac{dN}{dt} - 2K_I \alpha'_0 \right)}{L\rho h_{-1}h_0(h_0 + 3P'_0) - 2K_s M h_0(h_0 + 3P'_0) - 6K_I M h_{-1}(h_0 + P'_0)} \quad (A2-14)$$

These equations are all that is required to implement a variable time step method for the diffusion problem presented in chapter 5.